EFFECT OF STEREO AND COMONOMER DEFECTS ON CRYSTALLINE AND AMORPHOUS PHASES IN POLYPROPYLENE

by

Cassandra Gallaschun

Bachelor of Science in Chemical Engineering, University of Pittsburgh, 2012

Submitted to the Graduate Faculty of

Swanson School of Engineering in partial fulfillment

of the requirements for the degree of

Master of Science in Chemical Engineering

University of Pittsburgh

2018

UNIVERSITY OF PITTSBURGH

SWANSON SCHOOL OF ENGINEERING

This thesis was presented

by

Cassandra Gallaschun

It was defended on

November 20th, 2018

and approved by

Sachin Velankar, Ph.D., Associate Professor
Department of Chemical and Petroleum Engineering

Robert Enick, Ph.D., Assistant Chair of Research and Professor
Department of Chemical and Petroleum Engineering

Lei Li, Ph.D., Associate Professor
Department of Chemical and Petroleum Engineering

Damodaran Krishnan Achary, Ph.D., Research Professor
Department of Chemistry

EFFECT OF STEREO AND COMONOMER DEFECTS ON CRYSTALLINE AND AMORPHOUS PHASES IN POLYPROPYLENE

Cassandra Gallaschun, M.S.

University of Pittsburgh, 2018

Solution state nuclear magnetic resonance (NMR) will be used to measure the tacticity and ethylene incorporation of a matrix of samples containing, homopolymer, random, impact copolymer and branched samples. Solid state NMR will be used to investigate the rigid and mobile thickness along with the fractions of each type. Annealed and thermal fractionation stepwise crystallization differential scanning calorimetry will be used to measure the lamella thickness and amorphous phase thickness of various types of polypropylene. The crystallinity will also be investigated by annealed differential scanning calorimetry (ADSC). Dynamic mechanical analysis will be used to further investigate the amorphous phase. The chemical and crystal structure data collected will then be used to compare against predicted trends in literature of a series of mechanical tests, such as, tensile, flex, and two types of impact. The work showed the initial application of spin diffusion solid state NMR and thermal fractionation for lamellae characterization on branched polypropylene. Branching was found to increase the rigid fraction and the lamellae thickness, as branching increased.

TABLE OF CONTENTS

LIST OF TABLES

LIST OF FIGURES

ACKNOWLEDGEMENTS

The author would like to thank all the contributors for their support and knowledge in the data collection, analysis, and writing of this thesis.

1. Dr. Sachin Velankar for his extensive advice, support and knowledge throughout the thesis.
2. Dr. Damodaran Krishnan Achary for his solid state NMR advice, knowledge and work in running the solid state samples.
3. Leslie Bockman and Dr. Joel Carr for their general advice and guidance throughout this thesis.
4. Dr. Raj Krishnaswamy for his support in developing the project.
5. Dr. Songsheng Zhang for his NMR knowledge and the collection of the solution NMR data.
6. Carlosa Roberts-Jackson for her support in the collection of the annealed DSC data.
7. Laura Schlimgen for her support in the collection of the thermal fractionation DSC data.
8. Kent Mueller and Dylan Siebert for the molding and collection of data for the mechanical testing.
9. Steve Yusko and Curt Kugel for the sample compounding work that made the mechanical testing possible.

10. Susan Columbus for her data collection of ethylene content by FTIR for sample validation.
11. Michael Schabowski for his work and support in generating GPC-IR data on branched samples.
12. Dr. Toshi Miyoshi for his solid state NMR knowledge which helped form the initial steps of the project.

The author would like to thank her wife, Faythe, for her continued support and patience during the completion of this thesis and master's program. As well, the author would like to thank her parents for their continued encouragement through undergraduate and graduate school.

1.0 INTRODUCTION

Extensive work has been done throughout the literature to understand the crystal structure of polypropylene[1]. The kinetics of the crystal's macro structures have also been extensively studied[2]. Marigo et al. work showed effects of catalyst on phases and the connection to regio errors which occur when the propylene unit get inserted backwards[3]. De Rosa et al. studied the connection between stereo, caused by methyl units being on opposite planes, and regio defects and crystal structure for metallocene samples[4]. Although much is known about the crystal structure of polypropylene, questions regarding the connection between comonomer defects and branches on crystal structure and the final physical properties remain an area of interest. The goal of this work is to leverage the current knowledge on crystal structure in polypropylene to study the effect of stereo, comonomer and branching in polypropylene. In this work solid state NMR will be used to determine the rigid and mobile interface thickness, as well as the rigid and mobile fractions. The solid state work uses the approach demonstrated by Zhu et al. in the literature[5].

In this thesis, the connections between defects to crystal structure and to the ultimate physical properties of the polypropylene samples will be probed. The defects studied will be stereoregularity defects, comonomer incorporation, and branches. The three types of defects will be probed using four sets of polymer groups. The first set is a group of homopolymer polypropylene with similar melt flow rate but decreasing crystallinity which will be used to

probe the effect of stereoregularity defects. The second and third group will be used to probe the effect of comonomer incorporation on crystallinity. The second group is a set of three random copolymer samples with increasing ethylene incorporated in the chain. A schematic of the homopolymer and random copolymer chains are shown in Figure 1. The third group is a set of three impact copolymer samples with increasing ethylene-propylene rubber fraction. The impact copolymer samples also have increasing ethylene in the rubber fraction over the sample set. A schematic of the macro structure is shown in Figure 2.The final set comprises three polymers, all with the same ethylene content: the first contains zero branching, and the following two branched samples have increasing branching. Figure 3 shows the schematic for a branched sample.

In section 2.0 , the background of the analytical techniques will be discussed. The chemical structure of the polymer was studied by solution state NMR to determine the stereoregularity and ethylene content. Differential scanning calorimetry was used to investigate the percent crystallinity and crystal structure. Both standard annealed DSC, and a thermal fractionation stepwise crystallization (SC) was used. Solid state NMR was used to further investigate the rigid and mobile structure, cross polarization magic angle spinning (CP-MAS) was used to determine the rigid and amorphous fractions and then spin diffusion experiments were used to determine the rigid and mobile interface phase thickness. Dynamic mechanical analysis, tensile, flexure, Izod and instrumented drop impact were all then used to investigate the final physical properties.

The experimental details for all experiments are further discussed in Section 3.0 . Details regarding the analysis methods are all contained in Section 4.0 , which details the process used to calculate crystallinity and lamella thickness using DSC data. The analysis for tacticity and

ethylene incorporation using the solution state NMR is also captured, as well as the fractions calculation and thickness of phases by solid state NMR. Section 5.0 contains all results and discussion of the work with a final conclusion in Section 6.0 .

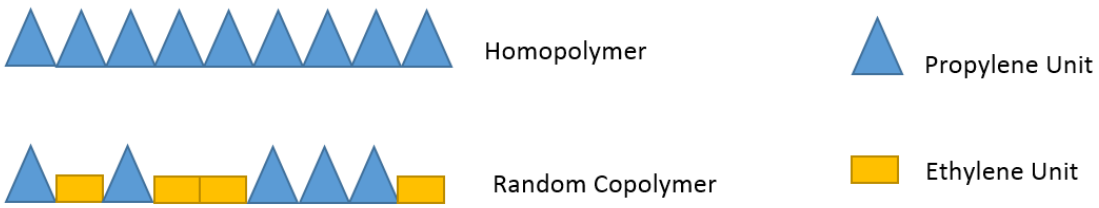

Figure 1.Schematic of Homopolymer Polyproplyene and Propylene Ethylene Random Copolymer

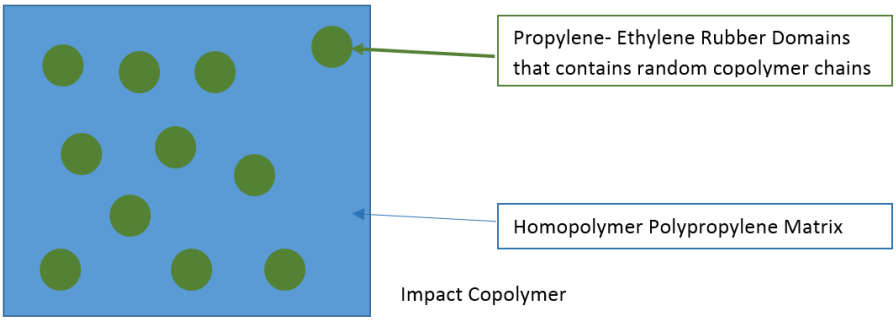

Figure 2. Schematic of Impact Copolymer that Contains a Homopolymer Polypropylene Matrix with Propylene-Ethylene Rubber Domains

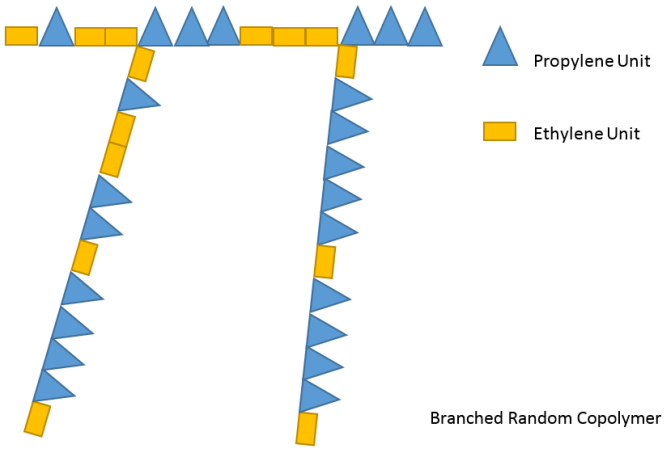

Figure 3. Schematic of Branched Random Copolymer

2.0 BACKGROUND

2.1 TYPES OF POLYPROPYLENE

In the work presented, four major polypropylene groups were tested. The first set of samples were homopolymer which are polypropylene chains that contain nearly zero comonomer. Homopolymer polypropylene (HP) can be used for a number of applications such as nonwovens, housewares, and caps/closures.

Random polypropylene (RP) are samples that contain a comonomer of some kind. Ethylene is the comonomer in all samples in this thesis. The ethylene is dispersed throughout the chain in a statistically random manner. Random polypropylene is often used in film applications due to its improved clarity and flexibility.

Impact copolymer polypropylene (ICP) samples are heterophasic reactor blends which typically contain a homopolymer matrix with propylene-ethylene random copolymer in the form of rubber particles. Impact copolymer polypropylene sample are often used for applications where toughness is important. This can include car bumpers, cold temperature food containers, and toys.

The final group of polypropylene samples studied are branched samples. The samples in this study are random copolymer samples that contain long chain branching in increasing level.

By adding branches, the melt strength of the polymer increases which makes foaming or blow molding applications more effective.

2.2 POLYPROPYLENE CHAIN STRUCTURE

Propylene when polymerized into polypropylene forms chains with methyl groups attached to the backbone. If only propylene is uses as the monomer, methyl groups are usually located on every other carbon in the backbone, giving a chain structure of -CH2-CH(CH3)-CH2-CH(CH3)- due to the polymerization progress. If an error occurs in which the monomer is inserted backwards, two secondary or methylene carbons will appear in a row corresponding to a chain structure such as -CH(CH3)-CH2-CH2-CH(CH3)-. These two structures are shown in

Figure 4 along with the carbon labeling used. This type of backward insertion is called a regio error, regiomistake, 2-1 insertion, or regio defect[6] and can affect the crystallization of the chain. Another more common error seen in polypropylene is called a stereo defect that can reduce the stereoregularity[7]. A stereo defect occurs when the methyl group is on the opposite plane as the nearest neighboring methyl. If the two methyls are on the same side they are labeled as meso and opposite sides are labeled as racemo[8]. NMR can then be used to analyze the pattern in different length segments, such as in groups of three, five, seven, or nine. For the purpose of this work, pentads (7) and triads (3) will be used. For the results shown, groups of fives methyl carbons were used or pentads.

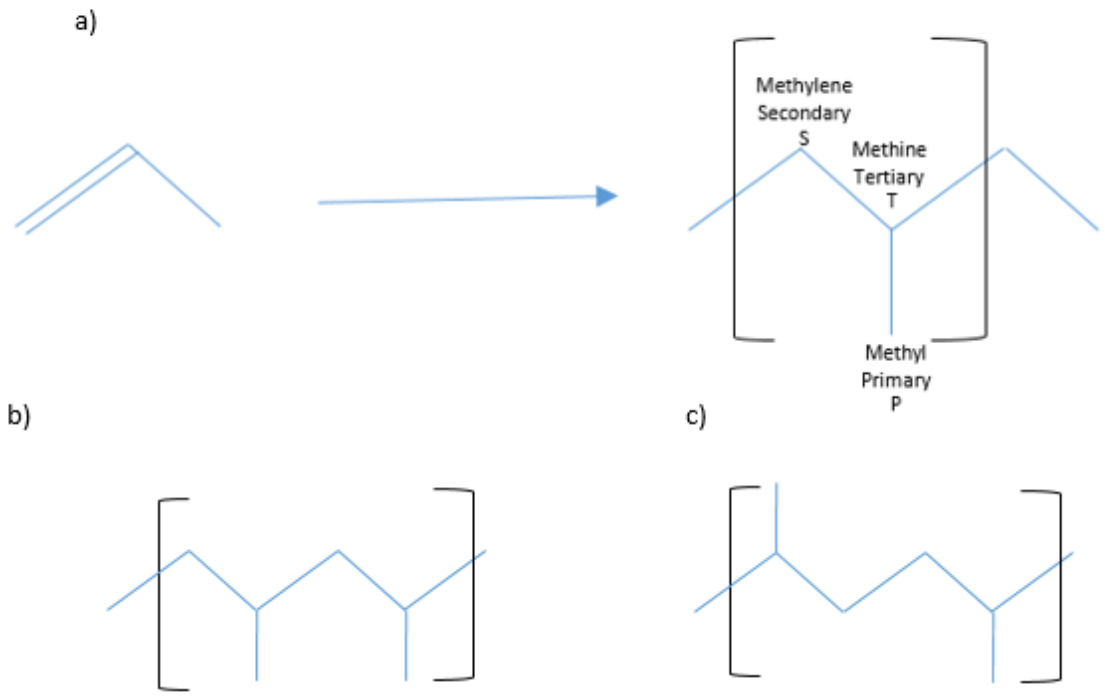

Figure 4. a) Polypropylene Formation Reaction and Carbon Labeling, b) Polyproplene with Noraml 1,2 –Insertion[6], and c) Polypropylene with Regio Error 2,1 – Insertion[6]

2.3 POLYPROPYLENE CRYSTAL STRUCTURE MODEL

Polypropylene chains crystallize into lamellae which are stacks of folded chains. A single chain may fold multiple times inside a given lamella. The chains may also crystalize in multiple adjacent lamellae; chains participating in multiple lamellae are called tie chains[9]. These lamellae often arrange further into macro structures like spherulites[10,11]. In semi-crystalline polymers, these spherulites can range from 3 to 500 um and are made up of crystalline lamellae that are 8 to

20 nm thick[12]. Between the stacked lamellae is an amorphous layer that cannot crystalize due to limited flexibility from being pinned between the lamella, or from defects in the chain making crystallization highly unfavorable. The thickness of the crystalline lamella (lc) and the amorphous interface (la) will be investigated in this work. A representation of the lamella and amorphous interface is shown in Figure 5.

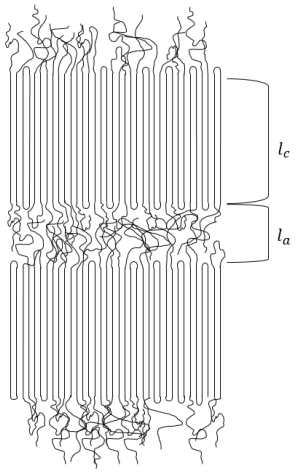

Figure 5. Polypropylene Crystal Lamella and Amorphous Interface Model

The amorphous interface contains defects, entangled chains, tie chains, and branches[13]. The amorphous phase deforms during the elastic deformation before the yield point[13]. More amorphous content would therefore lead to a lowering of elastic moduli. Sometimes this trend appears as a linear relationship between elastic modulus and percent crystallinity, although deviations can be found if samples with varying lamella thicknesses are selected. The elastic modulus depends on the balance of amorphous and crystalline as well as the lamella structure and its orientation[14]. The amorphous interface size controls the cavitation of the polymer during strain since the voids are typically formed in the amorphous interface and the size of voids are on

the size order of the amorphous inferface[15]. This highlights the importance of the amorphous thickness since the size of a crack or cavitation can predict whether it will cause a failure at a given stress, with larger cracks failing first. Small voids in the amorphous interphase have also been shown to heal[15].

The crystalline lamellar thickness also plays an important role in the yield stress: as the lamella thickness increase so does the yield stress of the sample[14]. Crystalline lamella thickness also determines the content of tie chains if molecular weight is kept constant. By having thinner crystalline lamella, the chances for a chain to crystallize in multiple lamella increase. This increase in tie chains has been shown to increase dart impact strength[16].

2.4 ANALYTICAL AND MECHANICAL TESTING

2.4.1 Solution State Nuclear Magnetic Resonance

For solution state NMR, a polymer sample is first dissolved in a deuterated solvent and placed in a NMR tube. It is important to heat the sample and fully homogenize it before analysis. For the solution state samples done for this project, the NMR active C^{13} nuclei was used[17].

A NMR spinner is used to hold the NMR tube and is placed in the magnet. A constant stream of air is used to suspend the sample inside the probe. The magnetic field is homogenized by "shimming" the magnet using the deuterated signal. The sample is then "tuned" which allows the exact irradiation frequency to be chosen which can vary slightly with solvent, but falls within the carbon range[17].

Once the instrument has been optimized, a pulse program is applied. The pulse program used was a ZGPG, 90 degree pulse power gated carbon-proton with waltz16 decoupling scheme, with an 4-10 sec delay. During the pulse, the C^{13} nuclei absorb energy and then release it after the pulse. The instrument records the signal from the release which decreases over time. The signal is then converted with a Fourier transformation to appear as the typical spectrum. The x axis is frequency and y is intensity. The frequency is determined by the chemical shift of certain types of C^{13} nuclei found in the sample. The tacticity is then determined by calculating the percent of each pentad in the sample. In addition, for copolymer samples, the ethylene insertion was calculated[17].

2.4.2 Solid State Nuclear Magnetic Resonance

When samples are in the solid state, the molecules no longer have the fast rotational motion that allows quadrupolar and dipole-dipole interactions to be averaged out. Due to these interactions, solid state spectra give very broad signals, but can be improved by a number of techniques. Cross polarization (CP) allows the higher population of H^1 nuclei to be leveraged. The pulse is transferred form the H^1 to the C^{13} and thereby allowing a better signal to be observed due to the higher population of the H^1 opposed to the C^{13}.The delay between pulses can also be shortened due to the faster relaxation of the proton. Magic angle spinning (MAS) can also be used, where the sample is spun at an angle of 55.44° which allows the internuclear interactions to be zeroed out giving a spectrum more similar to a solution state experiment[17].

The benefit of solid state experiments is that they allow the separation of the rigid and mobile components, thereby allowing a better calculation of the rigid and mobile fractions. Two CP-MAS experiments have been done for each sample, one with a spin lock and one without.

The spin lock allows only the slow relaxing rigid crystalline component to be captured. Without the spin lock, both mobile amorphous and rigid crystalline components are collected. The two spectra can be subtracted to determine the spectrum for the mobile component only. Proton spin diffusion experiments with dipolar filter can then be used to determine the thickness of the mobile or amorphous interface[5,9, and 18].

2.4.3 Differential Scanning Calorimetry

Differential Scanning Calorimetry is a technique in which the thermal properties of a sample can be characterized. Inside the DSC oven, an empty reference pan and a sample pan are both heated using customized methods. The difference in energy needed to heat the sample at the prescribed rate between the reference pan and sample pan are measured. The thermal transitions (melting, crystallization, and glass transition) can all be detected due to the sink or source of the energy for the sample. For the annealed method, samples are heated well over the melting temperature before the measurement begins. For the thermal fractionation method the sample is first annealed, and then cooled slowly to ensure that all chains that can crystalize at a given temperature actually crystallize. The thermal fractionation method is denoted as a stepwise crystallization (SC) approach[19].

2.4.4 Dynamic Mechanical Analysis

Dynamic Mechanical Analysis allows the probing of the balance of viscous and elastic properties of the polymer in the solid or molten state. The instrument applies a sinusoidal displacement and the resulting sinusoidal force is tracked. The phase shift between the force and displacement is

called the phase lag, and is related to the viscoelasticity of the material. The complex modulus is determined by dividing the maximum of each wave force by the maximum of the displacement and multiplying that by a geometric factor. The geometric factor is clamp and sample specific. The storage modulus is then calculated by taking the complex modulus and multiplying it by the cosine of the phase angle. The loss modulus is similarly calculated by taking the complex modulus and multiplying it by the sine of the phase angle. The tan delta is the ratio of loss modulus divided by storage modulus or can be calculated by taking the tan of the phase lag[20].

2.4.5 Tensile

Following ASTM D638, the tensile bar is stretched at a constant strain rate of 2.0 in/min and the resulting stress is measured. The stress and strain is then plotted allowing the points of interest to be viewed, an example plot is shown in Figure 6. The break strain and stress are the graph values at the point where the tensile bar breaks. The yield strain and stress are determined from reading the graph values from the yield point. The yield point is the point where increases in strain does not increase the stress at the same rate as when the sample was elastically deforming. The tangent modulus and 1% secant modulus are both slopes of the linear region of the graph. The 1% secant modulus is less sensitive to any noise in the low strain region of the graph since noise is removed by taking the slope between the origin and 1% strain value. The tangent is simply the tangent of the linear region of the graph. The two modulus values are shown in Figure 7.

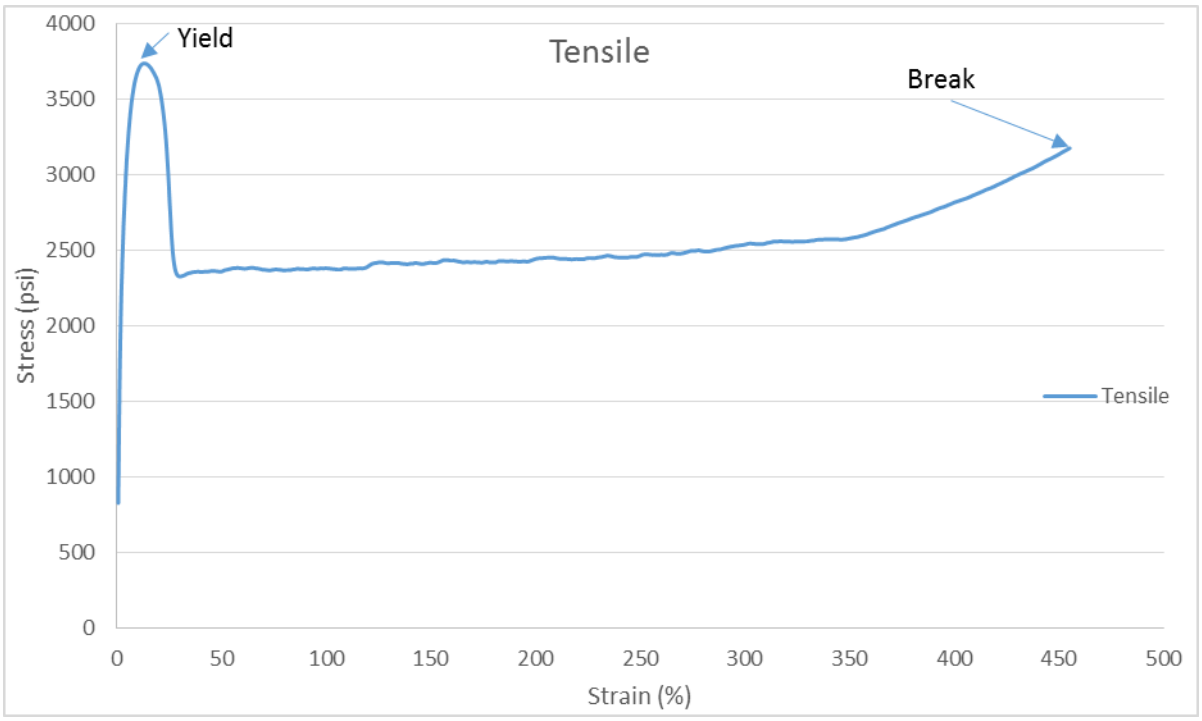

Figure 6. Tensile Stress Strain Example Curve with Yield and Break Labeled

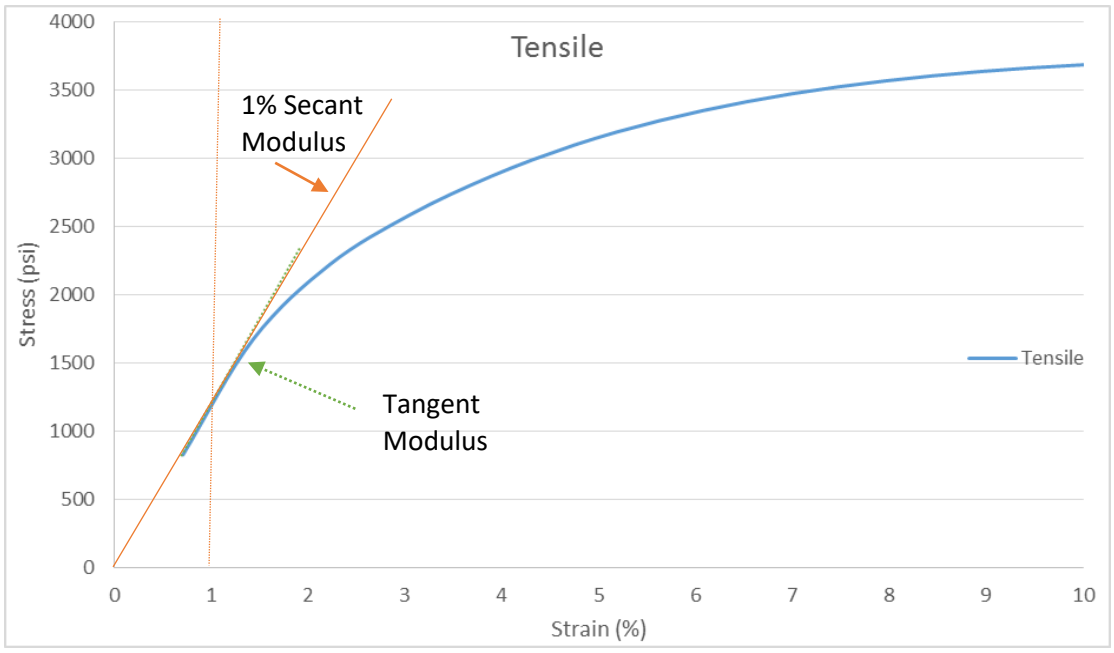

Figure 7. Tensile Stress Strain Example Curve with 2% Secant and Tangent Modulus Labeled

2.4.6 Flex

A three-point bend fixture is used on the same bar type as the tensile test following ASTM D790. Similarly to the tensile test, a constant strain rate is applied and the resulting stress is recorded. The strain rate used is 0.05 in/min. Again the stress strain curve is plotted which allows the modulus values to be calculated[22].

2.4.7 Izod Impact

The inner area of the tensile bar is cut out and notched using an Izod notcher. Test method ASTM D256 is used. The sample is mounted in a clamp with the notch facing the area of impact for the swing arm. The swinging arm is released and hits the sample. The arm continues to swing and the height is recorded to calculate the energy that was absorbed by the sample, given the fact that the initial potential energy of the arm is equal for all runs. The break type is classified as complete, hinge, partial, or non-break and the break strength is recorded[23].

2.4.8 Instrumented Drop Impact

For the instrumented drop impact testing (IDI), 3.175 mm thick round plaques are used following ASTM D3763. The test measures the puncture energy. The plunger travels at 2.73m/s hitting the sample. The maximum load is the peak of the graph, a single sample with multiple test specimens shown in Figure 8. The instrument also measures the plunger position. The energy at maximum load is then calculated by multiply the deflection by the load[24].

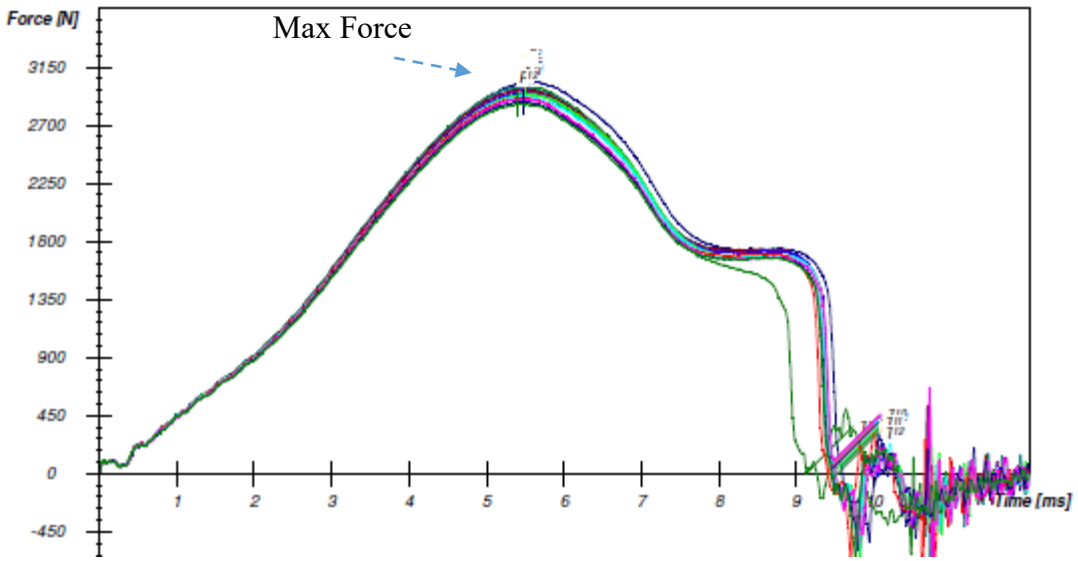

Figure 8. Instrumented Drop Impact Graph Showing Force (N) and Time (ms)

3.0 EXPERIMENTAL

3.1 SAMPLES STUDIED

In order to cover all areas of interest in polypropylene, four groups of samples were studied homopolymer, random, impact copolymer, and branched samples. Three homopolymer polypropylene samples were chosen for the study. The homopolymer samples are labeled as HP1, HP2, and HP3 going forth. The homopolymer samples have decreasing crystallinity from sample HP1 to HP3. Another set of three propylene ethylene random copolymers were chosen and are labeled as RP1, RP2, and RP3. The random samples have both decreasing crystallinity and increasing ethylene as you move from sample RP1 to RP3. Three impact propylene-ethylene copolymers were selected and are labeled at ICP1, ICP2, and ICP3. The crystallinity of the impact copolymer samples decrease from the ICP1 to ICP3 samples. The amount of rubber in the impact copolymer samples increases in the sample direction for ICP1 to ICP3 and the rubber becomes more ethylene rich(increasing levels of comonomer content). For the branched group, two branched propylene ethylene copolymer samples were selected, as well as, a reference unbranched random propylene ethylene copolymer sample. The set is labeled as BR1, BR2 and BR0 with the last being the unbranched reference. The two branched samples were provided as pellets and all other samples were provided in the form of powder. The level of branching

increases from BR1 to BR2. The crystallinity and ethylene content is constant across the branched set. The full sample set was provided by Braskem and are show in Table 1.

Table 1. Sample Description Key

Sample	Code	Type	MFR^	Crystallinity◊	Ethylene Content ○ (wt. %)	Rubber Content●	Ethylene Content in Rubber‡	LCB/1000C*	Branched	Type
1	HP1	HP	2.6	64.5	0	0	0	0.000	No	Powder
2	HP2	HP	1.9	61.6	0	0	0	0.000	No	Powder
3	HP3	HP	2.6	59.7	0	0	0	0.000	No	Powder
4	RP1	RP	1.5	36.4	2.6	0	0	0.000	No	Powder
5	RP2	RP	5.5	35.4	3	0	0	0.000	No	Powder
6	RP3	RP	3.7	27.1	5	0	0	0.000	No	Powder
7	ICP1	ICP	4.1	48.1	4.8	11	46	0.000	No	Powder
8	ICP2	ICP	2.3	42.6	11.6	19	48	0.000	No	Powder
9	ICP3	ICP	6.8	36.6	15.6	27	51	0.000	No	Powder
10	Br0	Branched	33.6	38.2	2.7	0	0	0.000	No	Powder
11	Br1	Branched	18	38.2	2.7	0	0	0.008	Yes	Pellet
12	Br2	Branched	5.4	37.6	2.7	0	0	0.011	Yes	Pellet

◊ Value determined by DSC

○ Value determined by NMR

●‡ Value determined by FTIR

*GPC-IR IV Detector

^ MFR (Melt Flow Rate)

3.2 SAMPLE PREPARATION-EXTRUSION

The powder samples were stabilized with a basic additive package of 750 ppm of primary antioxidant, 750 ppm of secondary antioxidant, and 500 ppm acid scavenger. The powder and additives were initially blended and then fed into a 30 mm twin screw extruder. The zone temperatures of the extruder were set based on the melt flow of the individual powder samples. The zone temperature and recorded extrusion data is shown in Table 2.

Table 2. Extrusion Parameters and Data

	Set (•C)	HP1	HP2	HP3	RP1	RP2	RP3	ICP1	ICP2	ICP3	Set (•C)	Br0
TEMPERATURE												
ZONE 1 (Feed Throat)	140	165	148	141	134	140	140	145	138	140	140	134
ZONE 2	180	179	183	176	178	176	179	181	181	173	180	173
ZONE 3	210	204	205	202	206	202	202	203	211	201	200	185
ZONE 4	210	223	209	207	214	208	207	212	216	204	200	195
ZONE 5 (Extruder Outlet)	210	221	210	209	215	211	211	213	217	208	200	197
ZONE 6 (Melt Pump)	210	210	210	210	210	210	210	210	211	210	200	200
ZONE 7 (Screen Changer)	210	209	210	210	210	210	210	210	210	210	200	200
ZONE 8 (Die)	210	210	210	210	210	210	210	210	210	210	200	200
Extruder												
RPM		250	250	250	250	250	250	250	250	250		250
% TORQUE		90	87	95	93	79	89	95	94	81		69
Pressure		281	300	288	378	266	280	230	281	183		114
MELT TEMP (•C)		228	224	224	226	222	223	224	227	221		208
SME		0.0908	0.0786	0.0996	0.0950	0.0678	0.0720	0.0974	0.0997	0.0742		0.0537
Melt Pump												
RPM		31.9	30.4	33.8	34.0	34.4	34.0	35.0	33.0	33.2		33.9
Amps		1.9	1.9	2.0	2.0	1.9	1.9	1.9	1.9	1.9		1.9
Suction Pressure		253	236	214	250	231	240	250	240	231		253
Discharge Pressure		733	809	809	1040	674	670	701	826	585		354
FEEDER												
Gravimetric lb./hr.		60.0	60.0	60.0	60.0	60.0	60.0	60.0	60.0	60.0		60.0
% Motor Speed		82.0	90.0	66.0	60.0	58.0	66.0	59.0	56.0	62.0		82.0
Melt Flow g/10min		2.6	1.9	2.6	1.5	5.5	3.7	4.1	2.3	6.8		33.6

3.3 SOLUTION STATE NMR

The solution state NMR samples were prepared by first using a hot press to melt a thin film. The film was then cut to an area corresponding to roughly 60-65 mg mass. The film was then curled

into a cylinder and dropped down into the 5 mm NMR tube. The tube was then blanketed with a constant flow of nitrogen. After letting the nitrogen flow for 5 minutes, 0.6 ml of a 50/50 blend of 1,1,2,2-Tetrachloroethane-d2(TCE-d_2) and 1,2,4-Trichlorobenzene (TCB) was added while the nitrogen flow remained. The nitrogen tube was raised to the top of the tube to stop splashing during the filling process. A needle was inserted around the side of the nitrogen tube allowing a constant blanket during filling. The sample was left under the blanket for another 5 minutes to purge and then the sample was capped while the nitrogen flow was left on.

The NMR sample tube was then heated to ~ 130 ^{o} C using a sample heating block. After the sample has been heated for an hour, a hot gun was used to boil the TCE and TCB solvent in the sample and allow the solution to be mixed inside the tube. The sample solvent surface was first heated with the hot gun to ensure that the polymer was not acting as a cap inside the tube. The sample tube was then heated at the bottom up to fully mix the sample. Once the sample was free of gels and fully heated the sample was run.

The NMR experiment was performed at 120 ˚C on a Bruker 500 MHz instrument using a 5mm BBO probe. The homopolymer set were tested with a 4 second delay time (d1) and the copolymers were tested with 8 second delay time. The tests were done using a "ZGPG" power gated carbon-proton with a 16 waltz decoupling scheme program. Around 2,000-5,000 scans were collected for each sample. The chemical shifts were referenced using the center of the central peak of the solvent at 73.80 ppm.

3.4 SOLID STATE NMR

The solid state nuclear magnetic experiments were done using a Bruker 500 Wide Bore spectrometer with a 4 mm probe. Pellet samples were converted into a powder using a cryo-grinder and then packed into the spinner. The mobile amorphous and rigid crystalline fractions were determined using two CP-MAS programs, one without spin lock and the other with spin lock at 8 um. The collection with spin lock allowed the collection of only the crystalline phase. The magic angle spinning (MAS) was set to 4000 Hz and a 90 pulse was applied for 4.5 us. The recycle delay was set to 2 seconds with a 1 ms cross-polarization. Proton two pulse phase modulation (TPPM) decoupling at 100 kHz was used for the 120 ms acquisition time. The proton spin-lattice relaxation time was 8 ms at a field strength of 62.5 kHz. The approach is the same as done in Kang[18].

For the spin diffusion experiment, the spin diffusion filter was optimized to suppress the crystalline fraction. The purpose of the spin diffusion experiment is to polarize only the mobile fraction and then measure the transfer of polarization to the crystalline phase, thereby allowing the physical spacing between the mobile and crystalline fraction to be detected. The 1H spin diffusion pulse program used contained 12 dipolar pulse filters(x,-y,x,x,-y,x,-x,y,-x,-x,y,-x) with spin diffusion delay of tau between each pulse. Tau of 25 us was used for the sample set. The 12 pulses were repeated 2 times to provide the best polarization followed by a pair of 90° pulses. A varying mixing time from 0- 2500 ms was used before the cross polarization was applied for 0.5 ms with a recycle time of 2 seconds[5, 19]. A proton spectrum was also collected with and without the filter in order to calculate the diffusion coefficients.

3.5 DIFFERENTIAL SCANNING CALORIMETRY ANNEALED

The extruded stabilized samples were also used in the annealed DSC experiment. The pellets were initially molded into a 0.2 mm thick film. A cylindrical disk punch was then used to cut out 6-11 mg of material that was then loaded and sealed inside of a "tzero" type DSC pans using tzero lids. The pan was then heated along with a standard empty pan/lid to 200 ˚C and held for 5 minutes. The sample was then rapidly cooled down to 45 ˚C at a rate of 10 ˚C /min. The sample then equilibrated to 0˚C and was heated back to 200 ˚C at a rate of 15 ˚C /min.

3.6 ANNEALED DSC THERMAL FRACTIONATION

The same prepared film for the annealed DSC experiment was also used in the thermal fractionation experiment. A new section was cut out using the cylindrical disk punch and sealed inside of a tzero DSC pan with a tzero lid. The sample was again loaded with a reference empty pan/lid and heated to 200 ˚C and held for 240 minutes. The sample was then cooled 10 degrees at a rate of 10 ˚C /min, held for another 240 minutes at 190 ˚C and then ramped down by another 10 degrees. The downward steps and holds are repeated until the sample reaches 100 ˚C. The graph in Figure 9 shows the full method which takes around 45 hours for one sample. Even after such a long heating, degradation of the samples is not expected since the stabilized pellets were used to produce the films. After the crystals have been fully formed, a standard ramp up from 100˚C to 200 ˚C at a rate of 10 ˚C /min was used to collect the melt peak which ultimately used for the calculations.

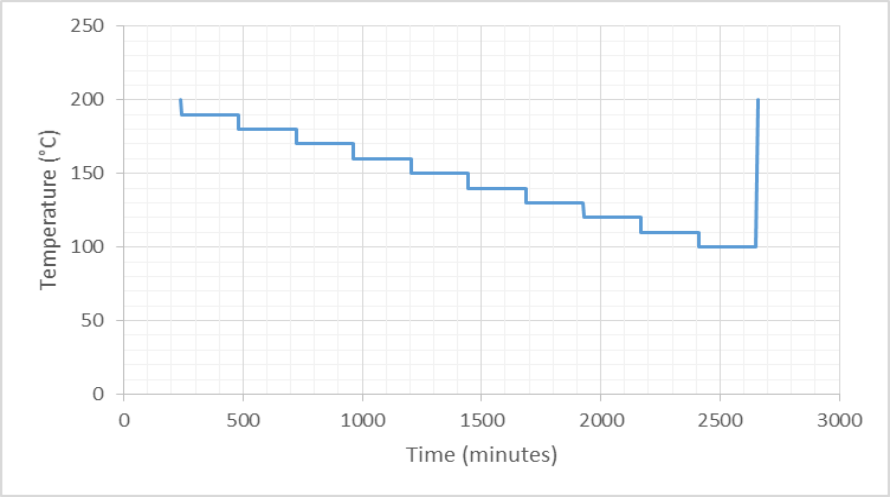

Figure 9. Temperature (◦C) versus Time (minutes) for Annealed Thermal Fractionation Method

3.7 DYNAMIC MECHANICAL ANALYSIS

The impact copolymer samples were initially melt mixed by using a hot press for repeatedly melting, cutting, restacking the film, and melting again until the samples each became homogenous and clarity differences across the film disappeared. After the initial melt mixing of the impact copolymer samples, all samples were handled identically for dynamic mechanical analysis (DMA) preparation. For the DMA samples, powder without antioxidants was used so some degradation is possible.

A mold (7.5 cm x 7.5 cm x 1.5 mm) was filled with the sample and then pressed between two aluminum sheets and further sandwiched by two platens. The platens and sample stack was then placed into the hot press set to 204 °C. Initially the sample was held for 2 minutes with only surface contact and no additional pressure to the top surface. The pressure was then raised to 12 metric tons and quickly released back down to zero. This process of increasing and dropping

pressure was repeated four times in order to ensure all bubbles and voids were removed from the sample. The pressure was then raised once more to 12 metric tons and held for 2 minutes. The stack was then moved to a chilled press that was set at 15 °C and held for another 2 minutes at 12 metric tons. The samples were then removed from the mold. A shear cutter was used to cut the samples into bars with the approximate dimensions of 1.5 mm X 13.68 mm X 35.64 mm. The bars were then aged at room temperature for 40 hours before testing.

Dynamic mechanical analysis was conducted on a TA instruments Q800 DMA. The testing was done using a single cantilever clamp in DMA Multi-Frequency- Strain mode with the Temp Ramp/ Freq Sweep test type. The samples were initially cooled to -70 °C and then the clamp screws were tightened with a torque controlled screw driving set at 8 lb. /in. The DMA temperature sweeps were done from -70 °C to 150 °C at a heating rate of 3 °C/min after an initial 5 minute soak time at -70°C. The amplitude was set to 30 um.

3.8 MECHANICAL TESTING

3.8.1 Sample Preparation-Molding

Two Cincinnati molders were used to make the tensile bars and impact disks. A standard ASTM tensile bar was prepared for the tensile, flex, and Izod testing. The molding parameters for the two specimens followed the ASTM D4101 and used stabilized extruded pellets referenced in Section 3.2.

3.8.2 Mechanical Testing Procedures

The tensile and impact specimens were aged for the required 40 hours after molding and then tested within 96 hours. An MTS 2GL was used to perform the tensile test using ASTM D638. The tensile jaw separation was set to 4.5 in with a load cell of 562 lbf. was used. The tensile testing speed was set to 2 in/min. The testing was performed until break or until the crosshead reached its maximum displacement. The flex testing was performed on an MTS 10GL unit following ASTM D790. The flex testing was conducted with a 100 lbf. load cell at a test speed of 0.05 in/min and a span distance of 2 in. Izod specimens were taken from the center of the tensile bar and an izod notch cutter was used to prepare the bar. The izod testing was run on a Tinius Olsen Impact 104 unit using ASTM D256. For the instrumented drop impact, 125 mil thick round plaques were molded. The instrumented drop impact was performed on a Ceast Fractovis unit using ASTM D3763. All mechanical testing was conducted at room temperature.

4.0 METHODOLOGIES OF ANALYSIS

4.1 TACTICITY DETERMINATION BY SOLUTION STATE NMR

The samples were analyzed for tacticity by integrating the peaks between 22-19 ppm which is the methyl area of the spectrum. The pentad structures are shown in Figure 10 and the respective peaks are shown in Figure 11 and were calculated for pentads. The methyl carbon observed by the NMR is indicated with a *. If the two nearest neighboring methyl carbons on either side of the starred methyl are on the same side, those carbons are considered meso(m). If a flip occurs with the methyl unit, that methyl is considered raceme(r)[8]. The next methyl is then considered based on its orientation to the last referenced methyl. The peak areas then become pentad mole fractions by dividing by the total area of the nine peaks. The triads (mm%, mr% and rr%) were then calculated using Equation 4-1, Equation 4-2, and Equation 4-3[25,8].

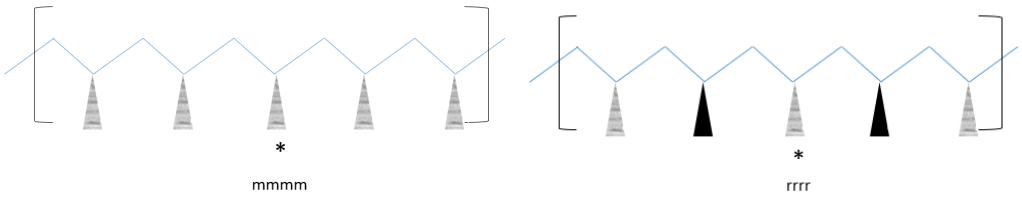

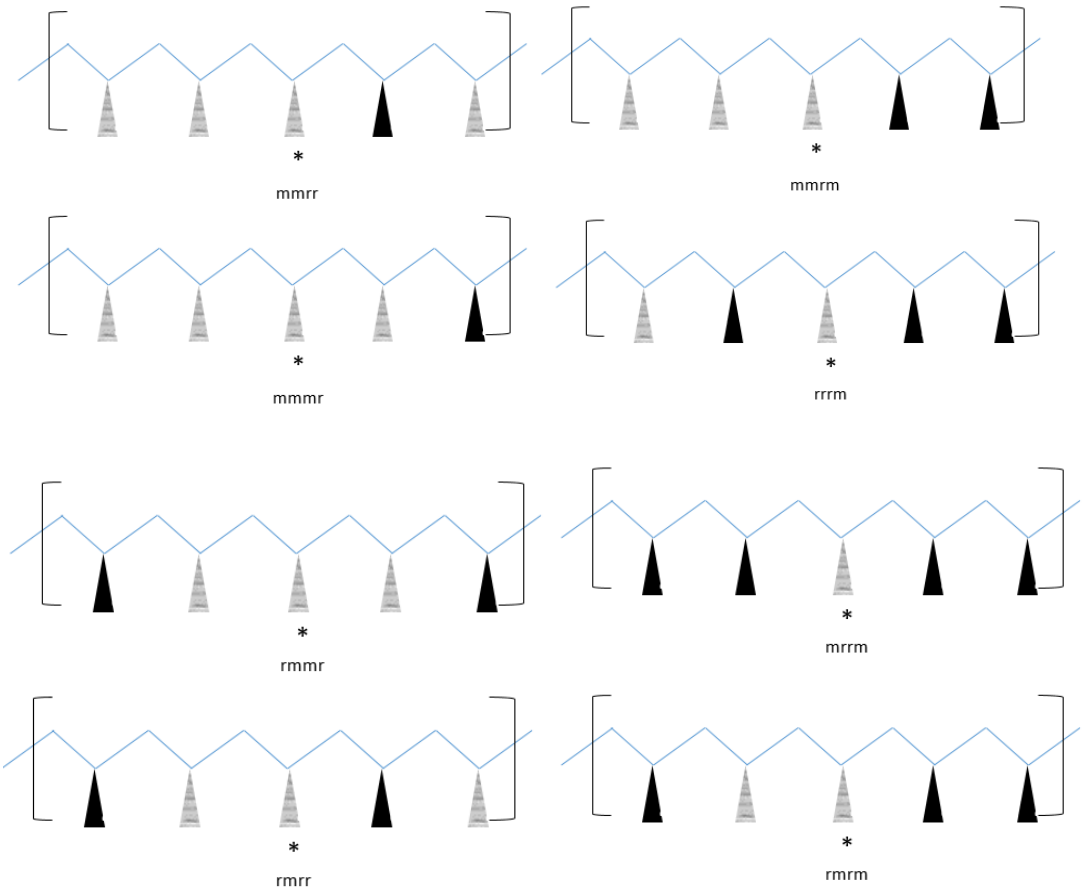

Figure 10. Polypropylene Pentad Structures

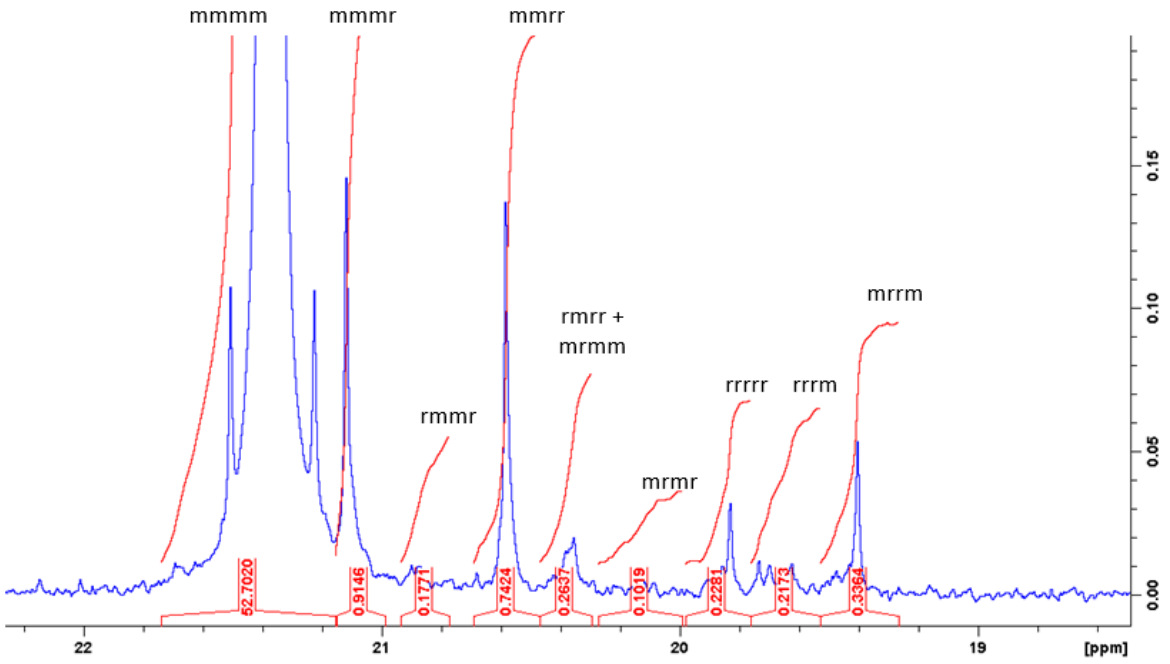

Figure 11. Tacticity Peaks[2, 3]

$$\text{mm(mole\%)} = \text{mmmm(mole\%)} + \text{mmmr(mole\%)} + \text{rmmr (mole\%)} \qquad \text{Equation 4-1}$$

$$\text{mr(mole\%)} = \text{mmrr(mole\%)} + \text{rmrr,mmrm(mole\%)} + \text{mrmr(mole\%)} \qquad \text{Equation 4-2}$$

$$\text{rr(mole\%)} = \text{rrrr(mole\%)} + \text{rrrm(mole\%)} + \text{mrrm (mole\%)} \qquad \text{Equation 4-3}$$

4.2 ETHYLENE INCORPORATION FOR IMPACT AND RANDOM BY SOLUTION STATE NMR

The ethylene incorporation for the copolymer samples (random, impact, and branched) was determined by first analyzing the spectrum in the secondary and tertiary carbon region. The peaks listed in Table 3 were integrated[26]. The dyads (two monomer units) and triads (three monomer units) areas are then converted to mole percent by dividing the signal intensity of each dyad type (PP, PE, and EE) over the total of all dyad signals. The same approach is used for triads[25, 26]. The dyad and triad structures are shown in Figure 12 and Figure 13.

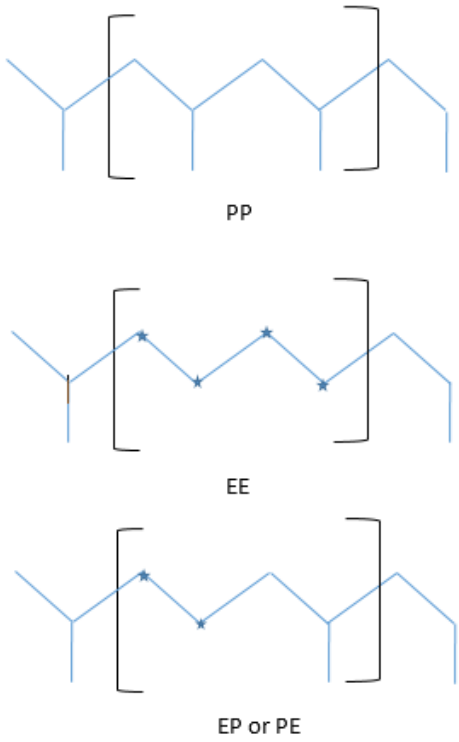

Figure 12. Dyad Ethylene- Propylene Copolymer Structure

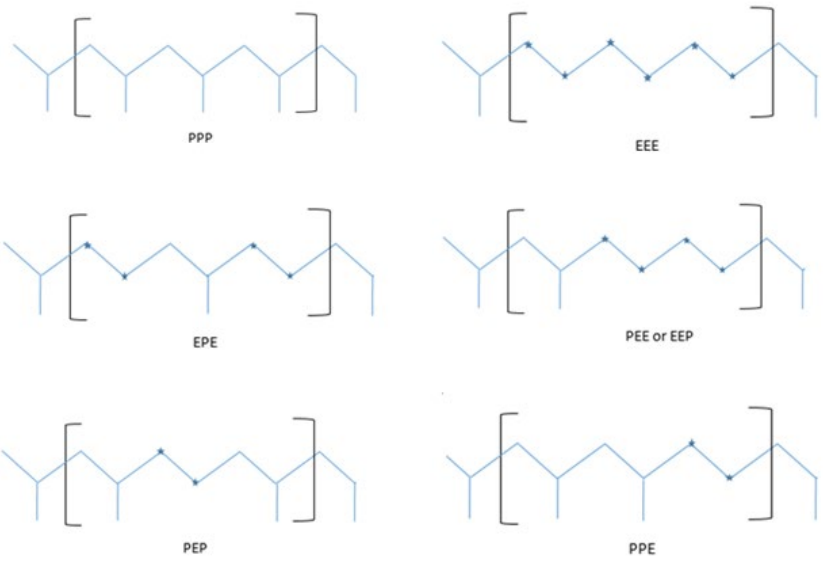

Figure 13. Triad Ethylene- Propylene Structures

Table 3. NMR Dyads and Triads[26]

Dyads	Peak Integration Area (ppm)
PP	47 to 45
PE	37.7 to 37.2 + 37.19 to 36.73
EE	1/2 26.9 to 26.60 + 1/2 29.50 to 29. 2 + 1/4 29.8 to 29.7
Triads	Peak Integration Area (ppm)
PPP	28.8 to 27.9
PPE	30.6 to 30.4
EPE	32.8 to 32.6
EEE	1/2 29.5 to 29.2 + 1/4 29.8 to 29.7
PEE	1/2 37.2 to 36.7 + 1/2 26.9 to 26.6
PEP	1/2 37.7 to 37.2

The percent moles of P and E were calculated by Equation 4-4 and Equation 4-5. The percent moles can be converted into weight percent by using the molecular weight of an ethylene and propylene unit.

$$P\ mole\% = PP\ mole\% + \tfrac{1}{2}\ PE\ mole\% \qquad \text{Equation 4-4}$$

$$E\ mole\% = EE\ mole\% + \tfrac{1}{2}\ PE\ mole\% \qquad \text{Equation 4-5}$$

The normalized triad calculations are shown in Table 4.

Table 4. Triads in Propylene or Ethylene[25, 26]

Triads in Propylene or Ethylene %	Using Calculated mole% values
PPP/P	PPP/(PPP+PPE+EPE)
PPE/P	PPE/(PPP+PPE+EPE)
EPE/P	EPE/(PPP+PPE+EPE)
EEE/E	EEE/(EEE+PEE+PEP)
PEE/E	PEE/(EEE+PEE+PEP)
PEP/E	PEP/(EEE+PEE+PEP)

4.3 RIGID AND SOFT FRACTION DETERMINATION BY SOLID STATE NMR

The two CPMAS solid state spectrums were used to determine the rigid crystalline and mobile amorphous components. The CPMAS spectrum with the spin lock at 8 um contained only the signal from the rigid crystalline sample, whereas, the other spectrum contained both the rigid crystalline and mobile amorphous components. By subtracting the rigid crystalline spectrum

from the total, the mobile amorphous spectrum was generated. The ratio of area of rigid crystalline to the area of the total was used to determine the rigid crystalline fraction[19]. Since the mobility is being measured and not a thermal transition, the rigid crystalline fraction determined by solid state NMR will be referred to as the rigid percent and the crystalline fraction determined by DSC will be referred to as the crystalline percent or crystallinity. The spin lock allows fast relaxing mobile amorphous signal to be removed. If branching was added to the sample in the amorphous domain, the relaxation might slow enough to appear to be part of the crystalline component. Since only relaxation rate is observed and no thermal changes are measured in the process the crystalline component is measured by observing the rigid fraction.

4.4 DOMAIN THICKNESS DETERMINATION FOR SOFT AND RIGID FRACTIONS BY SOLID STATE NMR

The thickness of the soft or mobile phase and the rigid phase was calculated using the spin diffusion solid state NMR experiments using the method done in Zhu et al and Kang[5, 19]. Initially the diffusion coefficient for the rigid fraction, D_r, was calculated using Equation 4-6 where $<r^2>$, the mean square distance between closest spins, is set to 0.08nm^2. The same spectrum was also used to determine width at half height, $\Delta\nu^r_{1/2}$.

$$D_r = \frac{1}{12}\left(\frac{\pi}{2ln2}\right)^{1/2} < r^2 > \Delta\nu^r_{1/2}$$

Equation 4-6[5]

The diffusion coefficient for the mobile or soft component, D_m, was then calculated using Equation 4-7 where $\Delta\nu^m_{1/2}$ is the width at half height of the mobile amorphous proton spectrum generated after subtracting the rigid crystalline components from the total proton spectrum and α is the width at the bottom of the peak.

$$D_m = \frac{1}{6} < r^2 > \left[\alpha \Delta \nu^m_{\frac{1}{2}}\right]^{1/2}$$

Equation 4-7[5]

Both diffusion coefficients were then used to calculate the $D_{eff,}$ shown in Equation 4-8.

$$\sqrt{D_{eff}} = \frac{2\sqrt{D_m}\sqrt{D_r}}{\sqrt{D_m} + \sqrt{D_r}}$$

Equation 4-8[5]

The intensity from the spin diffusion experiment was normalized by dividing the intensity of the experiment with the same mixing time but no spin diffusion. The intensity of the peak at 23 ppm was used since it was the largest and only clearly visible peak at the low mixing times. The normalized intensity was then plotted against $t_m^{1/2}$. The $t_{m0}^{1/2}$ value is then determined from the intersection of the initial linear slope and steady state value, shown in Figure 14. Due to the limited number of points used in the determination of the initial slope, sensitivity of the results calculated from the graph will be discussed in Section 5.2.2.The thickness of the rigid and mobile phases are then determined using Equation 4-9 and Equation 4-10, where ε is 1, since a lamella structure was assumed. The thickness of the mobile component (d_m) can then be determined using the rigid or crystalline fraction information obtained for solid state NMR. The rigid thickness will later be compared to the crystalline lamella thickness measured by DSC.

Both tests probe the same physical component but the approach shifts the observance limitations. The mobile thickness will similarly be compared to the amorphous phase thickness measured by DSC.

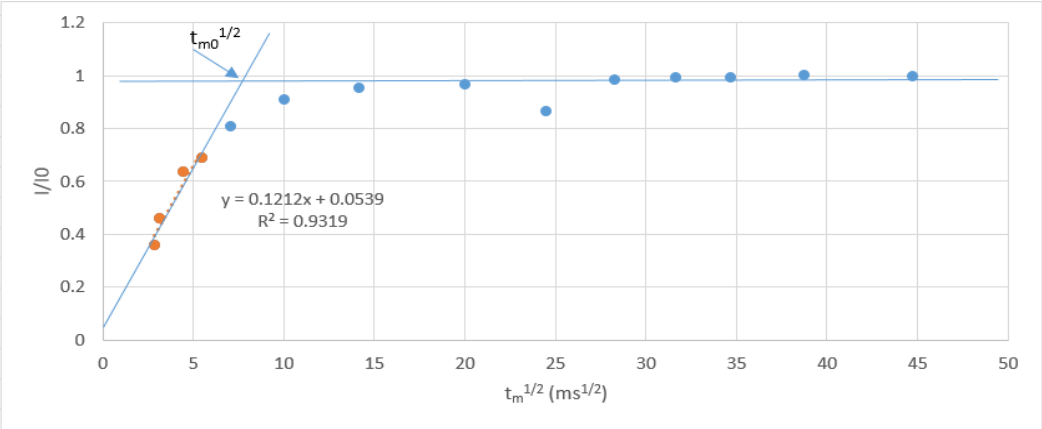

Figure 14. Plot of tm1/2 and I/I0

$$d_r = \frac{2\epsilon}{f_{am}}\sqrt{D_{eff}t_{m_0}/\pi}$$

Equation 4-9[19]

$$d_m = \frac{2\epsilon}{f_{cry}}\sqrt{D_{eff}t_{m_0}/\pi}$$

Equation 4-10[19]

4.5 CRYSTALLINITY ANALYSIS BY ANNEALED DSC

The annealed DSC data was analyzed by first integrating the melting and crystallization peaks. The melting peak was linearly integrated from 90 ˚C to 180 ˚C. The crystallization peak was

similar integrated but a constant spacing of 40° was used instead of an absolute range. The crystallinity was then calculated using Equation 4-11[27, 28].

$$X_c\,(\%) = \frac{\Delta Hf}{\Delta Hf_o}$$

Equation 4-11

The heat of fusion was taken from the integrated value for the melting peak. The hypothetical heat of fusion for a fully crystalline sample ΔHf_o was taken to be 165 J/g[18] or 207 J/g[29], the first being for homopolymer polypropylene and the second for copolymers of propylene and ethylene due to the enthalpy differences seen for a perfect polyethylene crystal and a perfect polypropylene crystal.

The Thomson-Gibbs equation was then used to calculate the lamella crystal thickness l_c, which is shown in Equation 4-12, where σ_e is the free energy of the folding lamella (0.122 J/m^2)[19], ρ_c is the density of the crystal (936 kg/m^3) [19], ΔH_f^o is the heat of fusion for isotactic polypropylene (165 J/g)[28], and T_m^o is the equilibrium melting point(481K) [19]. T_m was taken as the peak maximum in the anealed DSC melting peak.

$$T_m = T_m^o\left(1 - \frac{2\sigma_e}{\rho_c \Delta H_m^o \ell_c}\right)$$

Equation 4-12[19]

The crystallinity based on the homopolymer heat of fusion or weight fraction crystallinity was then converted to volume fraction using the denisty of the amorphos phase ρ_a (855 kg/m^3)[29]. The

amorphous phase thickness was then calculated assuming a two layer system using ℓ_c and the degree of crystallinity[28].

4.6 LAMELLA THICKNESS CALCULATION BY THERMAL FRACTIONATION DSC

Using a method similar to that shown in Horvath et al., the lamella thickness was calculated for the fractions produced with the thermal fractionation[19]. The melting thermal fractionation heat flow was normalized with the sample weight and plotted with temperature on the x axis. The temperature range between 105 ˚C to 185˚C was used in the analysis. Following the method in Horvath et al., the temperature range was divided into a fixed number of equal temperature span sections. The number of sections was set to the number of steps in the thermal fractionation method plus one. Since the thermal fractionation method used in this paper consisted of nine steps, the area was broken into ten sections of equal size. A data point every 1.67 ˚C was collected to be analyzed. Initially a linear baseline trend for each samples was established. The heat flow delta between each data point was determined and corrected with the linear base line to find the change in the y axis. The area of each change was then determined and collected into the ten sections to determine the area for each temperature range. The areas were then converted to fractions. Using the Gibbs- Thomson equation, shown in Equation 4-12, the temperatures were converted into lamella thickness (nm). The lamella thickness l was then converted into length of flawless regular sequence I in monomer units, using Equation 4-13, were c is the thickness of a propylene unit. The constants in Table 5 were used for the calculations[19].

$$I = 3 * l/c$$

Equation 4-13[19]

Table 5. Polypropylene Crystal Parameters[19]

T_m^o (K)	σ_e (J/m^2)	ρ_c (kg/m^3)	H_m^o (J/kg)	c (A)
481	0.122	936	146000	6.5

5.0 RESULTS AND DISCUSSION

5.1 SOLUTION STATE NMR RESULTS AND DICUSSION

5.1.1 Tacticity

The tacticity results for the homopolymer sample group are shown in Table 6. As the amount of amorphous polymer increased the level of meso pentad units (mmmm mole %) decreased which is expected since the samples were chosen to have decreasing crystallinity.

Table 6. Homopolymer NMR Tacticity Results (mole %)

Sample	HP1	HP2	HP3
mm	96.6	93.8	92.8
mr	2.0	3.4	3.8
rr	1.4	2.7	3.4
mmmm	94.7	90.9	89.7
mmmr	1.6	2.5	2.7
rmmr	0.3	0.4	0.4
mmrr	1.3	2.2	2.5
rmrr, mmrm	0.5	0.9	1.0
mrmr	0.18	0.4	0.4
rrrr	0.4	0.8	1.3
rrrm	0.4	0.8	1.0
mrrm	0.6	1.0	1.2

The random sample group's tacticity results are shown in Table 7. In the random group, as the level of ethylene increased the level of meso pentad units (mmmm mole %) dropped which was also expected.

Table 7. Random Copolymer NMR Tacticity Results (mole %)

Sample	RP1	RP2	RP3
mm	89.0	89.4	84.8
mr	8.3	8.5	12.1
rr	2.8	2.1	3.1
mmmm	82.0	81.8	74.8
mmmr	6.7	7.1	9.5
rmmr	0.3	0.6	0.6
mmrr	1.2	1.1	0.9
rmrr, mmrm	6.3	6.6	9.7
mrmr	0.9	0.8	1.6
rrrr	0.9	0.3	0.7
rrrm	1.3	1.3	2.0
mrrm	0.6	0.5	0.4

The impact copolymer samples group's results are shown in Table 8. As the samples increased in rubber content, the level of meso pentad units (mmmm mole %) decreased showing a drop in crystallinity which was also expected for this case.

Table 8. Impact Copolymer NMR Tacticity Results (mole %)

Sample	ICP1	ICP2	ICP3
mm	93.3	88.0	85.7
mr	4.0	7.0	8.2
rr	2.7	5.1	6.0
mmmm	90.4	84.2	81.6
mmmr	2.5	3.1	3.3
rmmr	0.4	0.7	0.9
mmrr	0.9	1.0	0.6
rmrr, mmrm	1.9	3.2	4.0
mrmr	1.2	2.7	3.7
rrrr	0.6	0.6	0.5
rrrm	1.7	4.0	5.1
mrrm	0.4	0.5	0.4

The results for the NMR branching tacticity are shown in Table 9. As the level of branching increased, the level of meso pentad units (mmmm mole %) increased slightly. However it is hard to say if in the increase was statistically significant.

Table 9. Branched NMR Tacticity Results (mole %)

Sample	Branch0	Branch1	Branch2
mm	89.6	89.9	90.0
mr	8.3	8.2	8.2
rr	2.1	1.9	1.9
mmmm	82.1	82.7	82.8
mmmr	7.1	6.9	6.8
rmmr	0.4	0.3	0.3
mmrr	1.0	0.8	0.8
rmrr, mmrm	6.6	6.6	6.6
mrmr	0.8	0.8	0.8

Table 9 (continued)			
rrrr	0.7	0.6	0.5
rrrm	0.9	1.0	0.9
mrrm	0.5	0.4	0.4

5.1.2 Ethylene Incorporation

The ethylene-propylene incorporation for the random copolymer group is shown in Table 10. In the random ethylene group RP1 has the lowest ethylene weight percent at 2.62 and RP3 has the highest at 5%. The EEE mole % area also similar for RP1 and RP2 but RP3 shows a more blocky ethylene incorporation. When looking at the EEE mole % normalized with ethylene level, EEE/E %, the same trend is seen; which indicated that the higher blockiness is not due to higher overall ethylene alone.

Table 10. Ethylene Incorporation for Random Set

Sample	RP1	RP2	RP3
P (wt. %)	97.4	97.0	95.0
P (mole %)	96.1	95.6	92.7
E (wt. %)	2.6	3.0	5.0
E (mole %)	3.9	4.4	7.3
PP (mole %)	92.7	91.7	86.7
PE (mole %)	6.8	7.8	12.0
EE (mole %)	0.5	0.5	1.3
PPP (mole %)	89.9	88.6	82.2
PPE (mole %)	5.9	6.6	9.6
EPE (mole %)	0.4	0.5	0.9
Sum (PPP,PPE,EPE) (mole %)	96.1	95.7	92.7
EEE (mole %)	0.1	0.2	0.5
PEE (mole %)	0.6	0.7	1.5

Table 10 (continued)			
PEP (mole %)	3.2	3.6	5.3
PPP/P (%)	93.5	92.6	88.7
PPE/P (%)	6.1	6.9	10.3
EPE/P (%)	0.4	0.5	1.0
EEE/E (%)	3.7	3.4	6.9
EEP/E (%)	14.6	15.1	20.6
PEP/E (%)	81.7	81.5	72.6

The ethylene-propylene incorporation for the impact copolymer group is shown in Table 11. The impact group has ethylene weight percent from 4.82 to 15.58 % for ICP1 and ICP3, respectively. Although the EEE mole % increase with increasing ethylene the normalized EEE mole%/E shows a smaller increase between samples.

Table 11. Ethylene Incorporation for Impact Copolymer Set

Sample	ICP1	ICP2	ICP3
P (wt. %)	95.2	88.4	84.4
P (mole %)	93.0	83.5	78.3
E (wt. %)	4.8	11.6	15.6
E (mole %)	7.1	16.5	21.7
PP (mole %)	90.5	78.2	71.6
PE (mole %)	4.9	10.7	13.4
EE (mole %)	4.6	11.1	15.0
PPP (mole %)	89.4	76.3	69.3
PPE (mole %)	2.3	4.3	5.4
EPE (mole %)	1.2	2.9	3.7
Sum (PPP,PPE,EPE) (mole %)	93.0	83.6	78.3
EEE (mole %)	3.4	8.3	11.4
PEE (mole %)	2.4	5.6	7.3
PEP (mole %)	1.2	2.5	3.0
PPP/P (%)	96.2	91.3	88.5

Table 11 (continued)			
PPE/P (%)	2.5	5.2	6.9
EPE/P (%)	1.3	3.5	4.7
EEE/E (%)	48.2	50.8	52.6
EEP/E (%)	34.6	33.8	33.5
PEP/E (%)	17.1	15.4	13.9

The ethylene-propylene incorporation for the branched copolymer group is shown in Table 12. The weight percent ethylene is similar for the three samples in the branching group. A slight decrease in ethylene weight percent was seen for the two branched samples, however this might be less than statistically significant.

Table 12. Ethylene Incorporation for Branched Copolymer Set

Sample	Branch0	Branch1	Branch2
P (wt. %)	97.2	97.3	97.3
P (mole %)	95.9	96.0	96.0
E (wt. %)	2.8	2.7	2.7
E (mole %)	4.1	4.0	4.0
PP (mole %)	92.2	92.3	92.4
PE (mole %)	7.4	7.3	7.2
EE (mole %)	0.5	0.4	0.4
PPP (mole %)	89.2	89.2	89.2
PPE (mole %)	6.4	6.4	6.4
EPE (mole %)	0.3	0.4	0.4
Sum (PPP,PPE,EPE) (mole %)	95.9	96.0	96.0
EEE (mole %)	0.1	0.1	0.2
PEE (mole %)	0.7	0.6	0.6
PEP (mole %)	3.3	3.4	3.3
PPP/P (%)	93.0	92.9	92.9
PPE/P (%)	6.7	6.7	6.6
EPE/P (%)	0.3	0.4	0.4
EEE/E (%)	3.4	3.0	3.8

Table 12 (continued)			
EEP/E (%)	16.1	14.0	14.3
PEP/E (%)	80.6	82.9	82.0

5.2 SOLID STATE NMR RESULTS AND DICUSSION

5.2.1 Soft and Rigid Fraction

The crystallinity calculated by DSC is compared to the rigid fraction measured by solid state NMR (ssNMR) and was calculated by dividing the integrated area from the CPMAS with 8 ms spin lock by the integrated area from CPMAS without a spin lock, since the two spectra represent the crystalline and total sample, respectively. The results are shown in Table 13. The homopolymer set shows the expected trend and similar relative magnitude as was seen in the DSC results. The random set shows the expected trend, however, the ssNMR values are significantly higher than the DSC results. The crystal defects caused by the comonomer could be effecting the crystal packing and causing the amorphous T1 to be longer then the homopolymer sample set. In the case of copolymer samples, a longer spin lock time may be needed to remove all mobile components from the signal. The impact copolymer set does not show the expected trend and similar to the random set, have significantly higher values to the DSC set. The first two impacts show the expected decrease in rigid fraction but the last sample is higher than the second sample. This could be due to the higher level of ethylene in the ethylene-propylene rubber that could be causing a small amount of crystalline polyethylene to form. This is supported by the additional peak in the DSC curve in Figure 20 area was not included in the DSC

crystallinity calculation since an ideal perfect polyethylene crystal has a different enthalpy so the area cannot be included in the crystallinity calculation used. The branched sample set had consistent crystallinity when measured by DSC but the ssNMR results show an increasing rigid percent as the level of branching increased. This increase is most likely due to the branches causing slower local movements and not an increase in crystallinity.

Table 13. Crystallinity by DSC Compared to Rigid Percent by ssNMR

Sample	Code	Type	Crystallinity(%) by DSC	Rigid(%) by ssNMR
1	HP1	HP	64.5	65.8
2	HP2	HP	61.6	63.3
3	HP3	HP	59.7	62.1
4	RP1	RP	36.4	58.1
5	RP2	RP	35.4	57.0
6	RP3	RP	27.1	55.8
7	ICP1	ICP	48.1	66.3
8	ICP2	ICP	42.6	59.8
9	ICP3	ICP	36.6	62.2
10	Br0	Branched	38.2	59.5
11	Br1	Branched	38.2	62.1
12	Br2	Branched	37.6	64.6

5.2.2 Domain Thickness for Soft and Rigid Fractions

The solid state NMR spin diffusion data was used to determine the $tm_0^{1/2}$, Dr, Dm, $D_{eff}^{1/2}$, dr, and dm. The results are shown in Table 14.

Table 14. Solid State NMR Diffusion Coefficients and Phase Thicknesses

Sample	Code	Type	$tm_0^{1/2}$	Dr ($nm/ms^{1/2}$)	Dm ($nm/ms^{1/2}$)	$D^{eff1/2}$ ($nm/ms^{1/2}$)	dr (nm)	dm (nm)
1	HP1	HP	7.5	0.23	0.80	0.63	15.5	8.1
2	HP2	HP	8.8	0.24	0.77	0.63	17.0	9.9
3	HP3	HP	8.5	0.23	0.77	0.62	15.8	9.6
4	RP1	RP	8.8	0.23	0.42	0.55	13.1	9.4
5	RP2	RP	9.5	0.23	0.37	0.54	13.3	10.1
6	RP3	RP	9.0	0.20	0.24	0.47	10.7	8.5
7	ICP1	ICP	7.6	0.02	0.12	0.21	5.3	2.7
8	ICP2	ICP	9.0	0.02	0.11	0.20	5.1	3.4
9	ICP3	ICP	7.8	0.02	0.11	0.20	4.6	2.8
10	Br0	Branched	8.8	0.23	0.33	0.52	12.8	8.7
11	Br1	Branched	8.8	0.23	0.25	0.49	12.9	7.9
12	Br2	Branched	8.8	0.24	0.26	0.50	13.9	7.6

It was noted that due to the small number of points used to calculate the initial slope of the intensity versus mixing time graph, significant variations in $tm_0^{1/2}$ are expected. Small changes in $tm_0^{1/2}$ can have a significant impact on the estimated rigid lamella thickness and mobile phase thickness. Figure 14 shows the $tm_0^{1/2}$ determination graph for HP1, only the first four points are used to create the initial slope line and the intersection with the steady state line is found to be 7.5 $ms^{1/2}$. However if the points after a $tm_0^{1/2}$ time of 20 $ms^{1/2}$ are used as steady state, the relative error in the test is 5%. If the initial four points are varied by 5% higher than measured and 5% lower than measured the shift in intersection is shown in Figure 15. If the three values determined for $tm_0^{1/2}$ are then used to calculate the dr and dm, the results can be seen in Table 15. Since 5% error was seen for the solid state NMR results for dr and dm, the results were graphed with error bars shown in Figure 16 and Figure 17. Table 16 shows the solid state NMR thickness results with the DSC results for the crystalline lamella thickness and amorphous phase thickness.

When comparing the results within a sample set, the relative differences in rigid and mobile thickness do not appear to be statistically significant.

The crystalline lamella thickness and rigid phase thickness for the homopolymer set do not show a consistent trend however the relative values are similar. The random set also shows similar relative values to the crystalline and rigid thicknesses. The trends are also consistent with RP1 and RP2 showing similar thicknesses and RP3 showing a reduction. The samples within impact copolymer set have a large difference in relative values from the crystalline results to the rigid results. This error is likely due to the broad signals used to calculate the diffusion coefficients which might be caused by the heterophasic nature of the impact samples. The branched samples show the same relative values and trends for the crystalline and rigid thickness. The thickness of the rigid phase increases as the level of branching increases. The thickness of the amorphous and mobile fraction for the homopolymer set had closest relative magnitude. All the ethylene containing samples had a large decrease in mobile thickness when comparing it to amorphous thickness. Consistent trends were not seen for the random or impact sample set. The branched set showed the opposite trend with the amorphous thickness increasing with increased branching and the mobile phase has decreasing with increased branching. The difference in trends may be due to the branching causing additional rigid like movement in the amorphous phase.

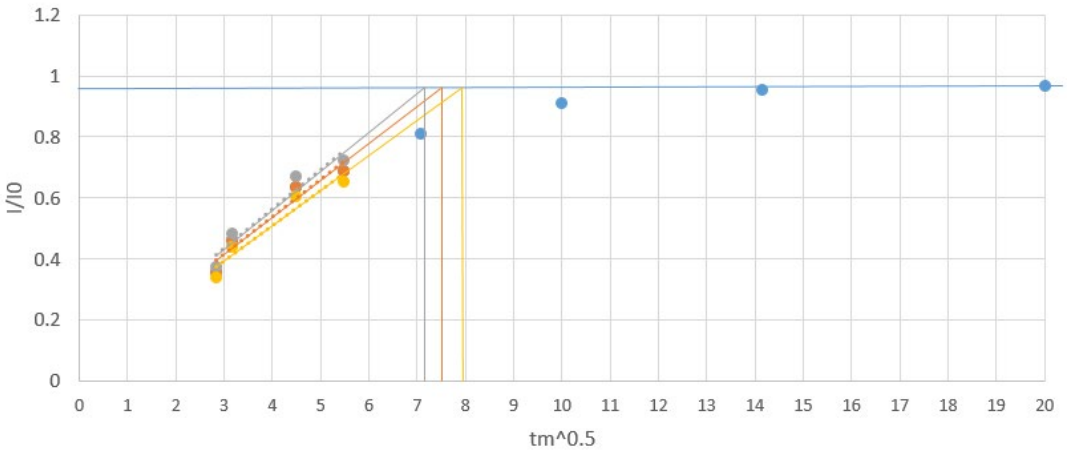

Figure 15. HP1 Variability in $tm_0^{1/2}$

Table 15. HP1 Variability in dr(nm) and dm(nm)

Sample	Code	Type	tm01/2	Dr ($nm/ms^{1/2}$)	Dm ($nm/ms^{1/2}$)	$D^{eff1/2}$ ($nm/ms^{1/2}$)	dr (nm)	dm (nm)
1	HP1	Recorded	7.5	0.2	0.8	0.6	15.5	8.1
1	HP1	5% High	7.9	0.2	0.8	0.6	16.4	8.5
1	HP1	5% Low	7.2	0.2	0.8	0.6	14.9	7.7
						Average	15.6	8.1
						Stdev	0.7	0.4
						RSD(%)	4.7	4.7

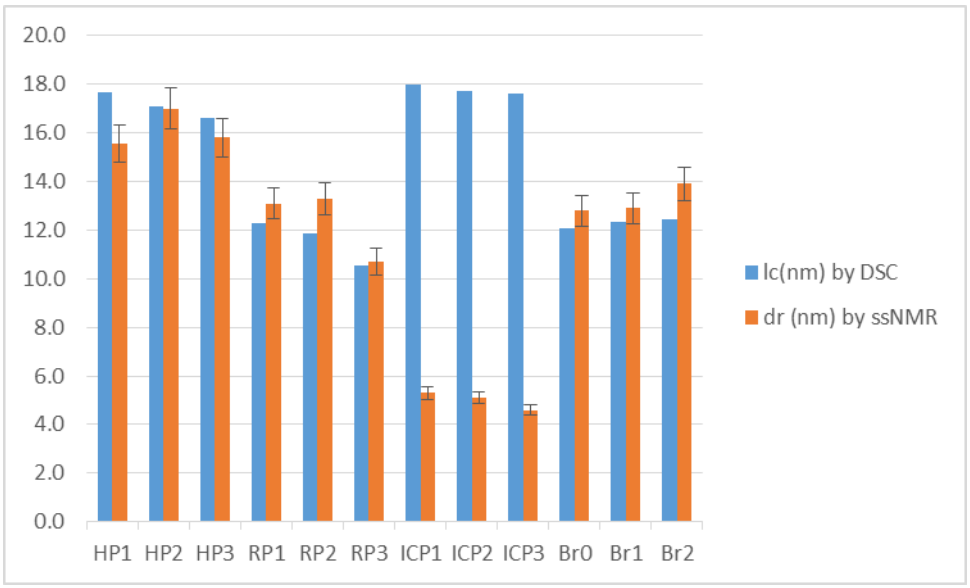

Figure 16. Crystalline Lamella Thickness by DSC and Rigid Phase Thickness by Solid State NMR

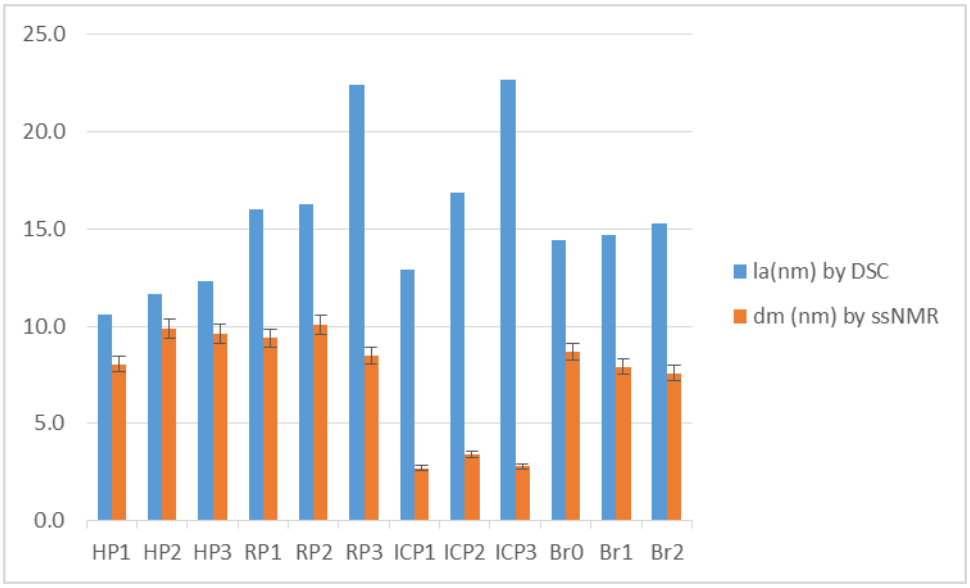

Figure 17. Amorphous Phase Thickness by DSC and Mobile Phase Thickness by Solid State NMR

Table 16. Phases Thicknesses by Annealed DSC and Solid State NMR

Sample	Code	Type	lc(nm) by DSC	la(nm) by DSC	dr (nm) by ssNMR	dm (nm) by ssNMR
1	HP1	HP	17.6	10.6	15.5	8.1
2	HP2	HP	17.1	11.6	17.0	9.9
3	HP3	HP	16.6	12.3	15.8	9.6
4	RP1	RP	12.3	16.0	13.1	9.4
5	RP2	RP	11.9	16.3	13.3	10.1
6	RP3	RP	10.5	22.4	10.7	8.5
7	ICP1	ICP	18.0	12.9	5.3	2.7
8	ICP2	ICP	17.7	16.9	5.1	3.4
9	ICP3	ICP	17.6	22.7	4.6	2.8
10	Br0	Branched	12.1	14.4	12.8	8.7
11	Br1	Branched	12.3	14.7	12.9	7.9
12	Br2	Branched	12.4	15.3	13.9	7.6

5.3 ANNEALED DSC CRYSTALINITY RESULTS AND DISCUSSION

The annealed DSC values for the crystallization peak are show in Table 17. As expected, with decreasing crystallinity, a drop in T_c and ΔHc was seen for the homopolymer set. The same downward trend was seen for increasing ethylene in the random set for T_c but ΔHc did not show a clear trend. The impact copolymer sample set showed the reverse with a decreasing ΔHc for increasing ethylene content but no trend for T_c. However for the branched set the T_c increases with increasing branching which is expected for branched samples since additional energy is required to crystalize the long side groups[30]. ΔHc decreased with increasing branching.

Table 17. Crystallization Temperature and Enthalpy

	Crystallization Peak Tc 1 (°C)	Crystallization Peak Δ H1 AVG (J/g)
HP1	123.37	101.2
HP2	122.6	97.0
HP3	120.5	93.7
RP1	108.9	72.5
RP2	107.3	74.6
RP3	99.5	61.5
ICP1	123.1	95.2
ICP2	121.8	83.2
ICP3	122.9	72.2
BR0	108.7	79.4
BR1	113.2	78.7
BR2	115.4	75.2

The melting peak data showed clearer trends with decreasing T_m values for decreasing crystallinity level for the homopolymer. The T_m also decreased with increasing ethylene for the random and impact copolymer samples. For the impact copolymer samples, this change is probably related to the reduction in the mmmm pentad percent of the sample and not the increase in ethylene. The heat of fusion ΔHf showed the same trend as seen in T_m for the homopolymer, random and impact sample sets. The branched samples mirrored the trend seen for T_c for T_m but showed no trend for ΔHf. The T_m and ΔHf data is shown in Table 18. A shoulder on the low temperature side of the melting peak around 135 ˚C is seen for the branched samples. The shoulder becomes larger as the branching increases.

Table 18. Melting Temperature and Enthalpy

	Second Melt Tm 1 AVG (°C)	Second Melt Δ H1 AVG (J/g)
HP1	164.9	106.5
HP2	163.6	101.7
HP3	162.3	98.5
RP1	146.2	75.3
RP2	144.0	73.3
RP3	135.9	56.1
ICP1	165.7	99.5
ICP2	165.1	88.2
ICP3	164.9	75.8
BR0	145.1	79.0
BR1	146.3	79.0
Br2	146.9	77.8

Since the crystallinity is calculated using the heat of fusion data, the weight percent crystallinity showed the sample trend as seen for ΔHf. The branched samples showed relatively no change in crystallinity with increasing branching, although it is possible that the nucleation density is still changing. The crystallinity for all samples was calculated using the idealized pure crystal heat of fusion for isotactic PP and then again for the samples containing ethylene using the heat of fusion for a fully crystalline copolymer sample, although a fully crystalline copolymer sample is not possible. The results are shown in Table 19.

Table 19. Weight Percent Crystallinity

	Xc ΔHm^0 = 156 J/g	Xc ΔHm^0 = 207 J/g
HP1	64.5	
HP2	61.6	

Table 19 (continued)		
HP3	59.7	
RP1	45.6	36.4
RP2	44.4	35.4
RP3	34.0	27.1
ICP1	60.3	48.1
ICP2	53.5	42.6
ICP3	45.9	36.6
BR0	47.9	38.2
BR1	47.9	38.2
Br2	47.1	37.6

The crystalline lamella thickness l_c is calculated using the Gibbs- Thomson equation, shown in Equation 4-12[19]**.**. The l_a value uses both the T_m and ΔHf and a volume conversion using the density differences between amorphous and crystalline polypropylene. The crystalline lamella thickness is converted into monomer units using Equation 4-13 . The homopolymer amorphous phase thickness shows increasing ℓ_a as crystallinity decreases and ℓ_c decreases. Similarly in the ethylene random case with increasing ethylene the ℓ_a increases and ℓ_c decreases. For the impact copolymer set, a very small decrease in ethylene ℓ_c was observed which would be due to a drop in mmm pentad percent of the sample. A large increase in ℓ_a was seen relative to the changes seen in the random and homopolymer samples. The large change in ℓ_a is due to the drop in crystalline fraction. For the impact samples, two phases exist, but the DSC values observed are from an average of both, the matrix and the ethylene-propylene rubber. For the branched samples both the ℓ_a and ℓ_c increases but only slightly, relative to the changes seen in the random and homopolymer samples. The raw data of the melting curve did show two populations for both branched samples but only one for the reference. The calculated values capture the average of the results. A more detailed analysis of the distribution and fraction of the lamellar thickness and

amorphous fraction is done using thermal fractionation in the next section. The annealed DSC calculated values are used to act as an average. The phase thicknesses are shown in Table 20. The branched samples did show an increase in the amorphous phase which could be caused by the additional branches being excluded into the amorphous domain[13].

Table 20. Calculations of Crystalline Lamella Thickness, Crystalline Volume Fraction and Amorphous phase Thickness

	ℓ_c (nm)	l (monomer units)	vc (volume fraction crystalline)	ℓ_a (nm)
HP1	17.7	81.0	62.5	10.6
HP2	17.1	79.0	59.5	11.7
HP3	16.6	77.0	57.5	12.3
RP1	12.3	57.0	43.4	16.0
RP2	11.9	55.0	42.2	16.3
RP3	10.5	49.0	32.0	22.4
ICP1	18.0	83.0	58.1	12.9
ICP2	17.7	82.0	51.2	16.9
ICP3	17.6	81.0	43.7	22.7
BR0	12.1	56.0	45.6	14.4
BR1	12.3	57.0	45.6	14.7
Br2	12.4	57.0	44.9	15.3

The overlaid graphs for all annealed DSC runs are shown in Figure 18 to Figure 25. The impact copolymer samples did show a small melting peak at 115 ˚C due to the crystallization of a small amount of polyethylene in the ethylene-propylene rubber particles. The respective crystallization peak was seen around 100 ˚C.

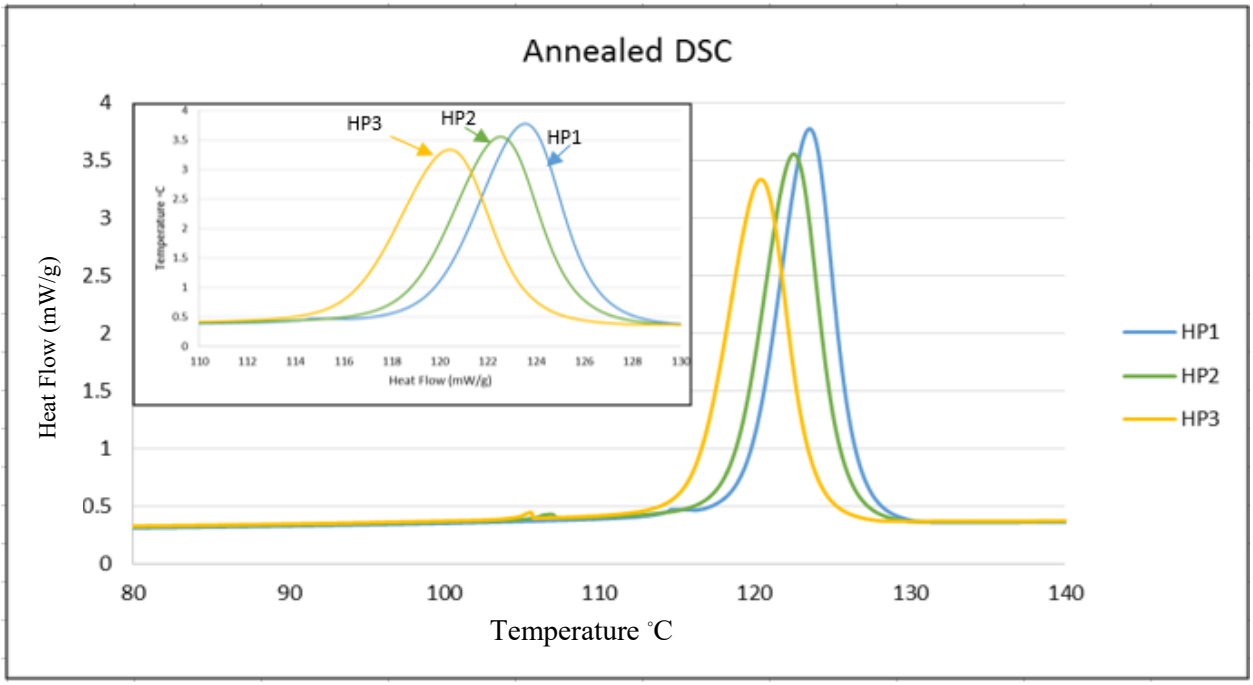

Figure 18. Crystallization Peak for Homopolymer Set

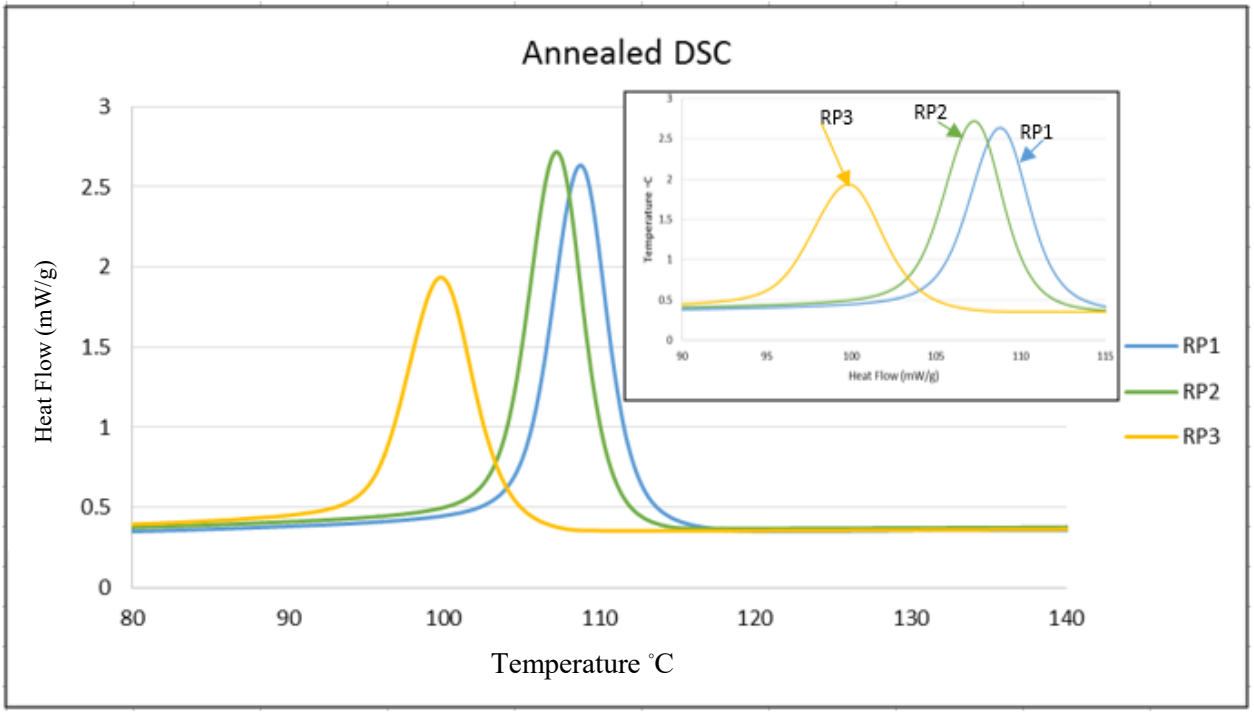

Figure 19. Crystallization Peak for Random Set

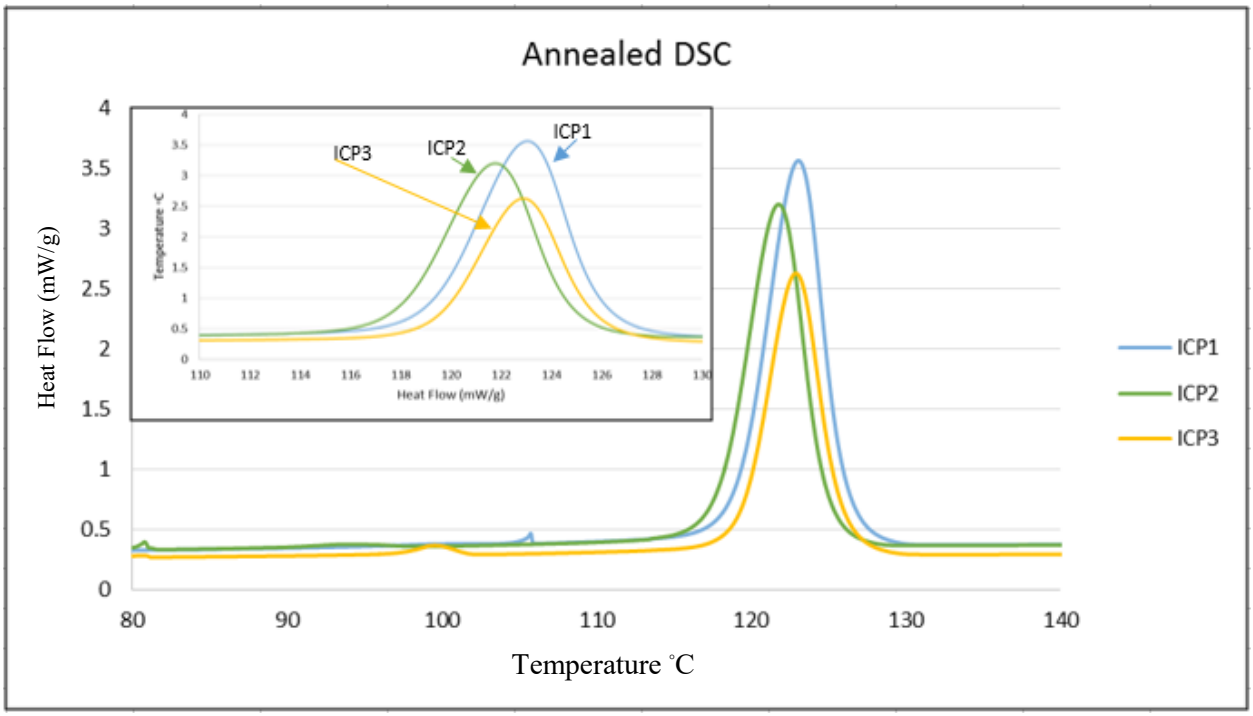

Figure 20. Crystallization Peak for Impact Set

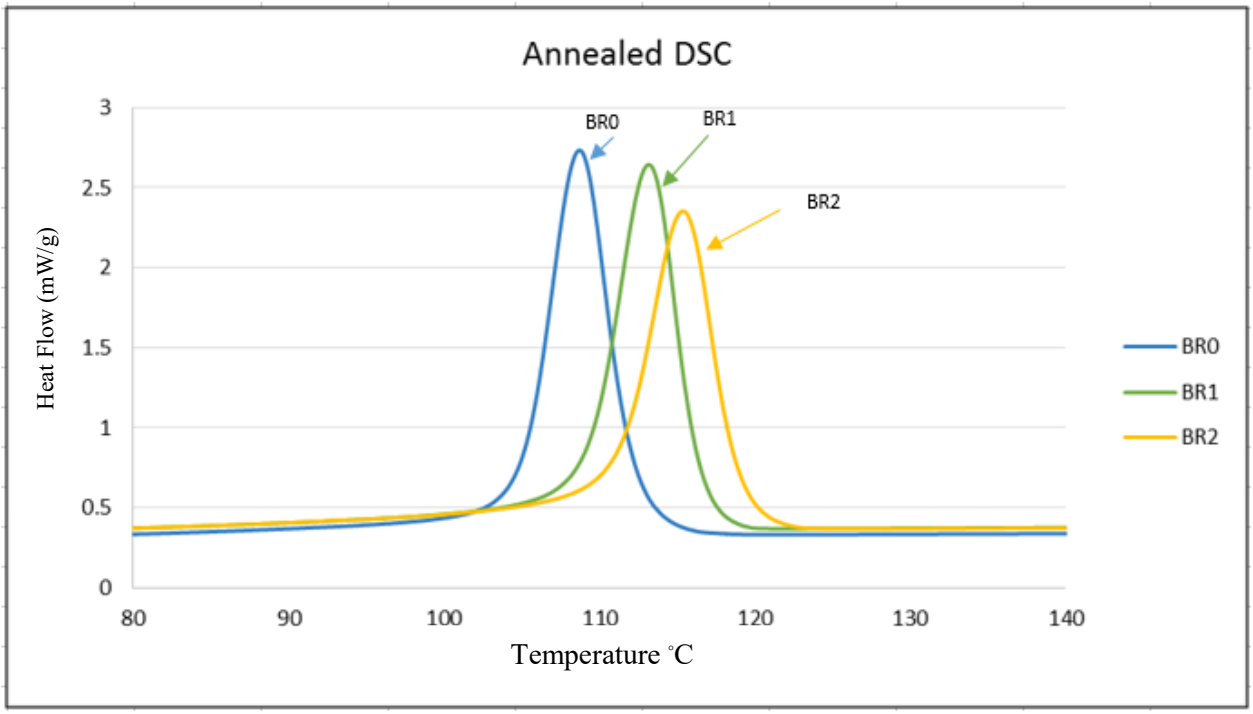

Figure 21. Crystallization Peak for Branched Set

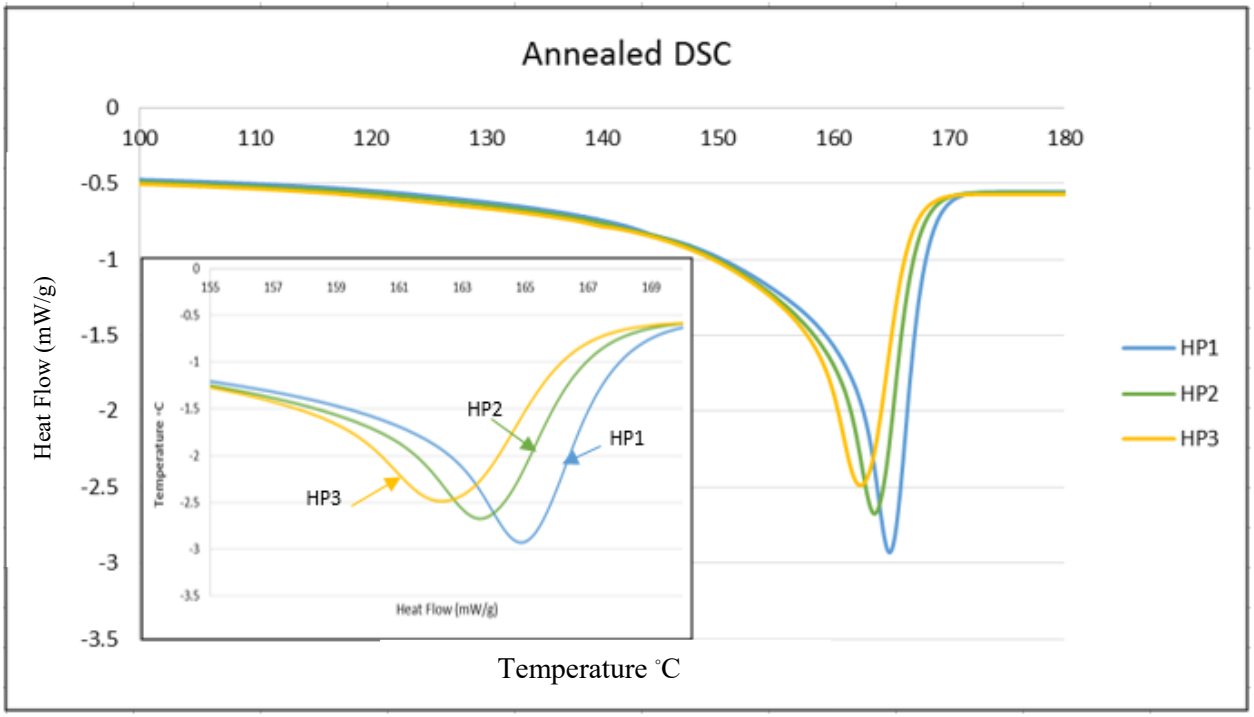

Figure 22. Melting Peak for Homopolymer Set

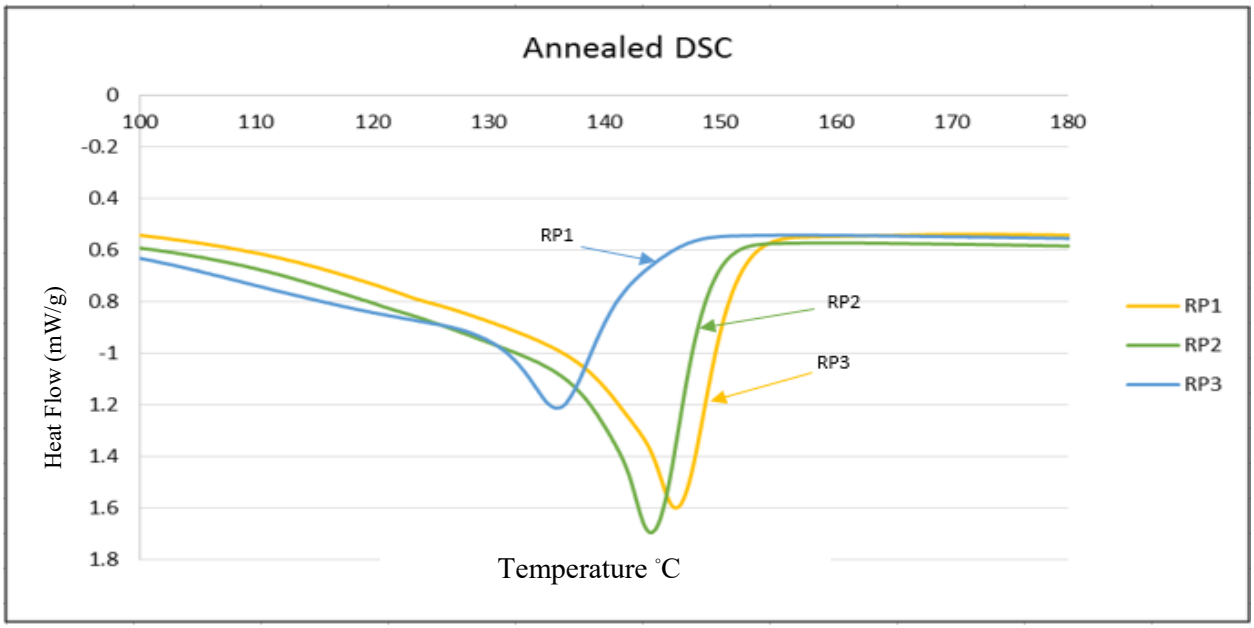

Figure 23. Melting Peak for Random Set

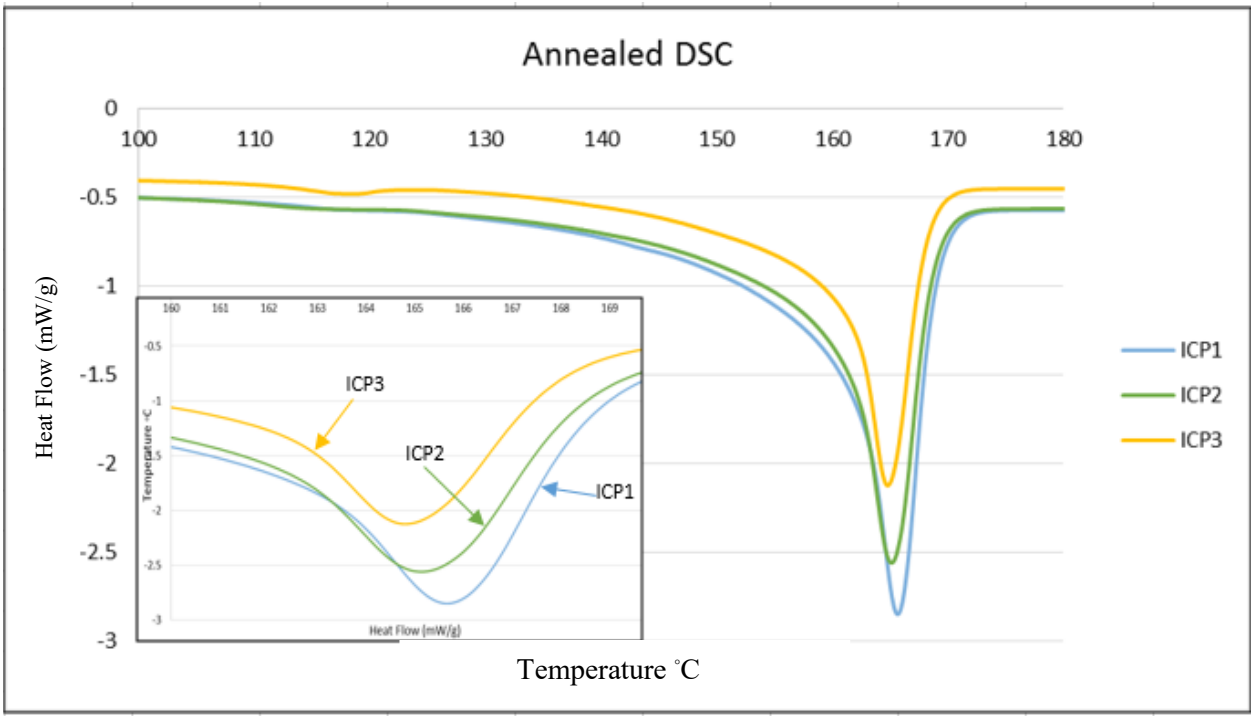

Figure 24. Melting Peak for Impact Set

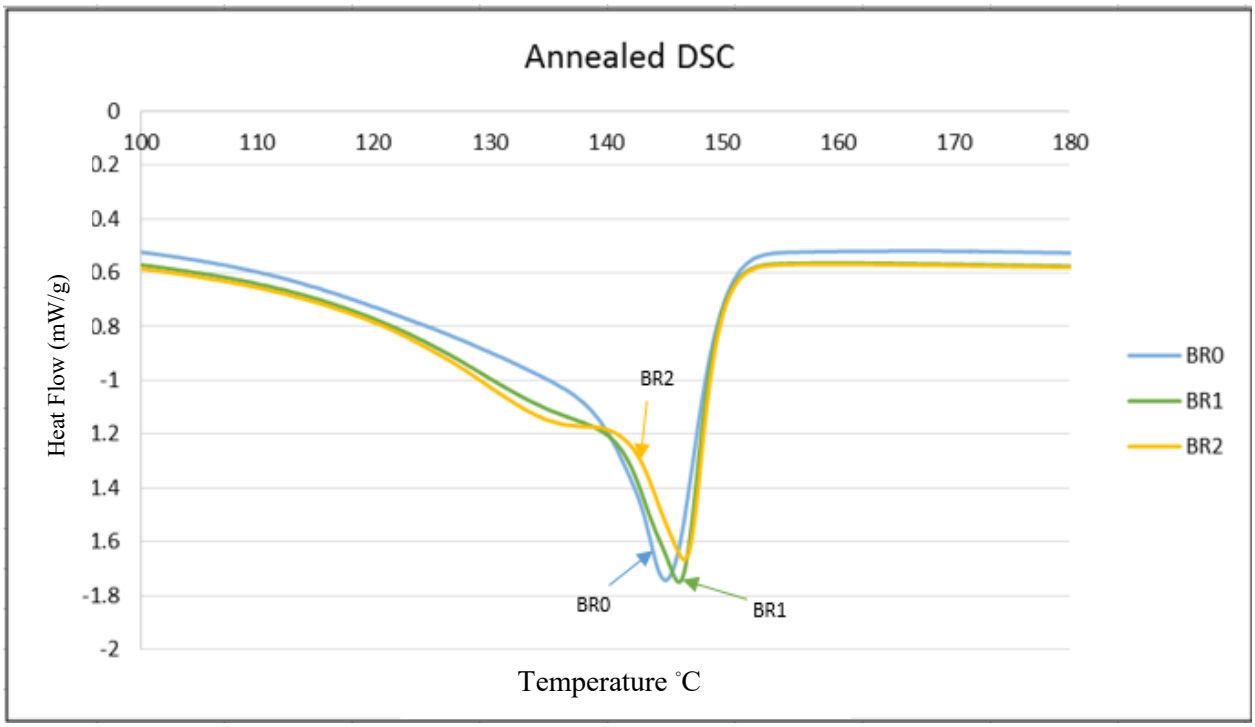

Figure 25. Melting Peak for Branched Set

5.4 THERMAL FRACTIONATION LAMELLA THICKNESS RESULTS AND DICUSSION

The homopolymer group's melting peak for the thermal fractionation run in shown below in Figure 26. As the crystallinity decreases so does that area under the curve in the higher temperature. Based on the Thomson-Gibbs equation shown in Equation 4-12[19], the higher the temperature of melting, the thicker the crystalline lamella melting in that range.

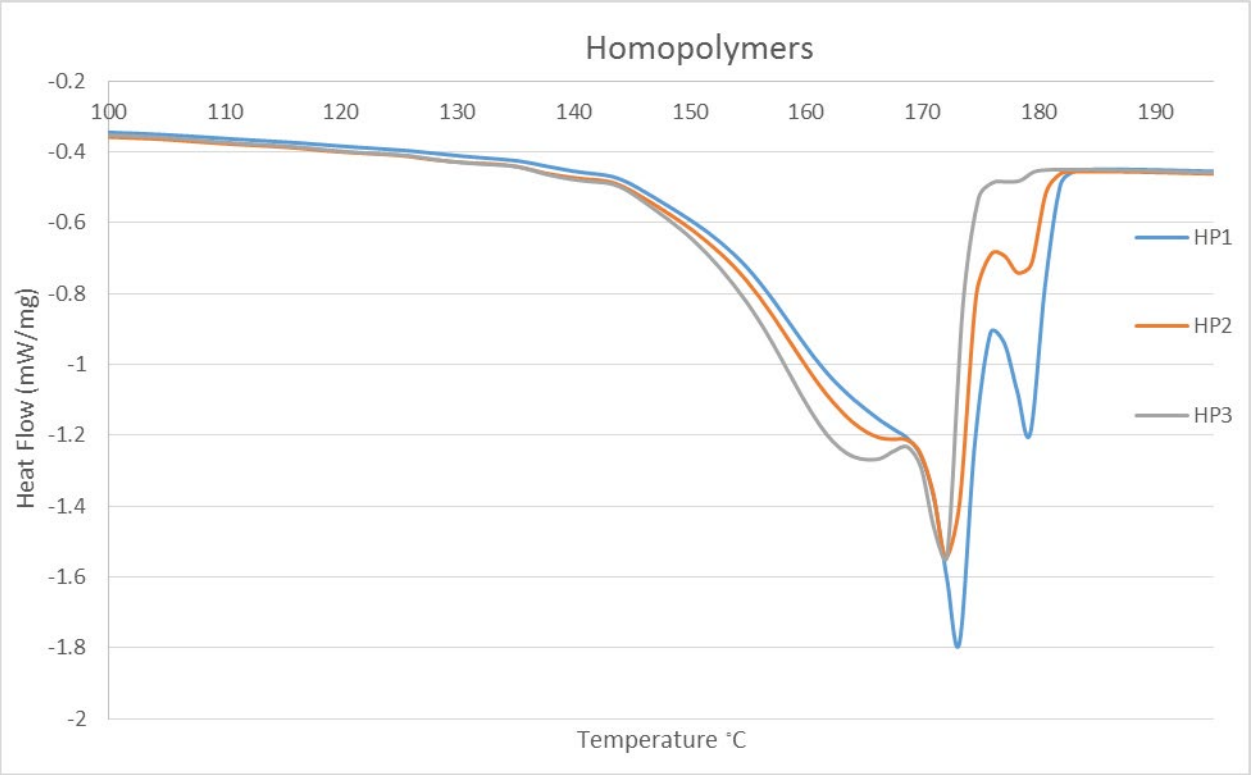

Figure 26. Homopolymer Thermal Fractionation Melting Peak

Figure 27 shows the homopolymer thermal fractionation result after the fraction of lamellar melting at a given temperature and the size of the lamellar that could melt at that temperature were determined. The lamellar thickness was converted to flawless regular sequence I in monomer units, using Equation 4-13.

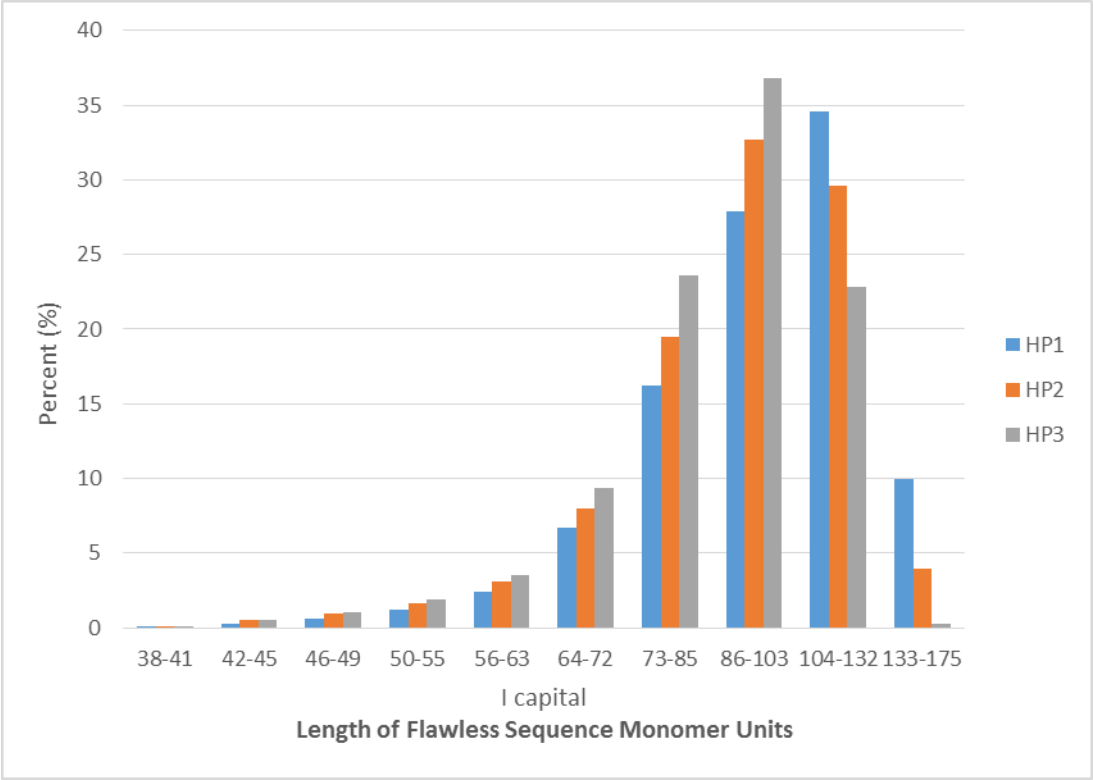

Figure 27. Homopolymer Percent of Crystalline Polypropylene at given Length of Flawless Sequence (Monomer Units)

The same approach was taken for the random copolymer group and the results are shown in Figure 28 and Figure 29. As the level of ethylene increases, the fraction of thicker lamella decreased. The magnitude of the change of ethylene also trends as expected, since only a small increase in ethylene is seen for RP1 to RP2 but a larger increase is seen in RP3. The results for the impact copolymer set is shown in Figure 30 and Figure 31. For the impact copolymer group, no consistent trend was seen for increasing ethylene which supports the idea that most of the ethylene propylene rubber is not undergoing crystallization and the observed signals is for the matrix. Figure 32 and Figure 33 show the branched case, as the level of branching increases the fraction of lamella melting at the higher temperature increase. This indicates that the branching

thickens the lamellae. When comparing the annealed and the thermal fractionation data, the branched samples showed a shoulder in the low temperature area for the annealed and a shoulder in the high temperature for the thermal fractionation data. The reduction of mobility of the long branches could cause the annealed run to be cooled too fast to fully perfect the crystals whereas the thermal fractionation run is long enough to perfect the crystal and form larger lamellae.

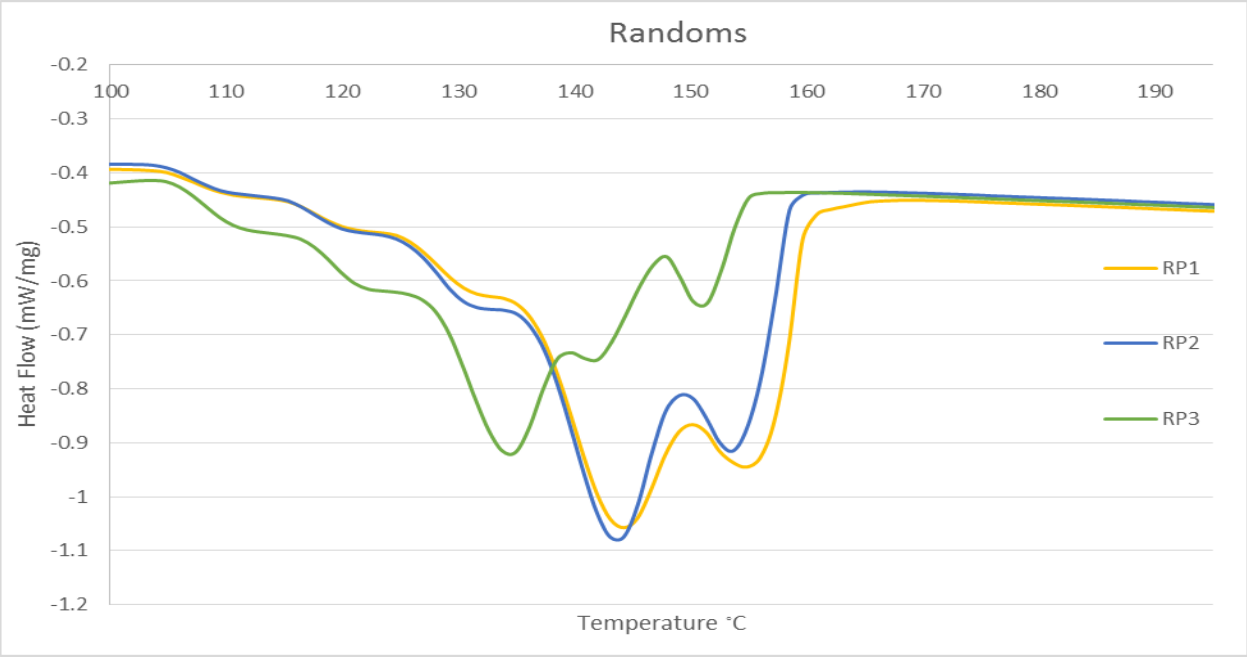

Figure 28. Random Thermal Fractionation Melting Peak

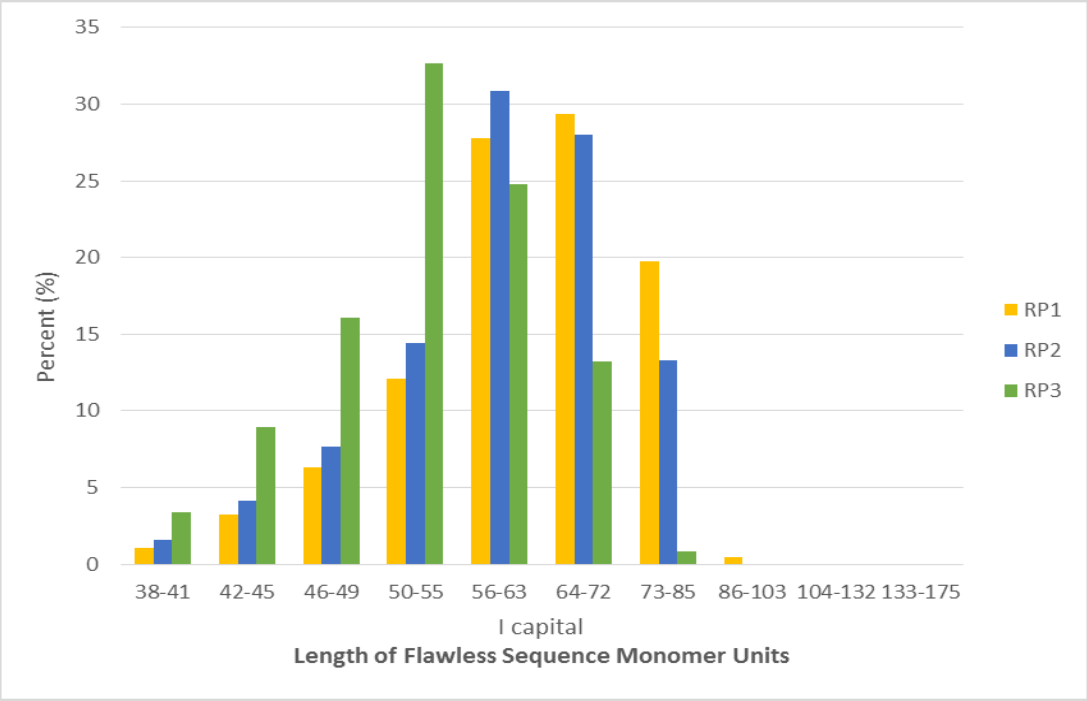

Figure 29. Random Percent of Crystalline Polypropylene at given Length of Flawless Sequence (Monomer Units)

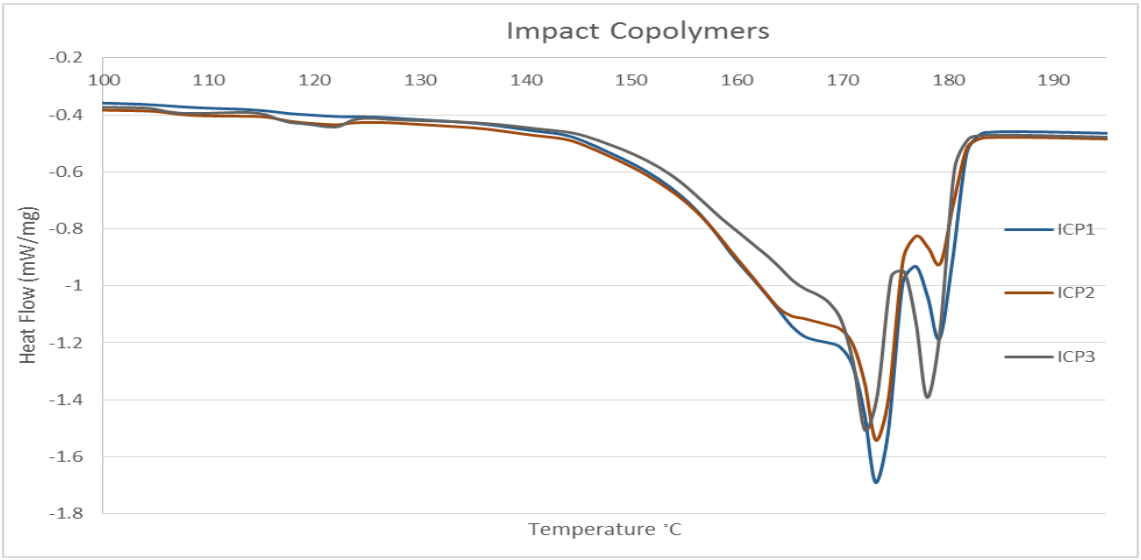

Figure 30. Impact Thermal Fractionation Melting Peak

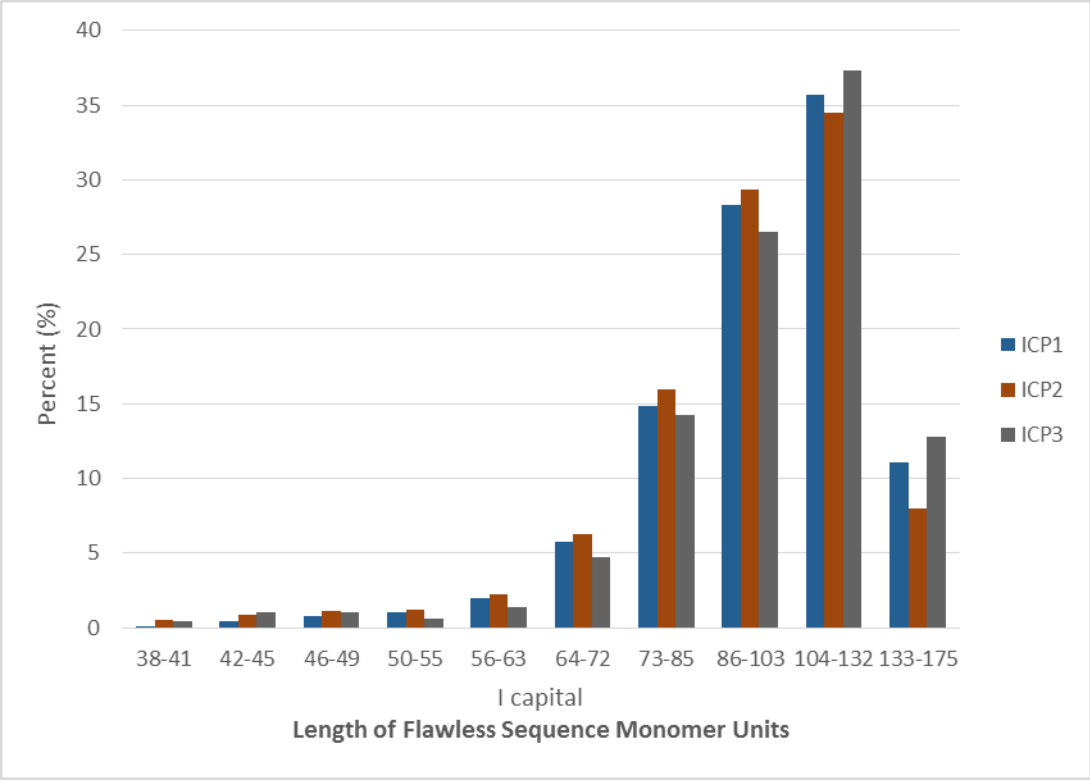

Figure 31. Impact Percent of Crystalline Polypropylene at given Length of Flawless Sequence (Monomer Units)

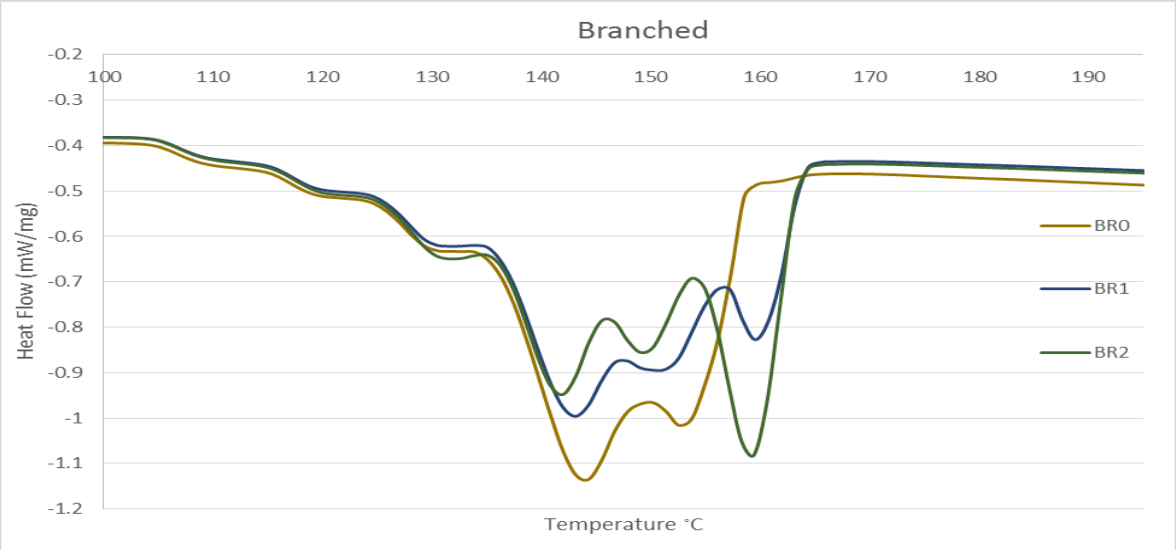

Figure 32. Branched Thermal Fractionation Melting Peak

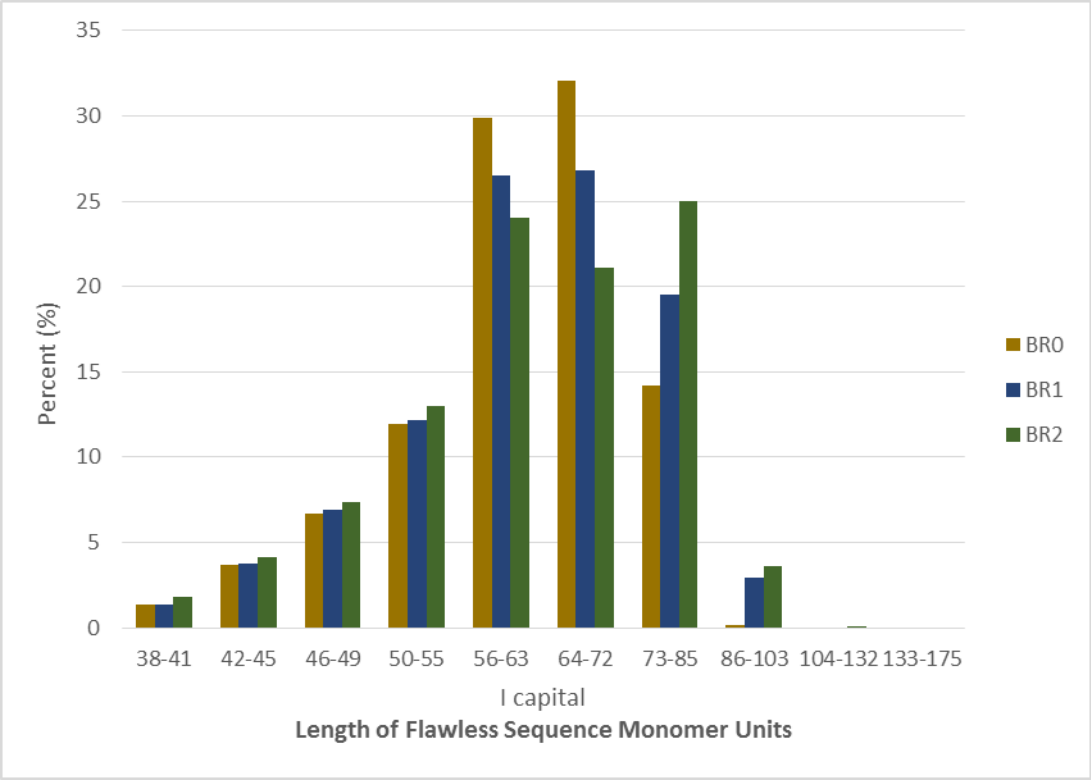

Figure 33. Branched Percent of Crystalline Polypropylene at given Length of Flawless Sequence (Monomer Units)

The area under the thermal fractionation melting peak showed a similar a consistent trend with the annealed DSC crystallinity calculation. The homopolymer had a decrease in crystallinity as the sample identifier increases which was done to probe the effect of crystallinity. The random copolymers and impact copolymer samples had a smaller area as the ethylene content increase. The branched samples had a consistent area which was also seen in the DSC crystallinity. The addition of the branches seem to have no effect on the amount of crystalline lamellae but the thickness of the lamellae increased with high levels of branching. Table 21 contains the values for the area under the curve.

Table 21. Area Under Thermal Fractionation Melting Peak

	HP1	HP2	HP3	RP1	RP2	RP3	ICP1	ICP2	ICP3	BR0	BR1	BR2
Area	20.09	18.10	17.85	13.75	13.25	10.03	19.28	17.36	15.76	14.21	14.05	14.88

Figure 34 shows the comparison between the average lamella thickness by thermal fractionation and by the standard annealed method. The slower crystallization produces slightly thicker lamella compared to the standard annealed. Trends between the two sets of results are still consistent. When the annealed lamella thickness is compared to the rigid phase thickness by ssNMR no clear trend is seen, the graph is shown in Figure 35.

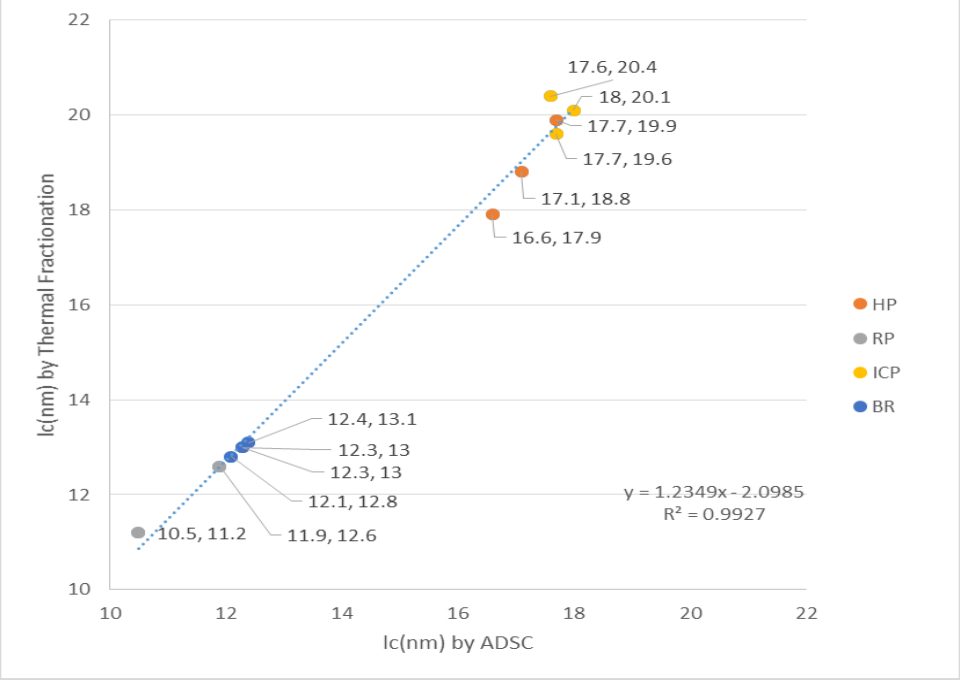

Figure 34. Average Lamellar Thickness for Thermal Fractionation and Annealed DSC

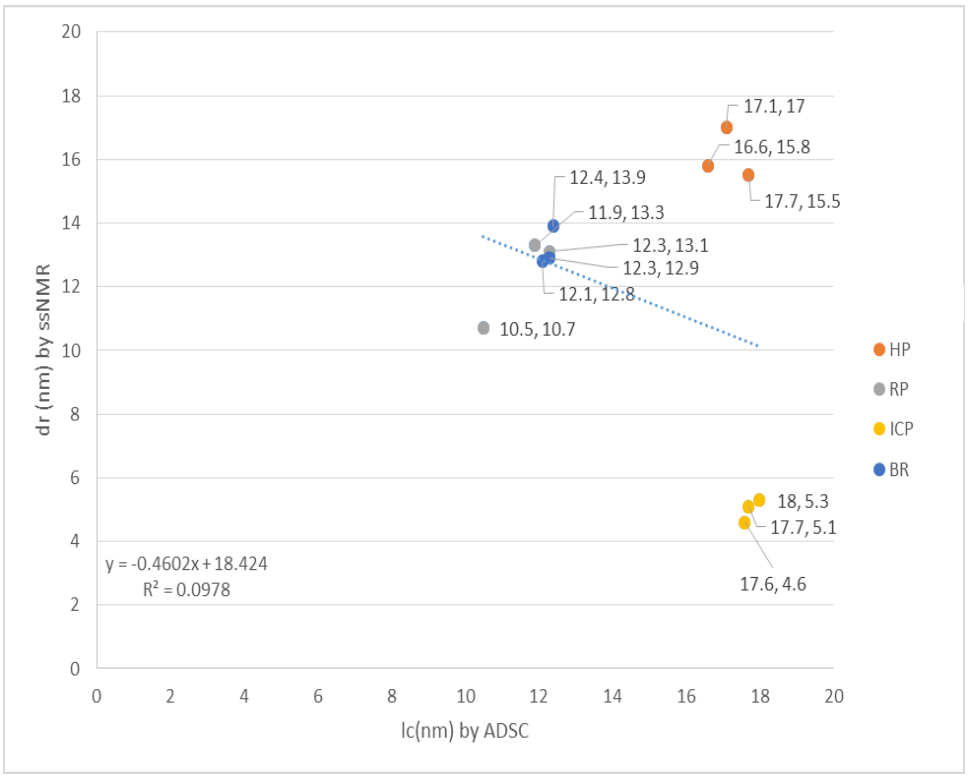

Figure 35. Average Lamellar Thickness by Annealed DSC and Rigid Phase Thickness by ssNMR

5.5 DYNAMIC MECHANICAL ANALYSIS RESULTS AND DISCUSSION

The dynamic mechanical analysis (DMA) results for the homopolymer group were unable to show large differences in the storage modulus results shown in Figure 36. Decreasing crystallinity is typically observed by sharper downward slope after the glass transition for the storage modulus, slight differences were seen but they may not be statistically significant. The first homopolymer samples did show a difference in the tan delta peak area for the glass transition. The expected trend of lower peak area for higher crystallinity was seen for the first

sample but the next two samples were not easily differentiated. The tan delta results are shown in Figure 37 for the homopolymer group.

In the random group, the first two random copolymers, RP1 and RP2 did not show differences in storage modulus or tan delta but RP3 did show the steeper drop in storage modulus after the glass transition and a large area in the tan delta glass transition peak. The increase in the tan delta peak area trends well with the ethylene only slightly increasing from sample RP1 to RP2 but then more dramatically increasing in RP3. The storage modulus shows that same trend where the increasing level of ethylene in RP3 drops the storage modulus. The glass transition also shifts to a lower temperature range as the level of ethylene comonomer increase. This followed the expected trend since polyethylene has a lower glass transition than polypropylene[31]. The random results are shown in Figure 38 and Figure 39.

The impact copolymers showed the best differentiation with increasing ethylene, the storage modulus showed a steeper slope after the glass transition. Also the area under the glass transition curve in the tan delta data showed increasing area with increasing rubber content, as expected. The storage modulus and tan delta graphs for the impact copolymer group are shown in Figure 40 and Figure 41.

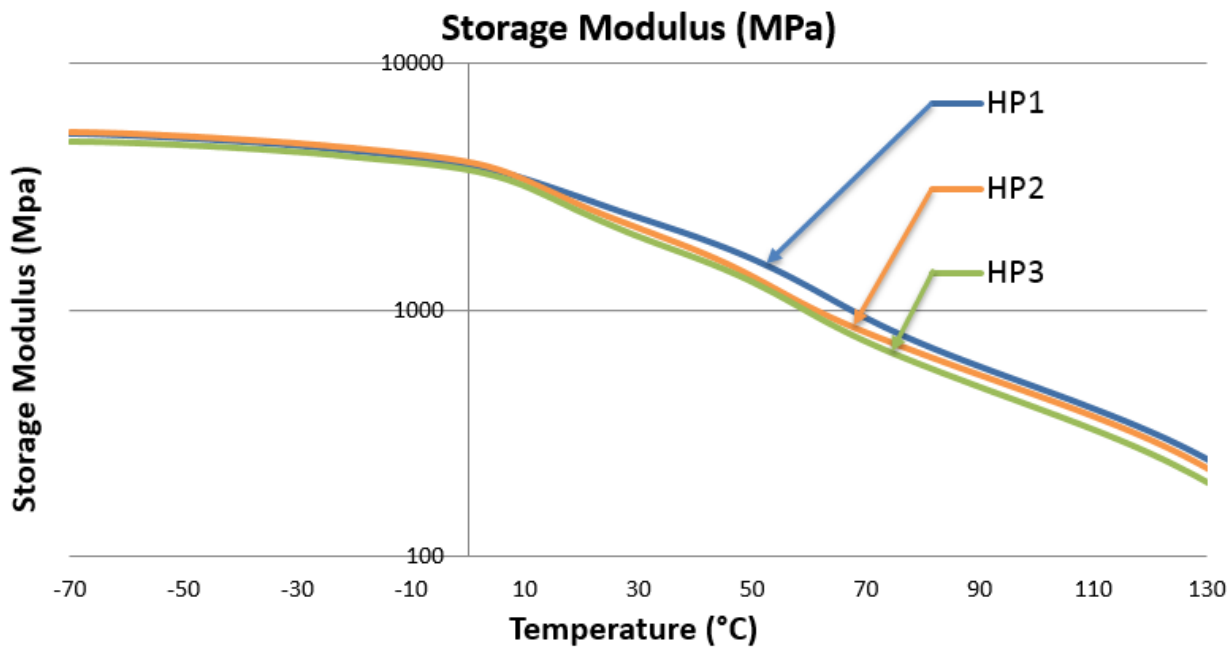

Figure 36. Homopolymer Group Storage Modulus (MPa)

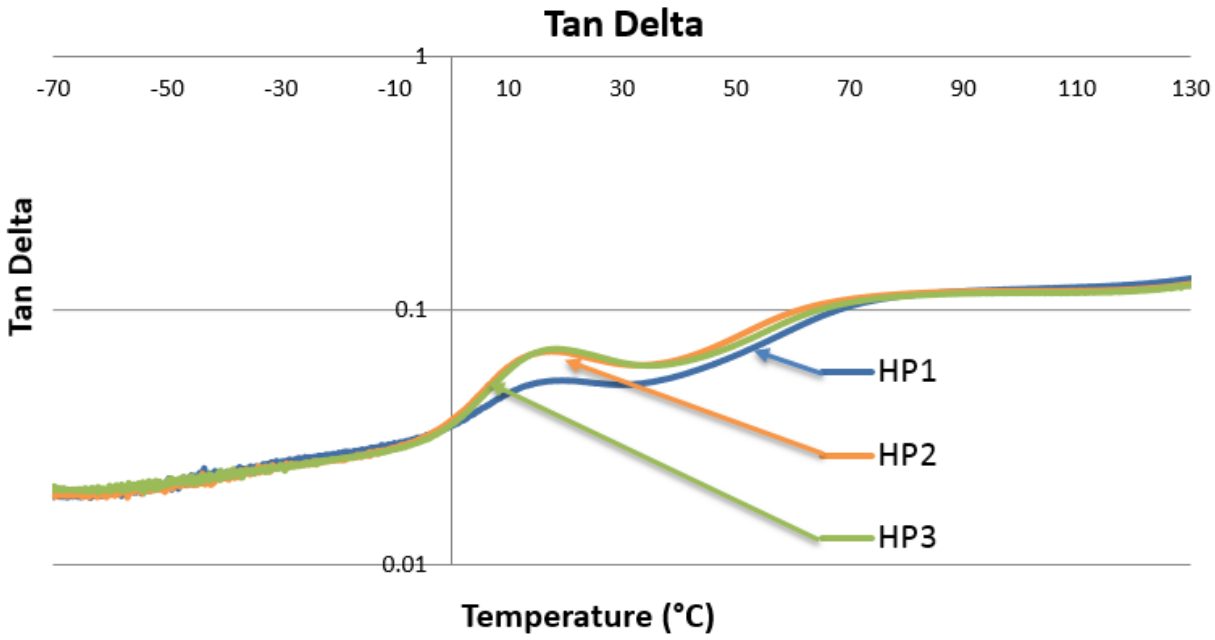

Figure 37. Homopolymer Group Tan Delta

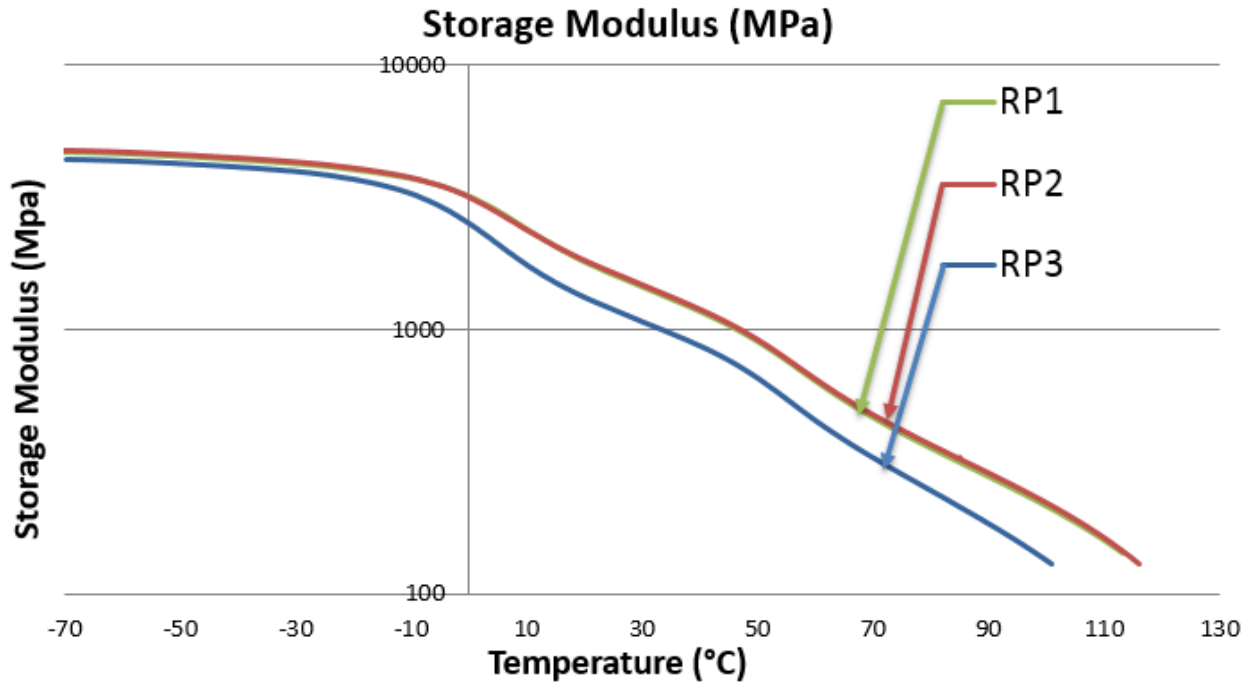

Figure 38. Random Copolymer Group Storage Modulus (MPa)

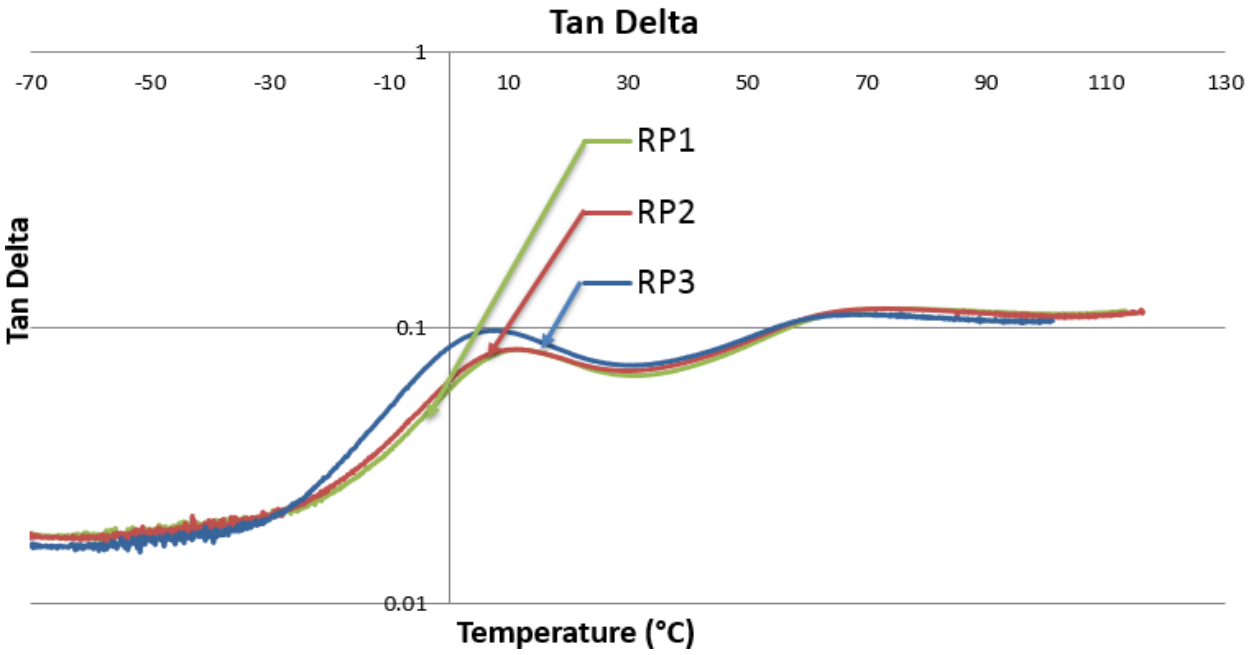

Figure 39. Random Copolymer Group Tan Delta

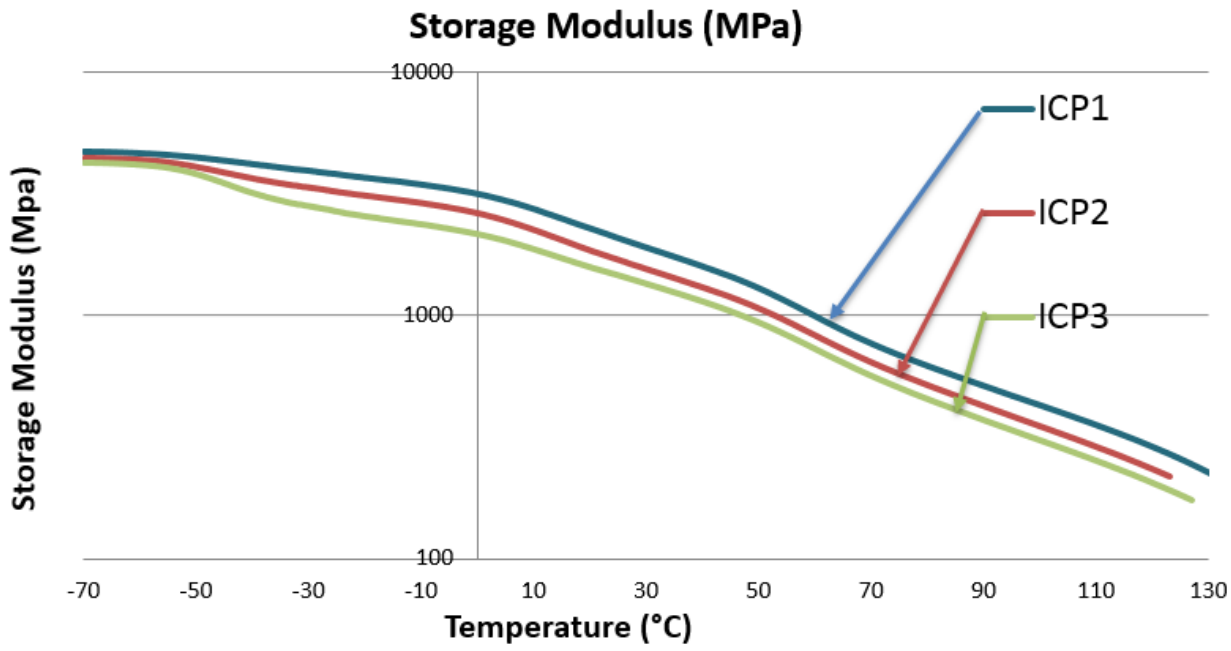

Figure 40. Impact Copolymer Group Storage Modulus (MPa)

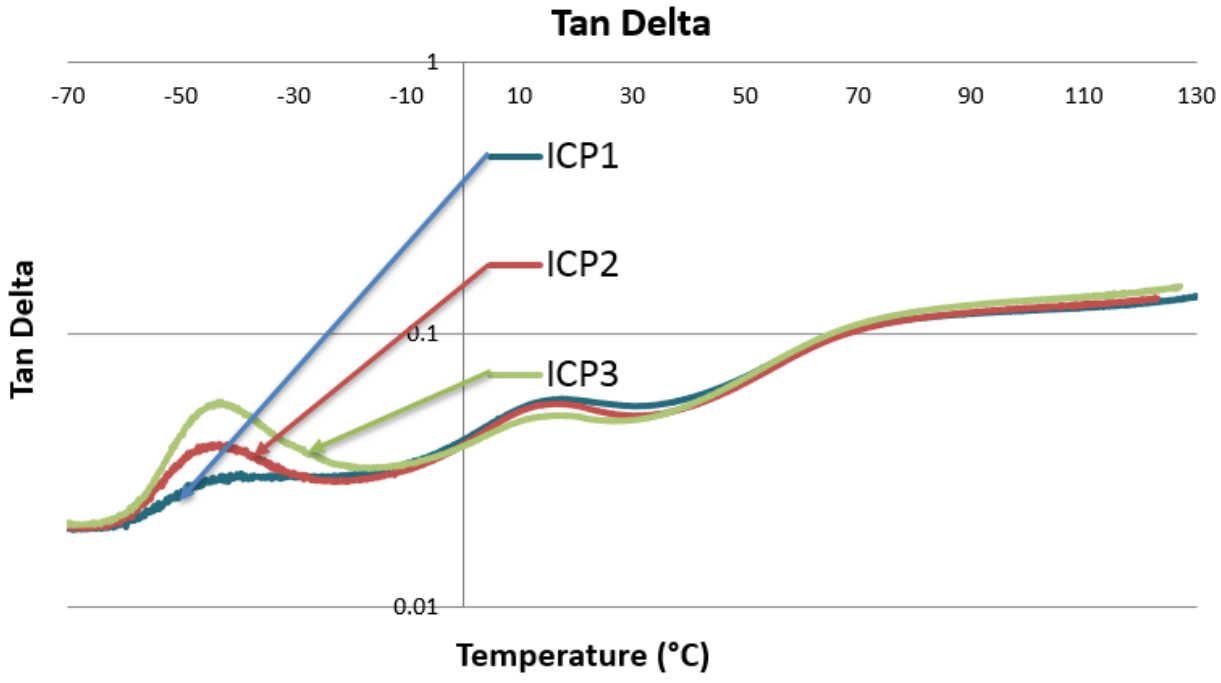

Figure 41. Impact Copolymer Group Tan Delta

The branched sample set showed a steeper slope after the glass transtion for the unbranched referecne Br0 which could be due to additional orientation caused by the long chain branches. Although the crystallinity between the branched and unbranched set does not change, a response similar to increasing crystallinity is seen. This is due to the effect of the entangled long chain branchs in Br1 and Br2. The two branched samples did not show a differentiation in storage modulus or tan delta. The tan delta for the unbranched reference was also very similar to that of the two branched samples. The branched results are shown in Figure 42 and Figure 43.

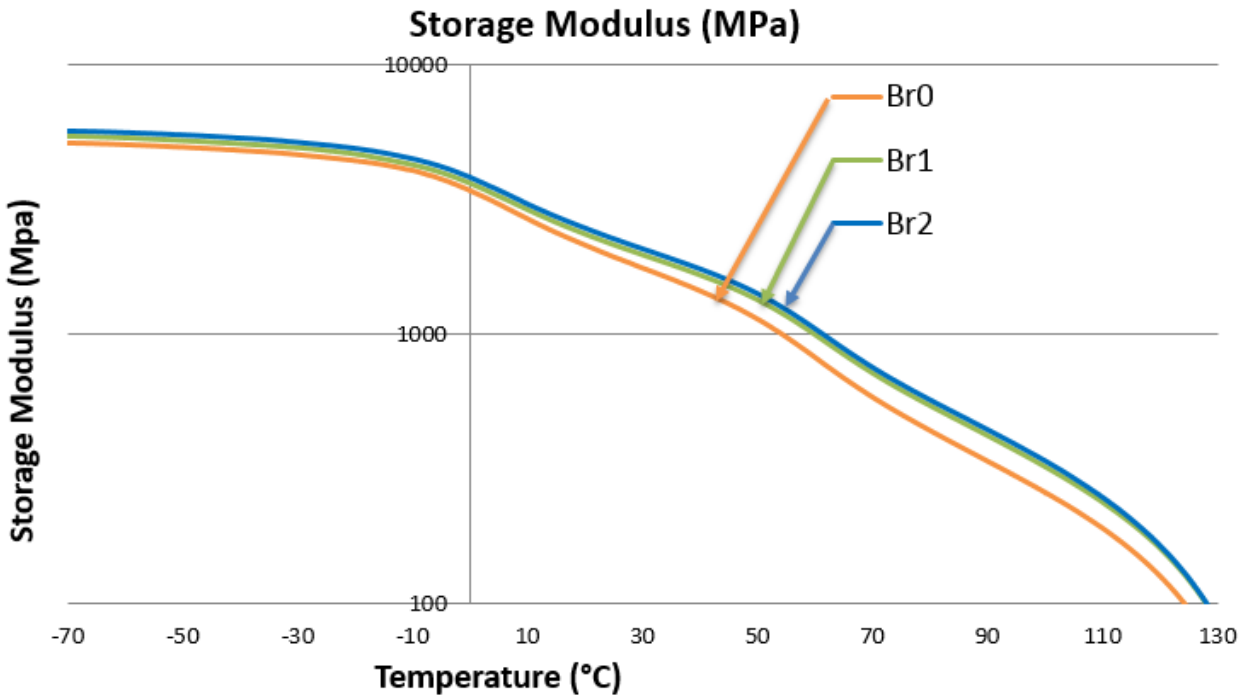

Figure 42. Branched Group Storage Modulus (MPa)

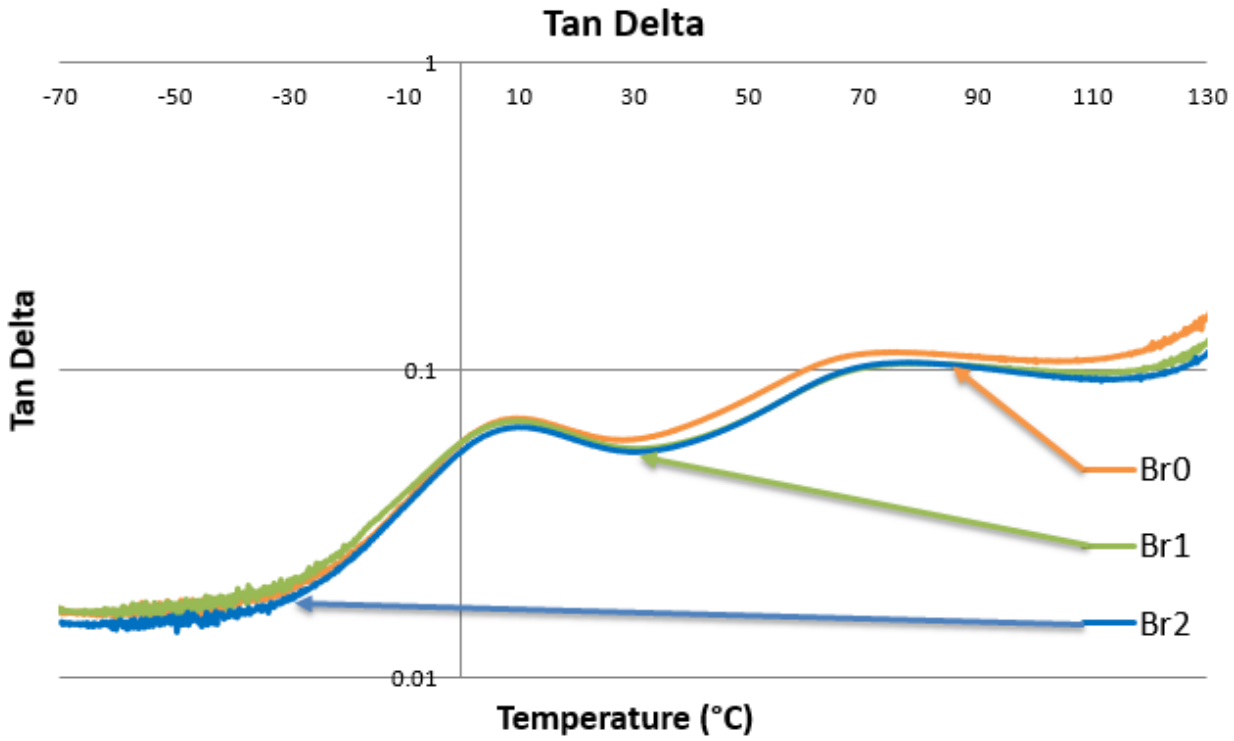

Figure 43. Branched Group Tan Delta

5.6 MECHANICAL RESULTS AND DISCUSSION

The MTS instrument used for the tensile testing, combined with the specimen length used, has a maximum strain of 450 %. If the sample did not break at that point, zeros are recorded for that sample's ultimate stress and break strain indicating a non-break. For the tensile test, samples RP2, RP3, Br1 and Br2 experienced no break at the max strain. No clear trend was seen in stress of the homopolymer set with decreasing crystallinity but this may be due to the high relative standard deviation of 49% for the break stress. The strain results did not show a statistically significant trend greater than the 30% relative standard deviation seen in the test set. The impact

copolymer samples showed increasing strain as ethylene level increased from ICP1 and ICP2 to ICP3. The trends in ultimate stresses were not statistically significant. The addition of branches moved Br0 from break to no break in tensile testing for Br0 to Br1 and Br2. Although the molecular weight of the backbone is similar the addition of branches reduces the MFR of the samples, as seen in Table 1. The ultimate stress and break strain are shown in Figure 44 and Figure 45, respectively.

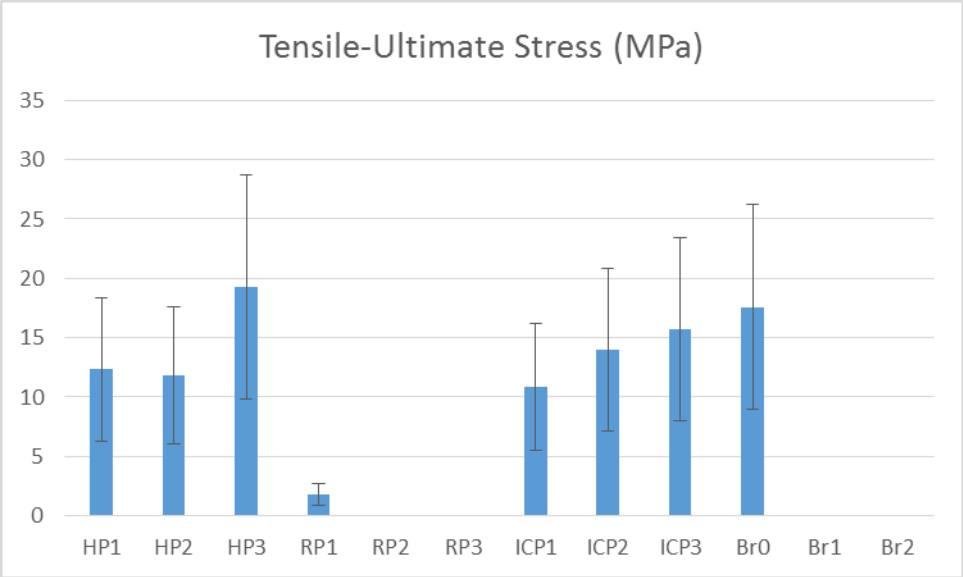

Figure 44. Tensile Break Stress (MPa)

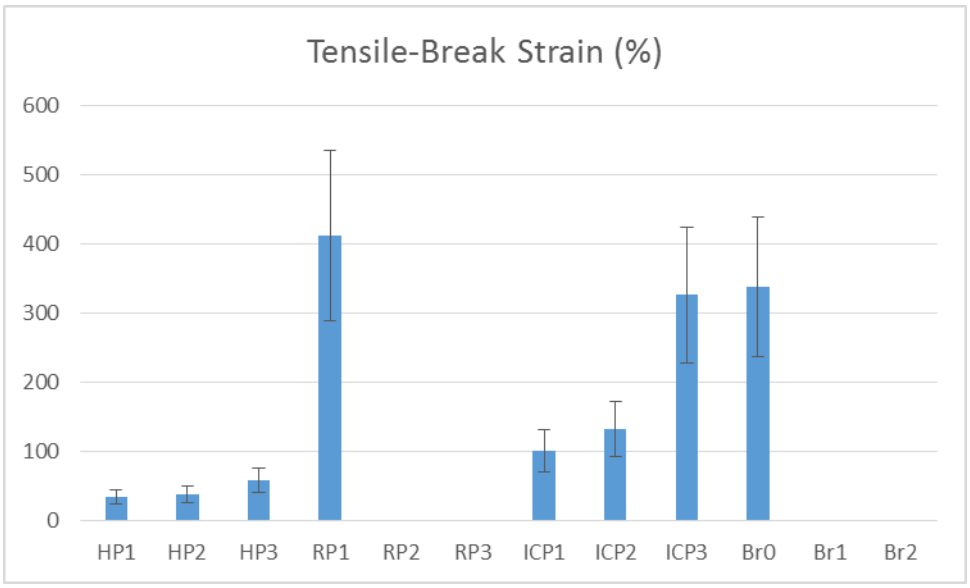

Figure 45. Tensile Break Strain (%)

For the homopolymer samples, as the crystallinity decreased the yield stess decreased and the yield strain increased. The random copolymers showed decreasing stress with increasing ethylene. The strain at yeild did also increase with increasing ethylene when comparing RP1 and RP3. The difference in ethylene between RP1 and RP2 was small and did not show a change in strain at yeild. The impact copolymer grouping showed decreasing stress and strain at yield as ethylene increased. The branched samples Br1 and Br2 showed a small jump in yield stess when compared to the unbranched linear Br0 reference, however, no increase was seen with increasing branching. The change in tensile yield strain was negligable for the branched samples. The results for the yield stress and yield strain are shown in Figure 46 and Figure 47.

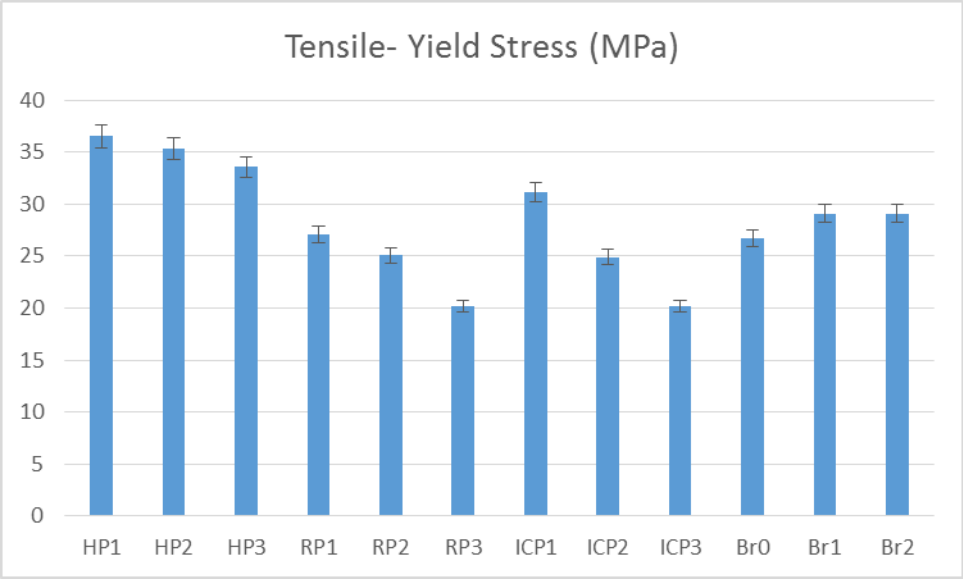

Figure 46. Tensile Yield Stress (MPa)

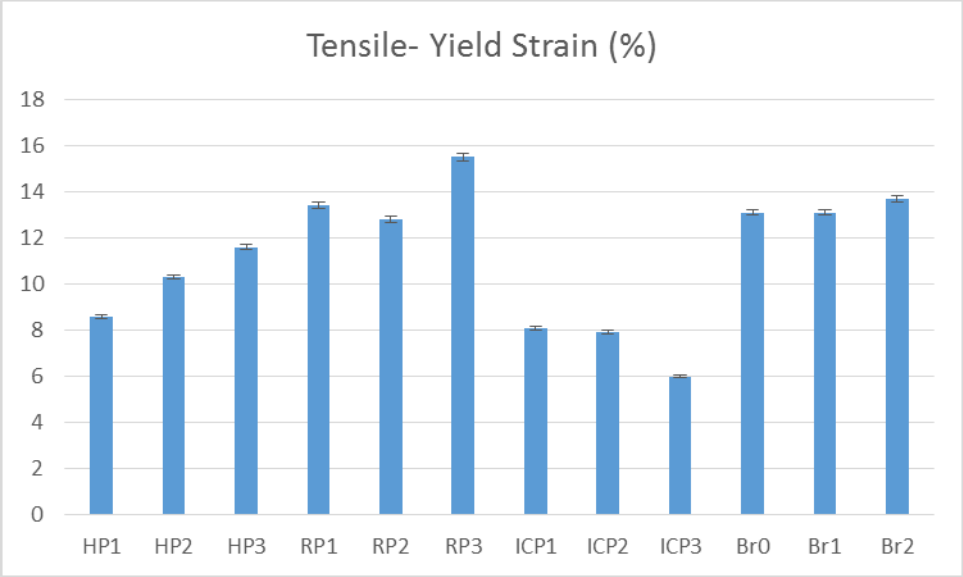

Figure 47. Tensile Yield Strain (%)

The tangent modulus shows clear trends for all four sample groups. As the level of crystallinity decreases for the homopolymer set, the tangent modulus reduces. Both random and impact copoymers show a decrease in the modulus as ethylene level increases. The branched samples showed no change with branching or increased branching. The results for tangent modulus are shown in Figure 48.

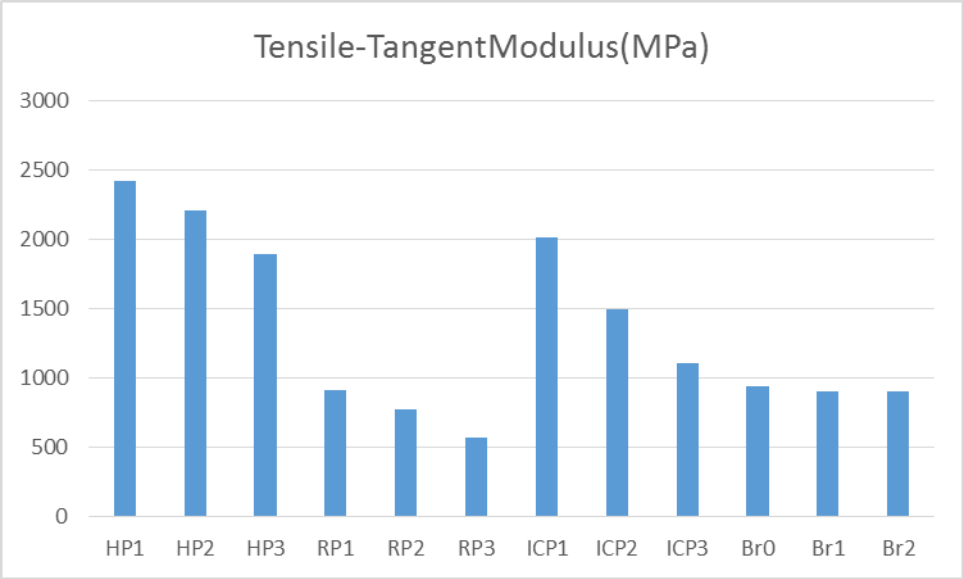

Figure 48. Tensile Tangent Modulus (MPa)

The flex results for 1% secant modulus show a decrease in modulus as the level of crystallinity decreases as expected. The random and impact copolymers also show the expected results, where in their case the drop in modulus is seen with increasing ethylene which also does reduce crystallinity. The branched samples again show an increase with branching compared to the linear control but no change between the levels of branching. The same trends are seen in the

four group's results for the flex's tangent modulus. The flex 1% secant modulus and tangent results are shown in Figure 49 and Figure 50.

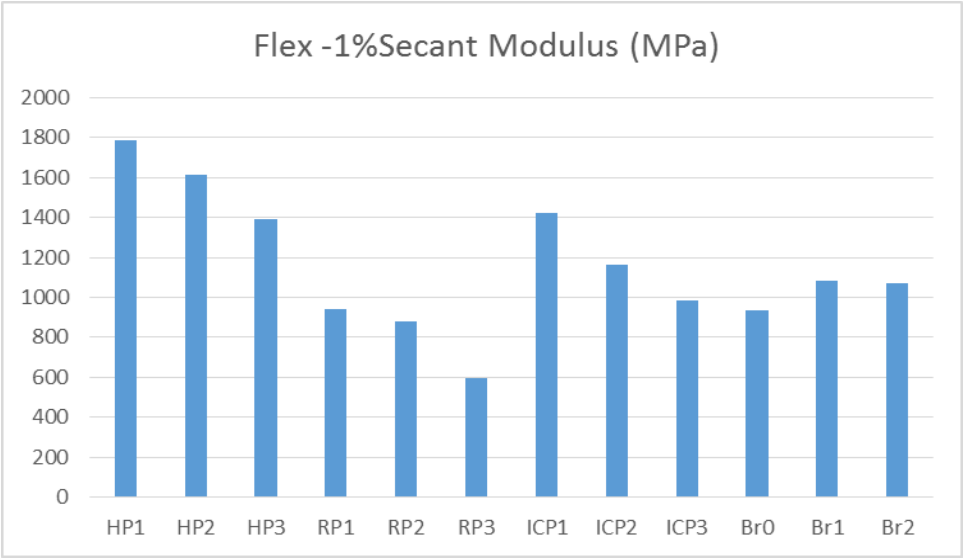

Figure 49. Flex 1% Secant Modulus (MPa)

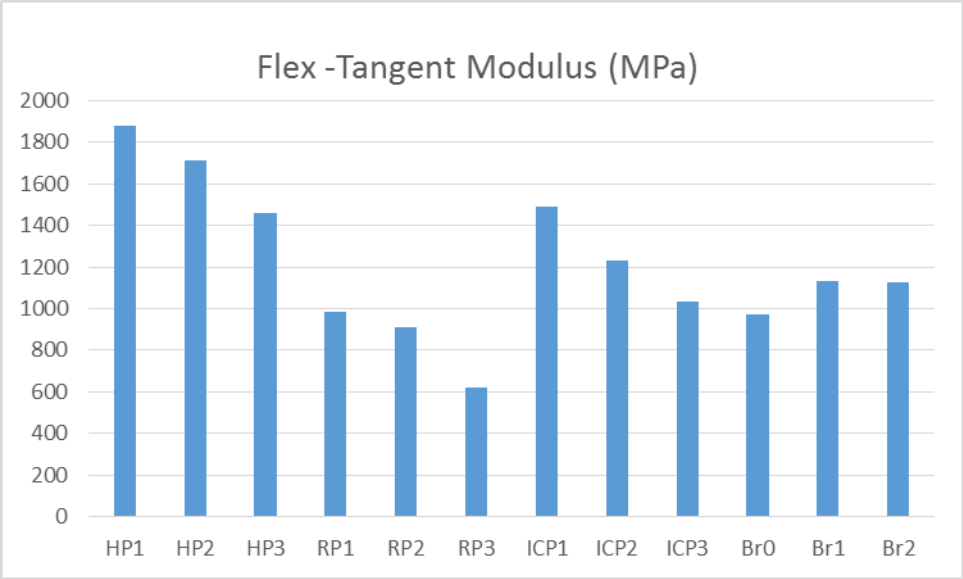

Figure 50. Flex Tangent Modulus (MPa)

The homopolymer samples all showed low average break strength with all complete breaks which is typical for homopolymer samples. The random samples were also all complete breaks but the break strength was higher than the homopolymer samples. The crystallinity of the random set were all lower than the homopolymer set and due to the improved energy absorption seen with amorphous materials the trend seen is expected. RP2 also has a slightly lower molecular weight which would cause a drop in the impact energy. As expected the ultimate strength increased with increasing rubber for the impact copolymer samples. The sample ICP3 showed all non-break performance. For the branched samples the presence of branching did increase the ultimate strength slightly but showed no difference with increasing level of branching. The increase in ultimate strength can be explained by an increase in entanglement or increasing crystallinity.

The homopolymer set all showed low Izod impact strength, as expected for homopolymer polypropylene. The random and branched set also had low Izod values but differentiation was seen for the branched set. In Zhou at el., both increased crystallinity and impact strength were seen for branched samples compared to a linear reference[32]. For Br0, Br1 and Br 2, no increase in crystallinity was seen in the DSC data indicating that the increase in impact strength is due to increased entanglements. As expected, the impact copolymer set showed the largest change in Izod strength. As the amount of ethylene increases, along with the amount of rubber, so did the impact strength. The first sample also showed a complete break type, whereas, the second was mixed with both complete and partial. The third sample showed non break indicating a ductile sample were the others were brittle or brittle ductile. The Izod results are shown in Figure 51.

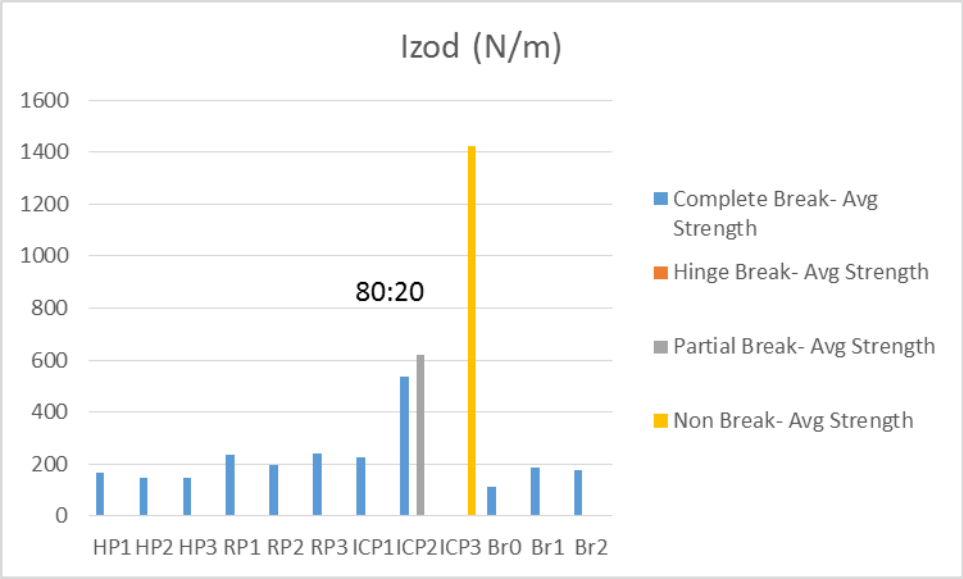

Figure 51. Izod Average Strength (N/m)

The instrumented drop impact (IDI) showed increasing average total energy with decreasing crystallinity for the homopolymer group. The maximum load, average energy at maximum load, and average deflection at maximum load, all showed the same trend as the average total energy in the homopolymer group. The break also changed from brittle to ductile as the crystallinity decreases for the homopolymer group. The IDI impact is an applied biaxial stress and did show improved impact as the crystallinity dropped. Whereas, in the previous Izod testing, the impact is tested with crack propagation in a notched sample and saw no difference with decreasing crystallinity. The random copolymer set showed little change with increasing ethylene for all parameters and they also all showed ductile break behavior. The impact samples showed decreasing average total energy, average energy at maximum load and average maximum load as the level of ethylene rubber increases. The average deflection at maximum load shows the opposite trend. All impact copolymer samples showed total ductile break. The branched samples

showed decreasing average total energy, average maximum load, average energy at maximum load, and average deflection at maximum load as the level of branching increased. The break type also transitioned from mixed ductile/brittle to fully brittle with increasing branching, which was not expected. It should be noted that the IDI testing showed the largest sensitivity for detecting differences in the amount of branching instead of simply the transition from linear to branched. It should be noted that the Izod showed improved impact with the addition of branching, however it should again be clarified that Izod and IDI probe different types of impact. The IDI results are shown in Figure 52 to Figure 56.

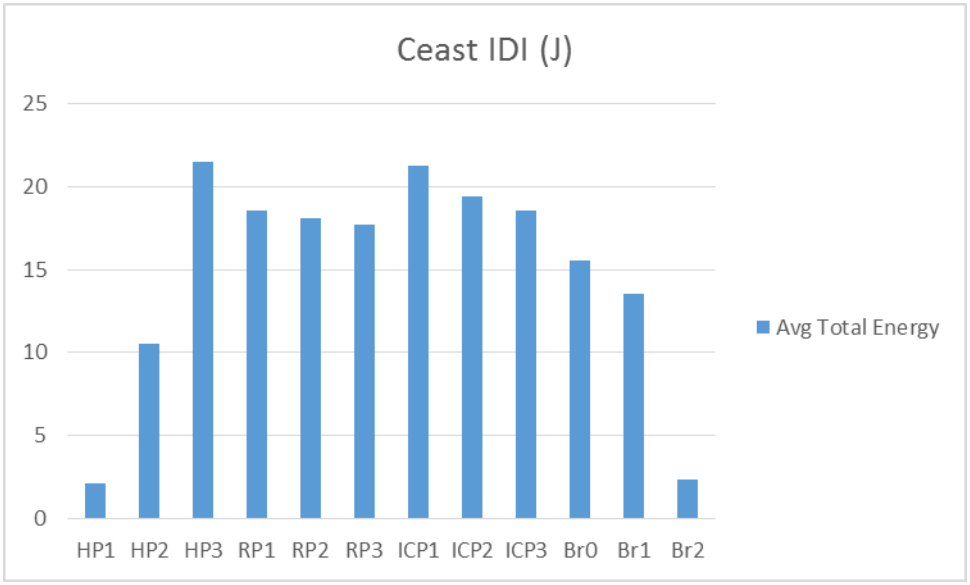

Figure 52. Instrumented Drop Impact Ceast Average Total Energy (J)

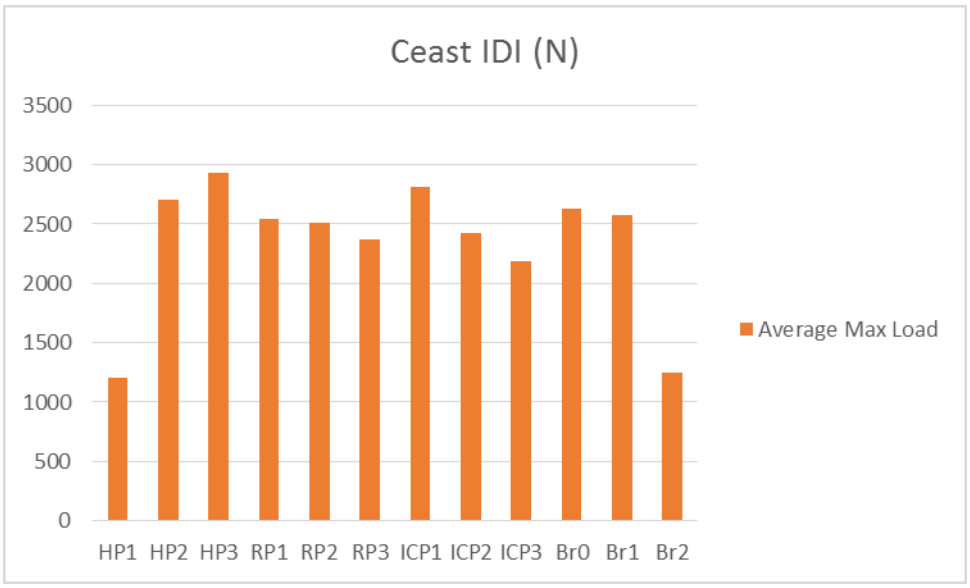

Figure 53. Instrumented Drop Impact Ceast Average Max Load (N)

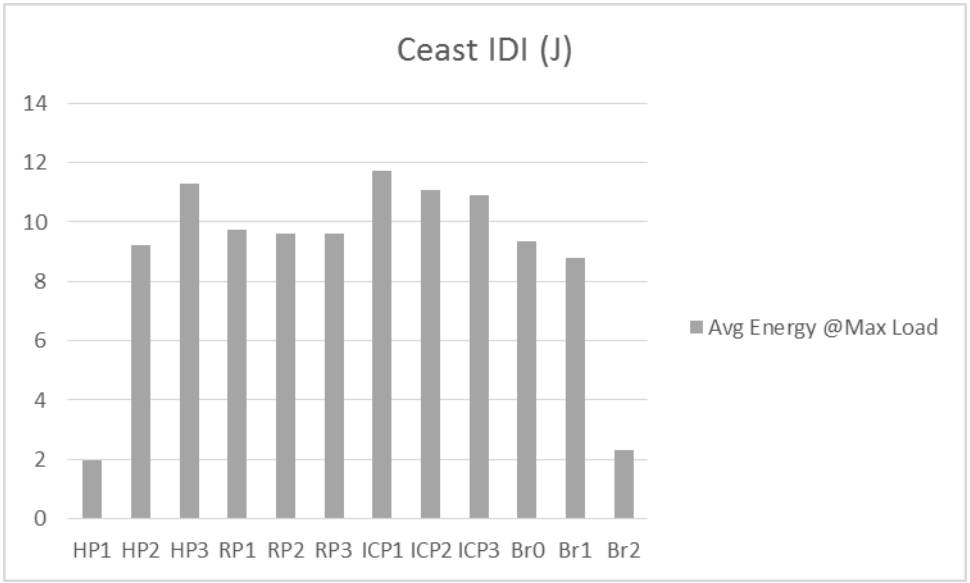

Figure 54. Instrumented Drop Impact Ceast Average Energy at Maximum Load (J)

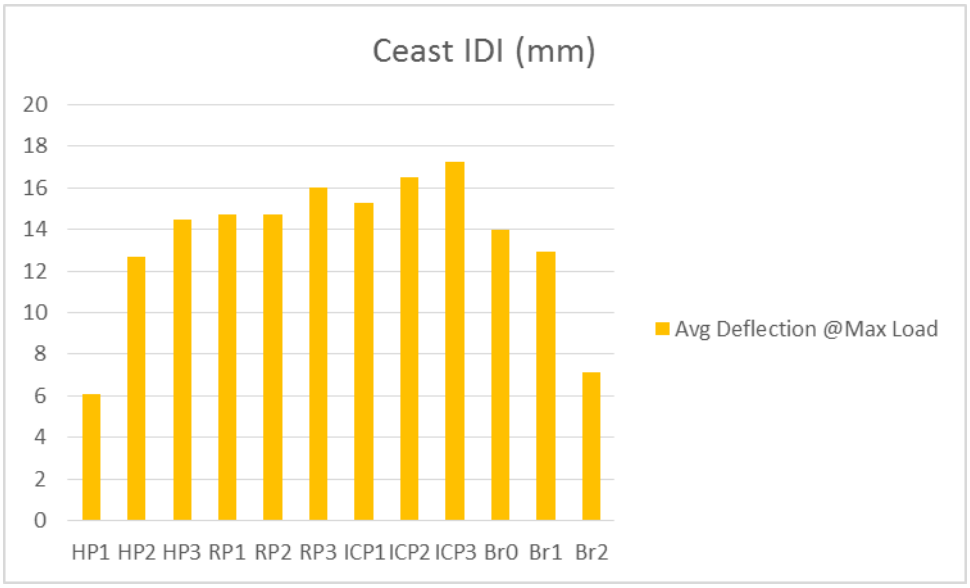

Figure 55. Instrumented Drop Impact Ceast Average Deflection at Maximum Load (mm)

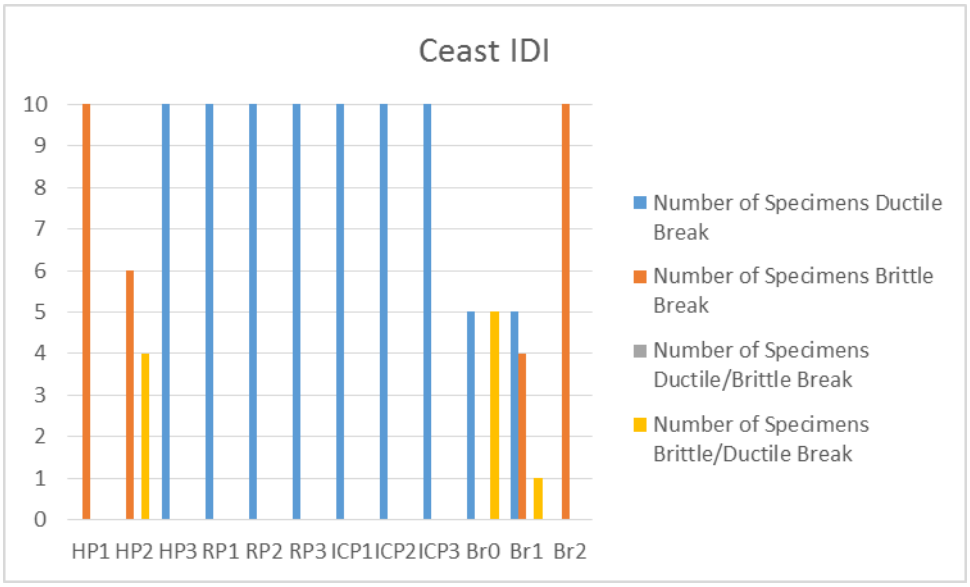

Figure 56. Instrumented Drop Impact Ceast Number of Specimens with Different Types of Breaks

The literature shows that increasing the amorphous content of a sample lowers the modulus if the lamellar thickness is relatively constant[14]. This effect was seen in the homopolymer, random, and

impact copolymer sets for the tensile tangent modulus, the flex tangent modulus, and the flex secant tangent modulus. Figure 57 to Figure 59 shows the linear trend of increasing crystallinity and modulus. Since the trends captured are a relatively good fit, the lamellae of the samples shown are relatively similar. This is supposed by the annealed DSC data that showed a range in lamella thickness of 10.54 nm to17.65 nm, which is a relatively small range.

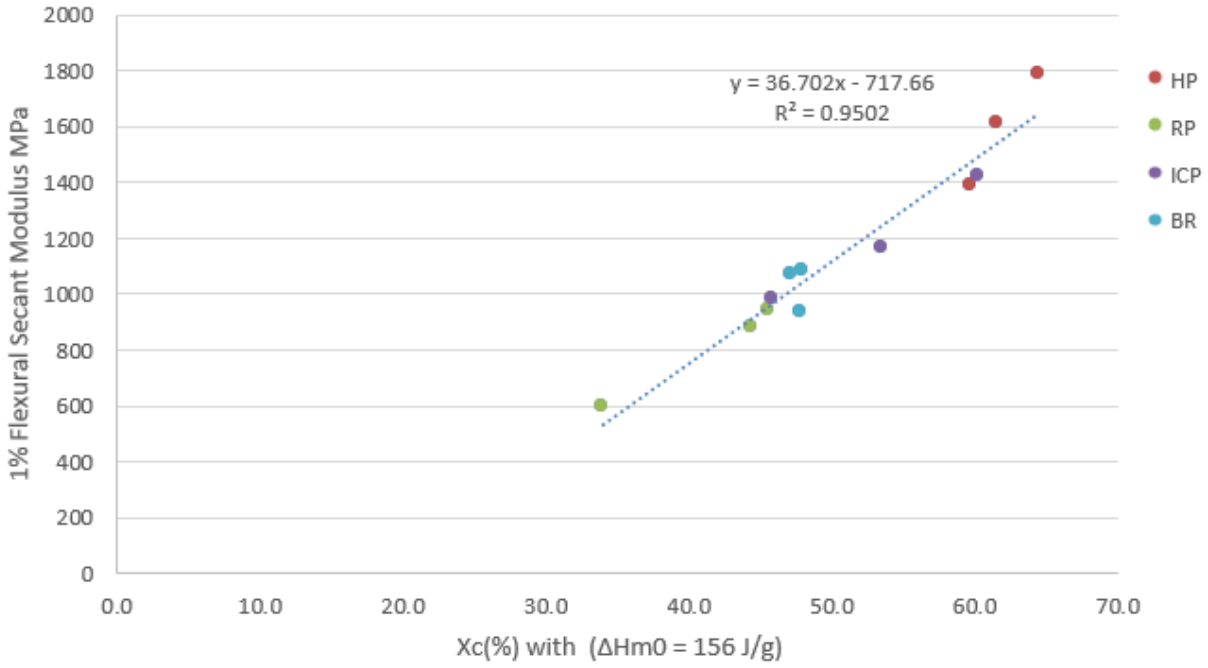

Figure 57. Sample Crystallinity's Effect on 1% Flexural Secant Modulus MPa

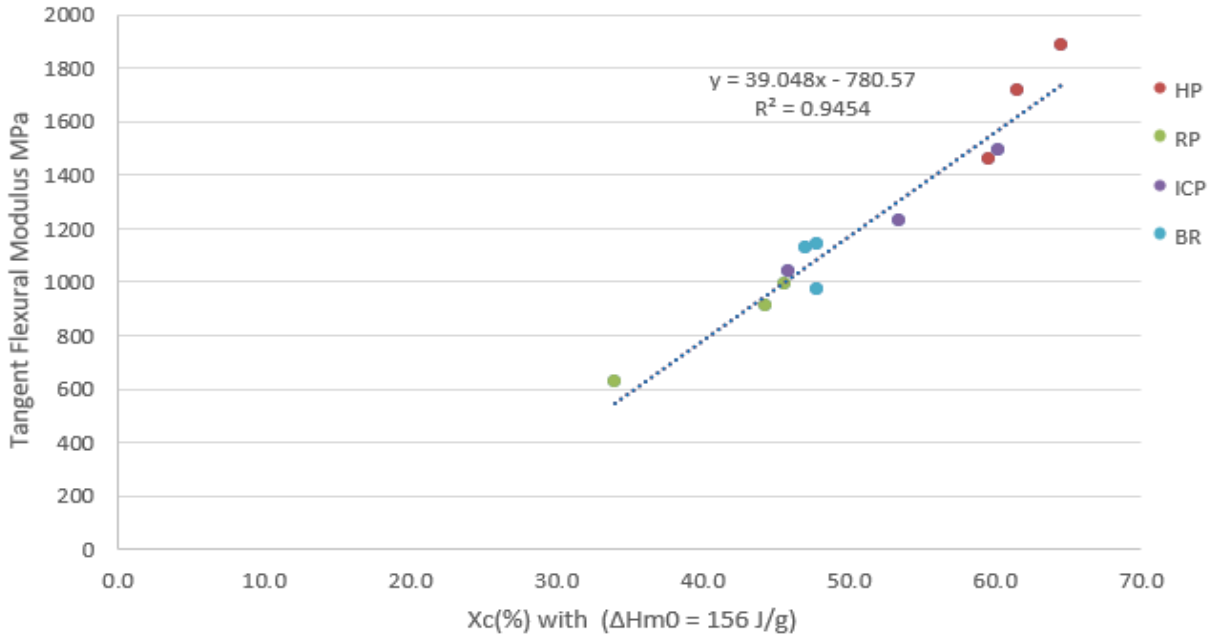

Figure 58. Sample Crystallinity's Effect on Tangent Flexural Modulus MPa

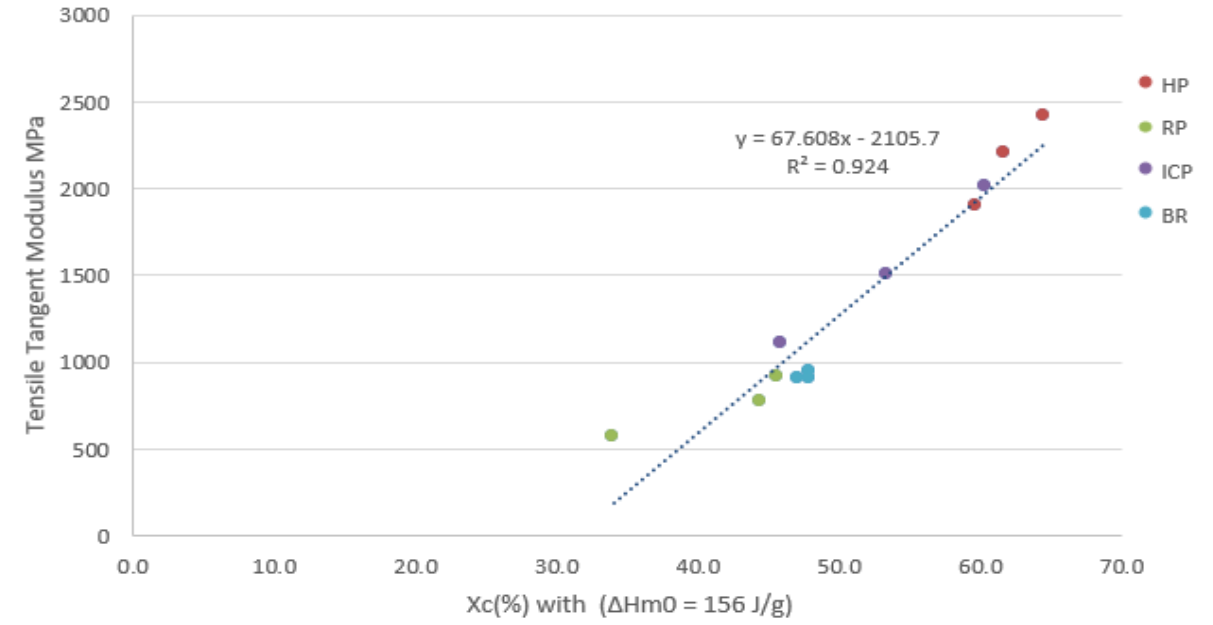

Figure 59. Sample Crystallinity's Effect on Tensile Tangent Modulus MPa

Yield stress has also been shown to increase as the lamella thickness increases[14]. The yield stress was found to increase with the ADSC l_c values for a given sample set which is shown in Figure 60. If the yield stress is compared based on crystallinity the samples collapse into a linear line expect for the impact copolymer sample set. The more rubber in the impact copolymer sample the farther the sample is shifted from the linear line, the graph is shown in Figure 61. A similar effect is seen with yield strain, all samples collapse onto a linear line, but the impact copolymers fall off the line. Again more rubber causes the samples to drop farther from the linear trend. The graph for yield strain and crystallinity is show in Figure 62.

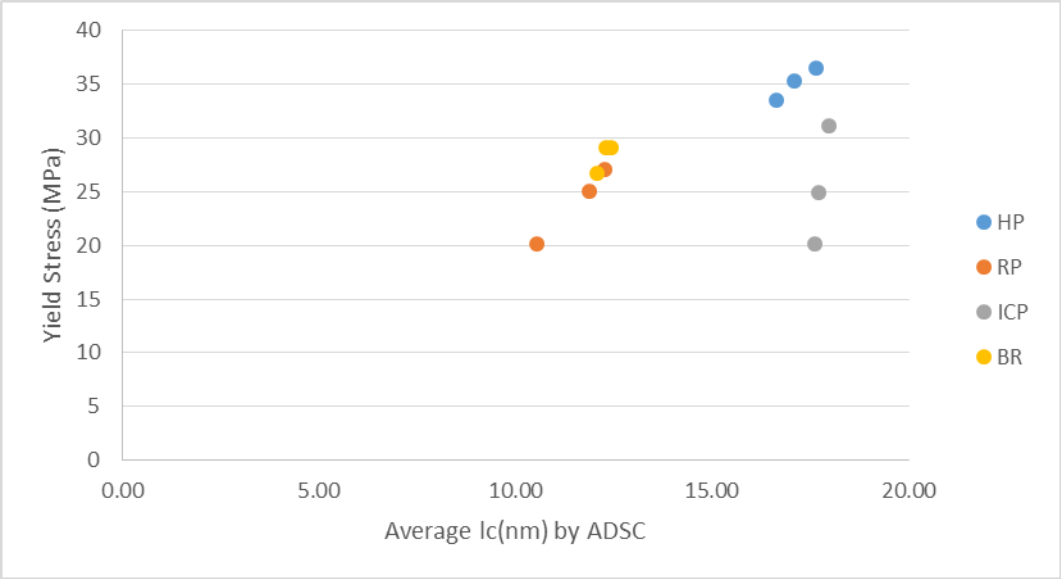

Figure 60. Crystalline Lamella Thickness and the Effect on Yield Stress

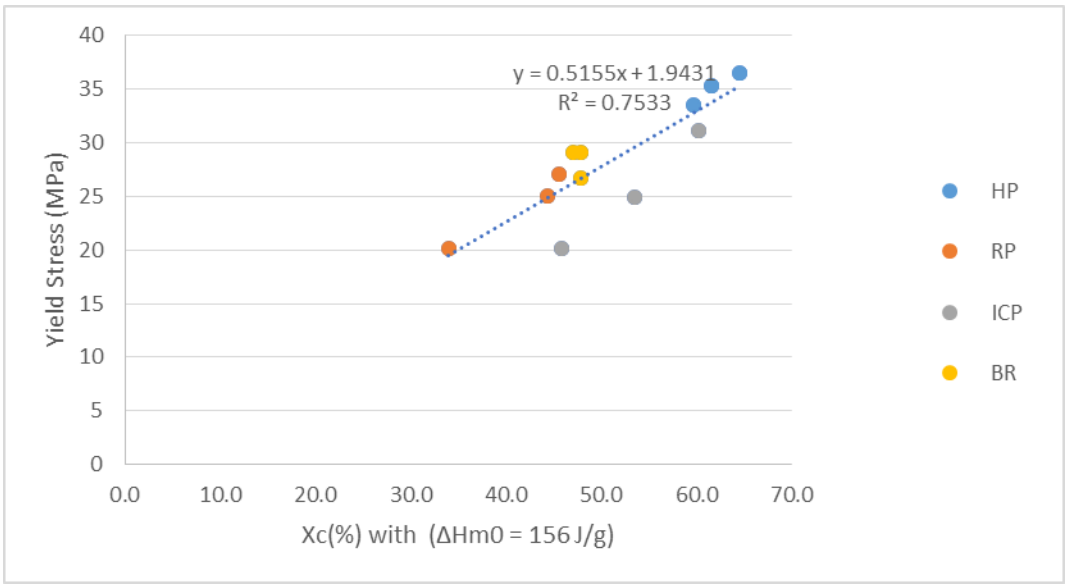

Figure 61. Crystallinity and the Effect on Yield Stress

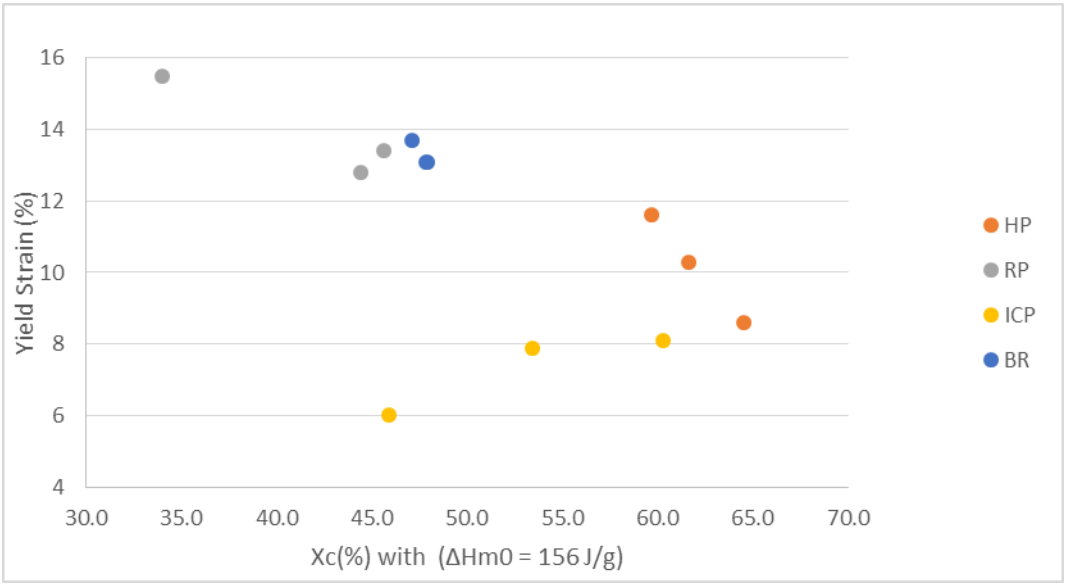

Figure 62. Crystallinity and the Effect on Yield Strain

Increasing lamella thickness has been shown to lower the dart impact strength due to a reduction in tie molecules if the molecular weight distribution is constant between samples[16]. The homopolymer and branched samples show the expected trend. No change is seen for the random samples and the oposite trend is seen for the impact copolymer set, however the increase in ethylene-propylene rubber is dramatically changing the impact properties. The amorphous lamella thickess of the impact copolymer samples were also show to increase which could be acting against the changes in the crystalline lamella thickness. Large amorphous phases allows for larger cracks to form and can lead to earlier breaks[15]. The plot is shown in Figure 63.

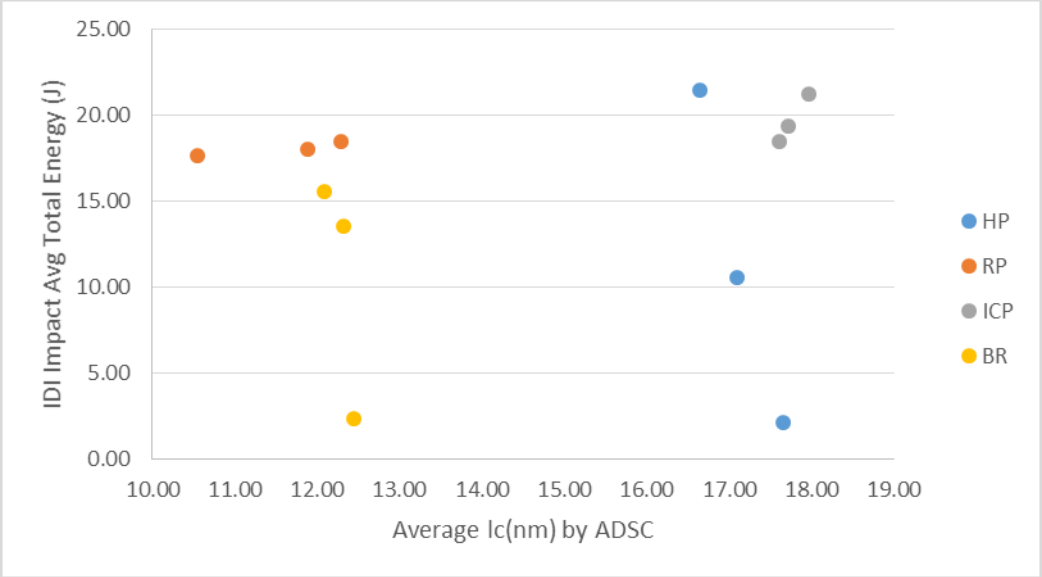

Figure 63. Crystalline Lamella Thickness and the Effect on IDI Impact

6.0 CONCLUSION

NMR solution state tacticity results showed that for the homopolymer sample set, decreasing crystallinity showed decreasing meso pentad percent, as expected. The random and impact copolymers showed the same trend: increasing ethylene caused the crystallinity and meso pentad to decrease across the individual sample sets. The branched samples showed a slight increase in meso pentad as the amount of branching increased, but the crystallinity across the samples were found to be constant. The slight change in meso pentad may not be statistically significant.

The NMR solution state ethylene incorporation results showed increasing ethylene weight percent across the random and impact copolymer as expected. Samples were chosen to achieve an increasing ethylene level. The blockiness (EEE mole%) of ethylene across the random set was found to be relatively constant. The impact copolymer set showed a sharp increase as the level of ethylene in the total samples, and ethylene in the ethylene-propylene rubber particle increased. The higher level of blocky ethylene in the ICP3 sample most likely contributed to the crystalline polyethylene detected in the annealed DSC results.

For the homopolymer samples, the soft and rigid fraction found by solid state NMR showed excellent agreement with the amorphous and crystalline fractions found from annealed DSC. For the set of random samples ss-NMR and DSC showed similar trends, but the solid state rigid fraction was found to be almost twice the crystallinity found from ADSC. The impact and branched samples, similar to the random set, showed significantly elevated values for the rigid

fraction measured by ssNMR when compared to the crystallinity by ADSC. This offset in values may be explained by small sections of ethylene rich regions in the chain that can't crystallize but are also not mobile due to being pinned by a crystalline lamella or constrained fold. The impact copolymer sample set shows the same trend for the crystallinity by ADSC and rigid fraction by ssNMR for the first two samples, showing a drop between ICP1 and ICP2. ICP3 showed a decrease in crystallinity for the crystallinity by ADSC but increases for the rigid fraction by ssNMR when compared to ICP2. This increase could be explained by the small amount of crystalline polyethylene detected in the ADSC but whose peak area was not included in the crystallinity calculation for ADSC. Finally, the branched set showed no change in crystallinity across the sample set, whereas the rigid fraction from ss-NMR increased with the level of branching.

Values of rigid and mobile phase thickness calculated from Solid state NMR were found to have an error in precision of 5%. When error bars were applied to the samples, changes within sample sets were not found to be statistically significant. In order to improve repeatability, additional mixing times (t_m) for the spin diffusion experiments would need to be added in both the low and high range to provide a more precise $t_{m0}^{1/2}$ value and thereby a more accurate rigid thickness. The method is effective only if large changes in rigid and mobile phase thickness are being observed.

Thermal fractionation stepwise crystallization differential scanning calorimetry was used to generate a histogram distribution of the lamellar thickness. The samples were slowly cooled which allows the chains to have more time to correct and thicken the lamellae. The area under the curve was found to trend with the crystallinity found by standard annealed DSC. Higher meso pentad levels were found to also correlate to higher lamellar thicknesses for the

homopolymer set. The increase ethylene in the random set was shown to decrease the fraction of lamellae between 73- 85 monomer units long. The impact copolymer set showed no clear trend which may be due to the fact that the ethylene is only within the ethylene propylene rubber and that the majority of the sample is still a homopolymer matrix. The branched showed thicker lamella as the amount of branching increased which was an unexpected result. The thicker lamellae were not seen in the ADSC results but the additional time in the thermal fractionation run may have allowed the required relaxation time for the chain to sufficiently untangle and crystallize.

The dynamic mechanical analysis data for the samples were used to probe the amorphous fraction of the sample. The area under the glass transition seen in the tan delta graph can be used to indicate the amorphous fraction. The DMA results showed sample HP1 had significantly less amorphous content then HP2 and HP3 but the latter two were not distinguishable. The random set's results showed clear differentiation between RP1 or RP2 and RP3. The difference between RP1 and RP2 was not judged to be significant. The impact copolymer samples showed the best differentiation in the area under the glass transition of the ethylene-propylene rubber domain. The glass transition of the polypropylene peak for the impact copolymer also showed that ICP3 had significantly less amorphous homopolymer. This supported the thicker lamella found by thermal fraction for the ICP3 sample compared to ICP2.

Annealed and thermal fractionation stepwise crystallization differential scanning calorimetry were shown to both effectively probe the lamella thickness and the amorphous phase thickness of homopolymer, random, impact copolymer, and branched polypropylene samples. Predictive trends were seen between crystallinity, meso pentad mole percent, dynamic mechanical analysis, mechanical properties, and the lamella and amorphous phase thickness.

Solid state NMR provided useful insight into the fraction of rigid and mobile phases in the samples. Rigid thickness and mobile thickness were calculated using spin diffusion solid state experiments but proved to have precision errors larger than the differences within a sample set.

The work discussed has shown a number of new techniques to investigate branched polypropylenes. Using GPC-IR and NMR, the number of branching points can be detected but the lengths of the branches are not accessible unless they are well below the entanglement limit. Rheology can be used to probe some of these effects, however model compounds may be needed. The solid state CPMAS runs were able to differentiate the two branched samples from each other which was impossible for a number of other techniques such as DMA, and solution state NMR. Future work could test the sensitivity of the CPMAS runs to determine if the rigid fraction calculated is strongly effected by only long chain branches and independent of shorter branches. However, additional work is needed to optimize the spin lock time to correctly separate amorphous and crystalline signals for copolymer samples.

Thermal fractionation and annealed DSC also proved effective in differentiating the two branched samples. With the application of the Thomson-Gibbs equation, the lamellae were shown to increase with increasing branching. In order to validate this effect, SAXS and AFM are recommended. However, it is important to note that the changes to average lamellar thickness were small, and understate the major difference evident when comparing the histograms in Figure 33 the thermal fractionation run, which shows the fraction of lamellae at bin lengths of flawless regular sequence I in monomer units.

In summary, the findings of the work are:

1. Branching was found to increase the rigid fraction.
2. The lamella thickness for branched samples increased with increased branching.

3. The rigid thickness increased with increasing branching.
4. The rigid fraction matched DSC values for crystallinity only for the homopolymer samples but not for copolymer samples, impact samples, or for the branched samples.
5. The lamella thickness matched the rigid thickness for all samples except the impact copolymer set.

For the branched set to have an increasing rigid fraction as branching increases but constant crystallinity some amorphous material must be behaving more like the lamella. It is believed that crosslinks or excluded branching points may cause the branches to appear rigid when measured in the solid state CPMAS spin lock experiment, Figure 64 is a proposed structure. The orange line represents a branched chain in which both the backbone and the branch are folded into the lamella.

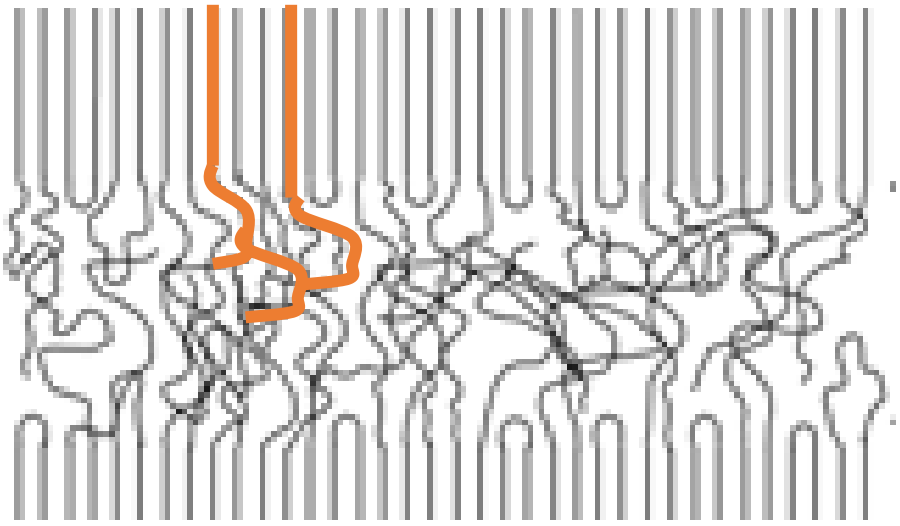

Figure 64. Lamellae Structure with Branch-Proposed Structure

Both solid state NMR and DSC show that increasing branching increased the lamella thickness. When the thermal fractionation melting peak is viewed in Figure 32, a distinct peak is seen for a crystal melting at ~160 ˚C for the two branched samples. The linear sample, BR0, is relatively flat at ~160 ˚C. The area of the peak also trends with the amount of branching, therefore its proposed that the larger molecular weight chains that are created with branching, crystallize after smaller lamella are already formed and due to encroaching thinner lamella, branched high molecular weight backbone and its neighboring own long branch forms into a thicker than normal lamella. The proposed mechanism is shown in Figure 65.

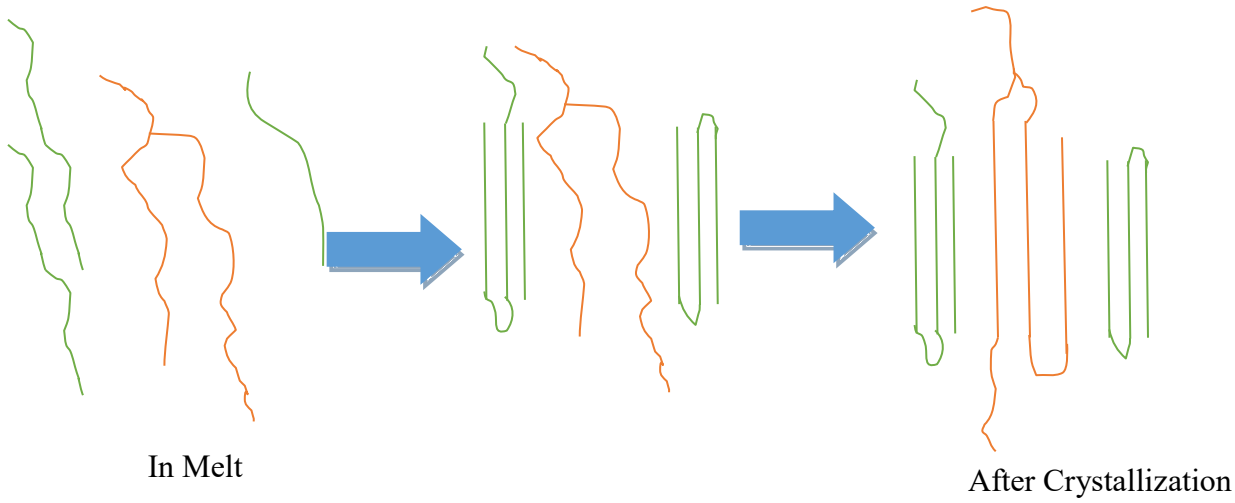

Figure 65. Proposed Mechanism for Thicker Lamellae Seen for Long Chain Branched Samples

The rigid fraction by solid state NMR only matched the crystallinity for the homopolymer sample set. The presence of comonomer in the amorphous domain may have affected the packing and made the relaxation slower, therefore a longer spin lock filter may be needed to allow the amorphous copolymer phase to fully relax.

The lamella thickness from DSC matched well the rigid thickness from ssNMR for all samples expect the impact copolymer set. The heterophasic nature may have caused the discrepancy since the ethylene proplyene rubber domain would be observed but is not present in a packed crystalline/amorphous macro structure.

BIBLIOGRAPHY

[1] Lotz, B., et al. “Structure and Morphology of Poly(Propylenes): a Molecular Analysis.” Polymer, vol. 37, no. 22, 1996, pp. 4979–4992., doi:10.1016/0032-3861(96)00370-9.

[2] Janimak, James J., et al. “Isotacticity Effect on Crystallization and Melting in Poly(propy1ene) Fractions. 2. Linear Crystal Growth Rate and Morphology Study.” Macromolecules, vol. 24, no. 1991, 1991, pp. 2253–2260.

[3] Marigo, Antonio, et al. “ Influence of Regioirregular Structural Units on the Crystallization of Isotactic Polypropylene.” J Appl Polym Sci, vol. 79, 2000, pp. 375–384.

[4] De Rosa, Claudio et al. “Structure-Property Correlations in Polypropylene from Metallocene Catalysts: Stereodefective, Regioregular Isotactic Polypropylene.” Journal of American Chemical Society, 2004, pp. 17040–17049.

[5] Zhu, Haijin, et al. “Solid-State NMR Characterization of the Multiphase Structure of Polypropylene In-Reactor Alloy.” Macromolecular Chemistry and Physics, vol. 211, no. 10, 2010, pp. 1157–1166., doi:10.1002/macp.200900661.

[6] Busico, Vincenzo, Roberta Roberta, Carmen Polzone, and Giovanni Giovanni. “Propene/Ethene-[1-13C] Copolymerization as a Tool for Investigating." Macromolecules. American Chemical Society, 20 Mar. 2003. Web. 23 June 2017.

[7] VanderHart, D. L., et al. “Observation of Resonances Associated with Stereo and Regio Defects in the Crystalline Regions of Isotactic Polypropylene: Toward a Determination of Morphological Partitioning.” Macromolecules, vol. 33, 2000, pp. 6078–6093

[8] Busico, Vincenzo; Cipullo Roberta. “Microstructure of Polypropylene, Progress in Polymer Science.” DeepDyve, Elsevier, 1 Apr. 2001

[9] Li, Zhen. “CHAIN PACKING AND CHAIN FOLDING STRUCTURES OF ISOTACTIC POLYPROPYLENE CHARACTERIZED BY SOLID-STATE NMR.” he University of Akron, ProQuest, 2015, pp. 1–173.

[10] Mamun, Al, et al. “Influences of the Chemical Defects on the Crystal Thickness and Their Melting of Isothermally Crystallized Isotactic Polypropylene.” Journal of Polymer Research, vol. 24, no. 145, 23 Aug. 2017, pp. 1–9., doi:10.1007/s10965-017-1304-6.

[11] JANIMAK, J J, and G C STEVENS. “Inter-Relationships between Tie-Molecule Concentrations, Molecular Characteristics and Mechanical Properties in Metallocene Catalysed Medium Density Polyethylenes.” JOURNAL OF MATERIALS SCIENCE, vol. 36, 2001, pp. 1879–1884.

[12] Thomas, C., et al. “Plastic Deformation of Spherulitic Semi-Crystalline Polymers: An in Situ AFM Study of Polybutene under Tensile Drawing.” *Polymer*, vol. 50, no. 15, 2009, pp. 3714–3723., doi:10.1016/j.polymer.2009.06.023.

[13] Nikolov, S.;Lebensohn, R.A.; Raabe, D.; ”Self-consistent modeling of large plastic deformation, texture and morphology evolution in semi-crystalline polymers.” Journal of the Mechanics and Physics of Solids, vol. 54, 2006, pp. 1350-1375

[14] Galeski, Andrzej. “Strength and Toughness of Crystalline Polymer Systems.” *Progress in Polymer Science*, vol. 28, no. 12, 2003, pp. 1643–1699., doi:10.1016/j.progpolymsci.2003.09.003.

[15] Pawlak, Andrzej, and Andrzej Galeski. “Plastic Deformation of Crystalline Polymers: The Role of Cavitation and Crystal Plasticity.” *Macromolecules*, vol. 38, no. 23, 2005, pp. 9688–9697., doi:10.1021/ma050842o.

[16] Janimak, J. J., and G. C. Stevens. “Inter-Relationships between Tie-Molecule Concentrations, Molecular Characteristics and Mechanical Properties in Metallocene Catalysed Medium Density Polyethylene.” *Journal of Materials Science* , vol. 36, 2001, pp. 1879–1884.

[17] Mitchell, Terence N., and Burkhard Costisella. NMR – From Spectra to Structures An Experimental Approach. Heidelberg: Springer-Verlag, Germany. Ser. 2. Springer-Verlag, 2007. Web. 8 Mar. 2018.

[18] Kang, Jia. “UNIAXIAL PLASTIC DEFORMATION OF ISOTACTIC POLYPROPYLENE STUDIED BY SOLID-STATE NMR.” The University of Akron, ProQuest LLC, 2016, pp. 1–163.

[19] Horva´th, Zsuzsanna, et al. “Chain Regularity of Isotactic Polypropylene Determined by Different Thermal Fractionation Methods.” Journal of Thermal Analysis and Calorimetry, vol. 118, 2015, pp. 235–245.

[20] “An Introduction to Dynamic Mechanical Analysis.” Dynamic Mechanical Analysis: A Practical Introduction, Second Edition, by Kevin P. Menard, 2nd ed., CRC Press, 2008, pp. 1–12.

[21] "D 638-02a Standard Test Method for Tensile Properties of Plastics." Annual Book of ASTM Standards 2003 Section 8 Plastics. Vol. 8.01. West Conshohocken: ASTM International, 2003. 46-47. Print.

[22] "D 790-02 Standard Test Method for Flexural Properties of Unreinforced and Reinforced Plastics and Electrical Insulating Materials." Annual Book of ASTM Standards 2003 Section 8 Plastics. Vol. 8.01. West Conshohocken: ASTM International, 2003. 146-147. Print.

[23] "D 256-02 Standard Test Methods for Determining the Izod Pendulum Impact Resistance of Plastics." Annual Book of ASTM Standards 2003 Section 8 Plastics. Vol. 8.01. West Conshohocken: ASTM International, 2003. 1-20. Print.(12)

[24] "D3763-02 Standard Test Method for High Speed Puncture Properties of Plastic Using Load and Displacement Sensor." Annual Book of ASTM Standards 2003 Section 8 Plastics. Vol. 8.02. West Conshohocken: ASTM International, 2003. 447-455. Print.

[25] Braskem Internal Report Determination of Ethylene Content, Molecular Distribution Sequence of P-E Copolymer, and Tacticity of PP Homopolymer Using 13C NMR Spectroscopy

[26] Ray, G. Joseph, et al. "Carbon-13 Nuclear Magnetic Resonance Determination of Monomer Composition and Sequence Distribution in Ethylene-Propylene Copolymers Prepared with a Stereoregular Catalyst System." *Macromolecules*, Macromolecules, 10 Jan. 1977.

[27] Stephens, C H, et al. "ISOTHERMAL CRYSTALLIZATION KINETICS AND MORPHOLOGY OF POLYPROPYLENES AND PROPYLENE/ETHYLENE (P/E) COPOLYMERS." SPE ANTEC May 2004, ser. 746-03501, May 2004. 746-03501

[28] Uan-Zo-li, Julie Tammy. "Morphology, Crystallization and Melting Behavior of Propylene-Ethylene Statistical Copolymers." Virginia Polytechnic Institute and State University, 2005.

[29] Rozanski, Artur, et al. "Physical State of the Amorphous Phase of Polypropylene -Influence on Free Volume and Cavitation Phenomenon." Journal of Polymer Science, Part B: Polymer Physics, vol. 54, 2016, pp. 531–543

[30] Tian, Jinghua, et al. "Crystallization Behaviors of Linear and Long Chain Branched Polypropylene." *Journal of Applied Polymer Science*, vol. 104, no. 6, 2007, pp. 3592–3600., doi:10.1002/app

[31] Stuart, Barbara H. "Thermal Behavior." Polymer Analysis. John Wiley & Sons, 2003. pp. 135-141.

[32] Zhou, Shuai et al. "Relationship between molecular structure, crystallization behavior, and mechanical properties of long chain branching polypropylene." *Journal of Material Science*, vol. 51, 2016, pp. 5598-5608